Dissertation

INFLAMMATORY PROFILING REVEALS TYPE 2 PREDOMINANT EOSINOPHILIC INFLAMMATION AND ASTHMATIC AIRWAY DISEASE IN THE FRA2 TRANSGENIC MOUSE MODEL

submitted by

MSc.

Anna GUNGL

for the Academic Degree of

Doctor of Philosophy (PhD)

at the

Medical University of Graz

Otto Loewi Research Center and

Ludwig Boltzmann Institute for Lung Vascular Research

under the Supervision of

PD Dr. Grazyna KWAPISZEWSKA

2019

Statutory Declaration and Disclosure

I hereby declare that this thesis is my own original work and that I have fully acknowledged by name all individuals and organisations that have contributed to the research for this thesis. Due acknowledgement has been made in the text to all other material used. Written permission was obtained to reproduce or reprint figures published elsewhere and submitted together with this thesis. Throughout this thesis and in all related publications I followed the “Standards of Good Scientific Practice and Ombuds Committee at the Medical University of Graz“.

Parts of this thesis has been published in:

Frontiers in Immunology, 2018 Sep 5;9:2018 (doi: 10.3389/fimmu.2018.02018).

Fra2 Overexpression in Mice Leads to Non-allergic Asthma Development in an IL-13 Dependent Manner

Anna Gungl[1], Valentina Biasin[2], Jochen Wilhelm[3,4], Andrea Olschewski[1,2], Grazyna Kwapiszewska[1,2], Leigh M. Marsh[2]*

[1]Otto Loewi Research Center, Medical University of Graz, Graz, Austria

[2]Ludwig Boltzmann Institute for Lung Vascular Research, Graz, Austria

[3]Department of Internal Medicine, Universities of Giessen and Marburg Lung Center, Giessen, Germany

[4]German Center for Lung Research, Justus-Liebig University, Giessen, Germany

All Co-authors have explicitly agreed to the use of their data in this dissertation.

Date …….

Foreword

I want to express my gratitude to my supervisors and members of my Dissertation committee: Dr. Grazyna Kwapiszewska, Dr. Andrea Olschewski, Dr. Akos Heinemann and Dr. Leigh Marsh.

A very special thank you belongs to Grazyna and Leigh for regularly pushing me outside my comfort zone to where the magic happens. I further want to thank Thomas Fuchs, Eva Grasmann, Bettina Schrenk and Lisa Oberreiter for excellent technical assistance; all members of the lab for support and a fun atmosphere to work in; Valentina Biasin and Slaven Crnkovic for guiding me through the first years and my PhD colleagues Davor Skofic-Maurer, Helene Thekekkara-Puthenparampil, Neha Sharma and Ceren Mutgan for all the laughs we had in- and outside the lab.

Last but not least, I want to thank Stefan and my family for always reminding me that there is more to life than work.

Acknowledgements

This work was conducted at the Ludwig Boltzmann Institute for Lung Vascular Research and at the Center for Medical Research (ZMF) of the Medical University of Graz. PhD student Anna Gungl received funding from the Jubilee Foundation of the Austrian National Bank ÖNB (grant number 16187 to GK), the Austrian Science Fund FWF (grant number P 27848-B28) and the Medical University of Graz through the PhD Program “Molecular Medicine” (MolMed).

The micro array gene expression analysis was performed by a collaboration partner, Dr. Jochen Wilhelm at the Justus-Liebig-Universität Gießen. Inflammatory profiling of mouse lungs was performed with the help of the translational platform of the Ludwig Boltzmann Institute for Lung Vascular Research and Dr. Leigh Marsh.

Table of Contents

Abbreviations and Definitions

AHR: airway hyperresponsiveness

AP-1: activator protein 1

ASMC: airway smooth muscle cell

ATF: activating transcription factor

BAL: bronchoalveolar lavage

BALF: bronchoalveolar lavage fluid

BSA: bovine serum albumin

CCL: CC-chemokine ligand

CD: cluster of differentiation

CD: cluster of differentiation

cDNA: complementary DNA

Clca1: chloride channel accessory 1

CRE: cAMP-responsive element

Crs: compliance of the respiratory system

Ct: threshold cycle

CTGF: connective tissue growth factor

CXCL: CXC-chemokine ligand

dcSSc: diffuse cutaneous systemic sclerosis

DNA: desoxyribonucleic acid

ECM: extracellular matrix

EDTA: ethylenediaminetetraacetic acid

EGFP: enhanced green fluorescence protein

ELISA: enzyme-linked immunosorbent assay

ERK: extracellular signal regulated kinase

Ers: elastance of the respiratory system

FCS: fetal calf serum

Foxa3: forkhead box A3

Fra: Fos-related antigen

Fra2: Fos-related antigen 2

G: tissue damping

H: tissue elastance

IC: inspiratory capacity

Ifnγ: interferon γ

IL: interleukin

JNK: c-Jun N-terminal kinase

kDa: kilodalton

lcSSc: limited cutaneous systemic sclerosis

LPS: lipopolysaccharide

MCP-1: monocyte chemoattractant protein 1 (also known as CCL2)

Muc5: mucin 5

OSM: oncostatin M

PAH: pulmonary arterial hypertension

PAS: periodic acid-Schiff staining

PBS: phosphate-buffered saline

PCR: polymerase chain reaction

PDGF: platelet derived growth factor

PFA: paraformaldehyde

PV-loop: pressure-volume loop

qRT-PCR: quantitative real-time PCR

Rn: Newtonian resistance

RNA: ribonucleic acid

Rrs: resistance of the respiratory system

SDS-PAGE: sodium dodecyl sulfate polyacrylamide gel electrophoresis

Spdef: SAM pointed domain containing ETS transcription factor

SPF: specific pathogen free

SRE: serum response element

SSc: systemic sclerosis

STAT6: signal transducer and activator of transcription 6

TAD: transactivation domain

TG: transgene

TGFβ: transforming growth factor β

Th2: T-helper-cell type 2

TPA: 12-O-tetradecanoylphorbol-13-acetate

TRE: TPA-responsive element

VWF: von Willebrand-factor

WT: wild-type

α: tumour necrosis factor α

α-SMA: α-smooth muscle actin

Abstract (German)

Überexpression des Transkriptionsfaktors Fos-related antigen 2 (Fra2 TG) in Mäusen führt zu vaskulären Veränderungen, systemischer Entzündung und Fibrose der Lunge, Haut und anderer Organe – Kennzeichen von systemischer Sklerose (SSc). Fra2 TG Mäuse wurden daher in den letzten Jahren zunehmend als Modell zur Untersuchung von SSc und damit assoziierter Lungenfibrose und pulmonaler Hypertonie verwendet. Eine detaillierte Beschreibung des zeitlichen Ablaufs ihres Phänotyps wurde bisher allerdings noch nicht publiziert. Das Ziel dieser Studie war daher eine genaue Charakterisierung des Lungenphänotyps von Fra2 TG im Vergleich zu WT Mäusen, inklusive Lungenfunktion, struktureller Umbau und Entzündung in der Lunge, um ein besseres Verständnis der zugrunde liegenden Pathomechanismen zu erlangen.

Vaskulärer Umbau in Fra2 TG Mäusen war in allen untersuchten Zeitpunkten (8, 16 und >20 Wochen) evident, während parenchymale Fibrose/Kollagendeposition erst später auftrat, in älteren Mäusen zunahm und zu einer Verschlechterung der Lungenfunktion in >20 Wochen alten Mäusen führte. Histologisch war keine Entzündung in 8 Wochen alten Mäusen ersichtlich. Im Alter von 16 Wochen waren hingegen deutliche peri-vaskuläre und peri-bronchiale inflammatorische Infiltrate ersichtlich, die in älteren Mäusen weiter zunahmen. Expressionsanalyse und Proteinquantifizierung wichtiger Zytokine des angeborenen und adaptiven Immunsystems zeigten erhöhte Level der Th2-Mediatoren IL-4 und IL-13. Gleichzeitig hatten 16 und 20 Wochen alte Mäuse signifikant mehr inflammatorische Zellen in der Lunge und in der bronchoalveolären Lavage, hauptsächlich bestehend aus Eosinophilen.

Nachdem erhöhte Typ 2 Immunität und Eosinophilie Markenzeichen von Asthma sind, wurde überprüft ob Fra2 TG Mäuse einen asthmatischen Phänotyp entwickeln. In der Tat zeigten Fra2 TG Mäuse peri-bronchiale Kollagendeposition, eine Verdickung der Glattmuskelzellenschicht, erhöhte Schleimproduktion und eine Hyper-Reaktivität der Atemwege. Behandlung mit Glucocorticoiden oder IL-13 Blockade über neutralisierende Antikörper führte zu einer Abschwächung des Phänotyps. Zusammenfassend wurde in dieser Studie durch detaillierte Charakterisierung des Fra2-induzierten pulmonalen Phänotyps herausgefunden,

dass Fra2 TG Mäuse ein neues Modell für nicht-allergisches Asthma darstellen, die wichtige Charakteristika dieser Krankheit, wie Atemwegsentzündung, - umbau und Hyper-Reaktivität zeigen.

Abstract (English)

Transgenic mice overexpressing the transcription factor Fos-related antigen 2 (Fra2 TG) exhibit vascular changes, systemic inflammation and fibrosis of skin, lung and other organs, the main hallmarks of systemic sclerosis (SSc). In the recent years, these mice became a commonly used model for SSc and associated pulmonary fibrosis and hypertension. However, a detailed assessment of the time-dependent phenotype of Fra2 TG mice was not conducted. Therefore, this work aimed to assess in detail the pulmonary phenotype of Fra2 TG mice in comparison to WT littermate control mice, including pulmonary function, remodelling and inflammation, to gain a better understanding of the underlying pathomechanisms.

Fra2 TG mice had increased vascular remodelling in all investigated time-points (8, 16 and >20 weeks), whereas parenchymal remodelling developed later on in a time-dependent manner, leading to increased collagen deposition and a concomitant decline in lung function in mice older than 20 weeks. Histologically, inflammation was not apparent in the lungs of 8-week-old mice, but at 16 weeks perivascular and peribronchial inflammatory infiltrates were observed which advanced in old mice. Expression analysis of key cytokines of the innate and the adaptive immunity (known to be associated with SSc) revealed increased levels of the Th2 cytokines IL-4 and IL-13, which were confirmed on protein level. At the same time, 16- and >20-week-old Fra2 TG mice had a significant increase of inflammatory cells in bronchoalveolar lavage and lung tissue, with eosinophils as the most predominant cell type in both compartments.

As increased levels of Th2 cytokines and eosinophils are hallmarks of allergic airway disease and asthma, the hypothesis that Fra2 TG mice have an asthmatic phenotype was investigated. Indeed, 16-week-old mice showed elevated peribronchial collagen deposition, smooth muscle thickening, mucus production and airway hyperresponsiveness in response to increasing doses of methacholine. Glucocorticoid treatment and blockade of IL-13 via neutralising antibodies partially ameliorated the asthmatic phenotype. In conclusion, by detailed characterisation of the Fra2-induced pulmonary phenotype, Fra2 TG mice were discovered as a novel model for non-allergic asthma that mimics key features of the disease, such as airway inflammation, remodelling and hyperresponsiveness.

1. Introduction

1.1. Activator protein-1 transcription factors

1.1.1. The AP-1 family of transcription factors

The activator protein-1 (AP-1) family of transcription factors is involved in a broad variety of physiological and cellular processes, such as tissue development and homeostasis. It directly couples extra- or intracellular stimuli and regulates genes involved in cellular proliferation, differentiation and apoptosis (1). It consists of Jun proteins (v-Jun, c-Jun, JunB, JunD) and Fos proteins (c-fos, FosB, Fra1, Fra2). AP-1 proteins form either homo- or heterodimers which then bind to their DNA consensus sequence (TGAG/CTCA) to activate or repress transcription (2) (Figure 1).

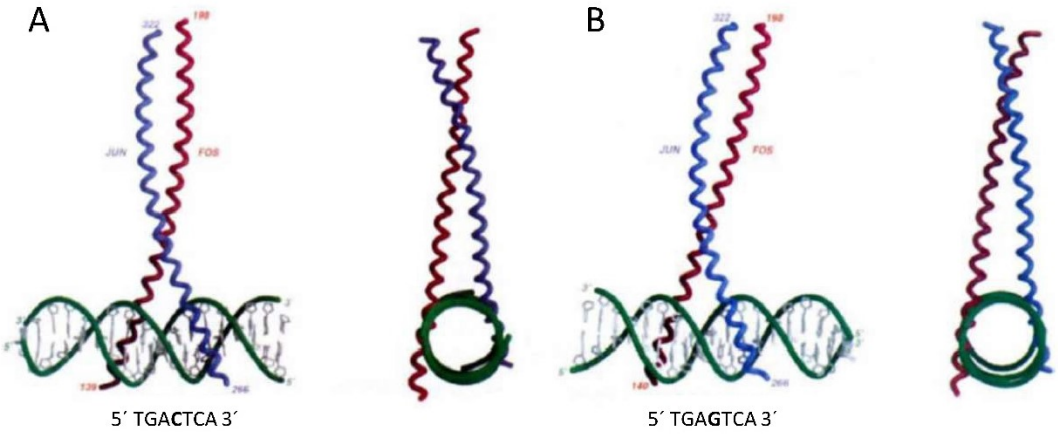

Figure 1: Structure of the AP-1 dimer bound to DNA. Jun (blue) and Fos (red) proteins bound to the DNA (green) consensus sequence A) 5´ TGACTCA 3´ or B) 5´ TGAGTCA 3´. Figure taken from reference (3) with permission of publisher (Springer Nature).

1.1.2. Structure and DNA binding properties of AP-1

AP-1 was first identified as the transcription factor inducing gene expression upon stimulation with the phorbol ester TPA (12-O-tetradecanoylphorbol-13-acetate), therefore the DNA consensus sequence (TGAG/CTCA) bound by AP-1 is called TPA-responsive element (TRE) (2). AP-1 proteins form dimers through leucine zipper motifs and bind to the DNA through positively charged basic regions (3). Jun proteins can either form heterodimers with members of the Fos family (Fos-Jun) or homodimerize with other Jun proteins (Jun-Jun), while Fos proteins can only form

heterodimers (Fos-Jun) and are not able to dimerise with other Fos proteins (4, 5). AP-1 proteins can also dimerize with ATF proteins (ATF2, ATF3/LRF1, B-ATF). Jun/Fos-ATF dimers have an altered DNA binding specificity and preferentially bind to cAMP-responsive elements (CRE; TGACGTCA). Additionally, Jun and Fos proteins can dimerize with Maf proteins (c-Maf, c-Maf) or JDP (Jun dimerizing partners) and bind to TRE, CRE or asymmetric DNA sequences (6).

The structure of different AP-1 proteins is partially highly conserved. However, they differ in some crucial aspects. In addition to the leucine-zipper dimerization domain and the basic DNA binding domain, the presence of a transactivation domain (TAD) is crucial for the transcription-activating properties of an AP-1 protein (Figure 2). While all Jun proteins possess a TAD, in the Fos family only c-Fos and FosB have one (7). Fra-1 and Fra-2 lack a transactivation domain and depend on their interaction partner to acquire transactivating properties (7).

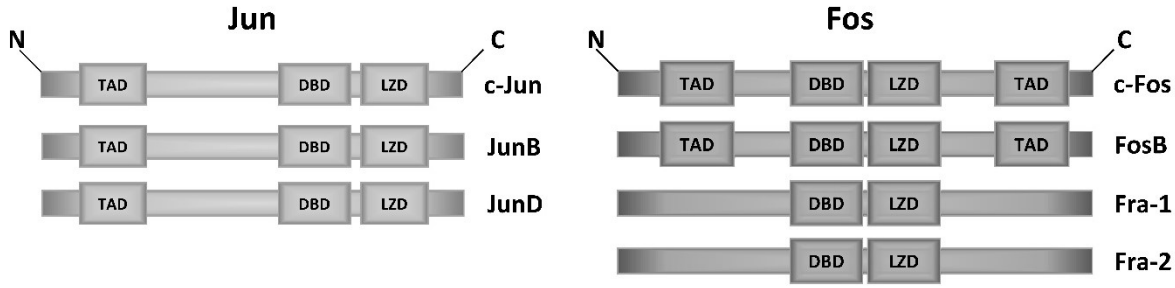

Figure 2: Schematic representation of the structure, dimerization and DNA binding properties of AP-1 proteins. Different domains within Jun and Fos proteins: TAD: transcription-activating domain; DBD: DNA binding domain; LZD: leucine-zipper domain.

Depending on the dimer composition, different DNA sequences around the consensus site are favoured and influence AP-1 binding to the DNA. The differential abundance and expression of specific AP-1 members upon intra- or extracellular stimuli in diverse cell types leads to a specific set of AP-1 dimers and allows for distinct time-, tissue- and cell-dependent regulation of specific sets of target genes (8).

1.2. The AP-1 subunit Fra2

1.2.1. Regulation of Fra2

Fra2 was the last member of the Fos family of proteins to be identified in 1990 as a 46 kDa protein in growth stimulated chicken embryo fibroblasts. At the same time, the human *FRA2* gene was cloned from a cDNA library (9, 10). Due to its homology to c-fos and its identification through an anti-fos antiserum, it was termed fos-related antigen 2 (Fra2) (10). In contrast to c-fos which is only detectable after stimulation, low levels of Fra2 can also be detected in unstimulated cells under basal conditions (11). Fra2 is expressed in response to phorbol esters (such as TPA), cAMP, Ca^{++} and serum. Compared to c-fos expression, Fra2 expression is delayed and more prolonged in stimulated cells. Furthermore, the time-period of Fra2 induction varies depending on the stimulus acting on a cell (12).

Several regulatory elements can be found in the Fra2 promoter region such as SCM-like (sis-conditioned medium) elements, SRE (serum response element), CRE (cyclic AMP response element) and several GC boxes. Further two putative AP-1 binding sites can be found. The AP-1 binding site found in the promoter regions of the Fra2 and other AP-1 genes indicates auto-regulatory mechanisms or cross-regulation of different AP-1 subunits (12). Indeed, it has been shown that c-fos/c-jun dimers bound to the Fra2 promoter strongly activate its expression. The c-fos/c-jun dimer is then exchanged with a fra-2/c-jun dimer, which has a lower transcriptional activity (13). Fra2 supresses the transactivational activity of c-jun, indicating a potential negative feedback loop in the regulation of Fra2 (14).

1.2.2. Target genes of Fra2

Fra2 forms stable heterodimers with all member of the Jun family, namely c-Jun, JunD and JunB (14), and can therefore act on a broad variety of target genes, involved in tissue homeostasis, extracellular matrix (ECM) production or inflammatory responses. It is activated and acts downstream of several stimuli such as growth factors like TGFβ (15) or PDGF-BB (16), and inflammatory mediators like IL-13 (17). Although Fra2 is one of the downstream mediators of TGFβ signalling, TGFβ1 in turn is regulated by Fra2 bound to its promoter site. Deletion of the AP-1 site in the TGFβ1 promoter inhibits transcriptional activity (18). Several cytokines such as IL-6 (19) or IL-13 (17) can activate AP-1. On the other hand, AP-1 binding

sites can be found in the promoter regions of typical Th2 cytokines such as IL-4, IL-5 or IL-13 and their expression can be regulated by AP-1 (20-23). Fra2 itself has been implicated in the regulation of IL-11 (24). In response to toxins, such as tobacco smoke, several pathways are activated, namely activation of ERK as well as JNK, which converge to Fra2 activating airway mucus production (25).

In fibroblasts Fra2 expression and activation leads to the production and release of collagen. Knockdown of Fra2 decreased the basal expression of *COL1A1*, *COL1A2* and *COL5A1* in SSc dermal fibroblasts (26). Overexpression of Fra2 in mice also led to the production of meprinβ (16), a metalloproteinase supporting collagen maturation and deposition in the lung (27). An additional mechanism by which Fra2 drives the maturation of collagen is via regulation of TGFβ-induced expression of lysyl oxidase-like 4 (*LOXL4*), an enzyme initiating the cross-linking and thereby stabilization of collagen fibrils (28). Fra2 is further involved in regulation of LAMA3A expression, a constituent of laminin-5 that is a major adhesion ligand expressed by keratinocytes anchoring them to the basal membrane (15).

Through this variety of actions including several feedback loops, Fra2/AP-1 is involved in pathways crucial for cell and tissue homeostasis which if erroneously regulated can significantly contribute to the development of disease and pathologic remodelling processes.

1.3. Fra2 in disease

1.3.1. Fra2/AP-1 in tumorigenesis

Both Jun and Fos proteins are important modulators in the development of tumours and can act both tumour-promoting or –repressing (29). Altered AP-1 expression has been implicated in several cancers, such as breast, endometrial, ovarian and gastric carcinomas, colorectal cancer and in diverse forms of leukaemia and lymphoma (30). Due to the lack of a transactivation domain, Fra1 and Fra2 themselves do not possess transforming properties in rodent fibroblasts, however, they can be found abundantly in transformed cells and may play a role in the maintenance and progression of the transformed state in cells (31). For example, in

transformed chicken embryo fibroblasts, Fra2 was hyper-phosphorylated and led to increased Fra2 and c-Jun expression via an auto-regulatory loop (32).

1.3.2. Fra2/AP1 in inflammation

In recent years, the use of AP-1 subunit-specific knock-out or overexpressing mice has led to a better understanding of the role of distinct AP-1 subunits and their implications in disease development beyond cancer. Jun proteins were found to be important for immune cell differentiation and regulation of the immune system (33). For example, c-Jun is critically involved in the regulation of T-cell development and differentiation (34).

Fos proteins, especially c-fos, play important roles in bone formation and homeostasis, by controlling osteoclast differentiation and extracellular matrix gene expression (35, 36). Mice lacking Fra2 die shortly after birth (37) and display impaired chondrocyte differentiation and matrix deposition in the growth plates of femur and tibia (38). Bone development and homeostasis are also closely linked to the immune system. In the bone marrow, immune cells exist in close proximity to osteoclasts and osteoblasts and they share a wide range of receptors, signalling molecules such as cytokines, and transcription factors (39). One of these transcription factors is AP-1. Throughout osteoblast differentiation, all AP-1 components are expressed, but in differentiated osteoblasts Fra2 and JunD are the major AP-1 components present (40). Indeed the close link between bone and immune system becomes apparent in a recent study showing that Fra2 overexpression in osteoblasts alone is sufficient to induce a systemic inflammatory state with high levels of pro-inflammatory cytokines and aggravates LPS-induced lung injury (41). The role of Fra2 in the development of inflammation and pulmonary pathologies also becomes apparent in mice overexpressing Fra2.

1.3.3. Fra2 overexpressing mice

In 2008, Eferl and colleagues created mice globally overexpressing Fra2 (Fra2 TG) (42). The whole genomic region of the *Fra2* gene was fused to the major histocompatibility complex class I promoter H2Kb and combined with a downstream EGFP reporter gene (Figure 3). To increase stability and expression of the *Fra2* mRNA, the 3' long terminal repeat sequence including a poly-adenylation sequence of the FBJ murine sarcoma virus was fused to the construct (37, 42).

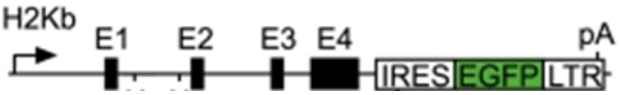

Figure 3: Genetic construct for the ectopic overexpression of Fra2 in mice. H2Kb: major histocompatibility complex class I antigen promoter; E1-4: exon 1-4; pA: polyadenylation sequence; IRES: internal ribosomal entry site; EGFP: enhanced green fluorescence protein; LTR: 3' long terminal repeat. (Figure from (42). © 2008 National Academy of Sciences of the USA).

Fra2 TG mice were fertile, and the transgene was passed on to the offsprings in a mendelian ratio. Although no obvious developmental defects were observed until an age of 12 weeks, and lung morphology looked normal, Fra2 TG mice developed severe pulmonary fibrosis within a few weeks and died at a median age of 17 weeks (42). In these mice, not only the lungs were affected, but they also developed fibrosis of skin and other internal organs such as liver, stomach, oesophagus, thymus and heart. Of note, Fra2 TG mice also exhibited increased bone mass and in rare cases tumour formation (42). Follow-up studies showed that Fra2 TG mice show a phenotype similar to that of systemic sclerosis patients (26, 43).

1.4. Fra2 TG mice as a model of pulmonary fibrosis associated with systemic sclerosis

It was shown that Fra2 is overexpressed in dermal fibroblasts from systemic sclerosis (SSc) patients compared to fibroblasts from healthy donors (26). Increased expression and nuclear localisation of Fra2 can be observed in skin biopsies from SSc patients, especially in endothelial and vascular smooth muscle cells (26). Furthermore, Fra2 levels were highly elevated in the lungs of patients with pulmonary fibrosis, in idiopathic disease as well as in SSc-associated lung fibrosis (42).

1.4.1. SSc pathology and pulmonary involvement

Systemic sclerosis (SSc) is a rare connective tissue disease with involvement of multiple organs, such as the skin, heart, lungs, kidneys, the gastrointestinal tract and the musculoskeletal system. It is characterized by aberrant immune activation and autoimmunity, fibrosis of the skin and internal organs, and vascular pathology

with damage and loss of microvasculature. The extent of fibrosis, organ involvement or vasculopathy can vary and disease manifestation can even change over time compared to its initial presentation (44). SSc is classified into two major subtypes, depending on the extent of skin involvement: limited cutaneous (lcSSc) or diffuse cutaneous SSc (dcSSc). LcSSc patients mostly show slow disease progression with skin fibrosis isolated to the lower extremities, dcSSc patients have a more rapid progression, generalized skin fibrosis and frequent organ involvement. SSc is a clinically complex and heterogeneous disease and can overlap with other autoimmune disorders. The American College of Rheumatology and the European League against Rheumatism (ACR/EULAR) have provided criteria to classify SSc (45-47).

Lung involvement occurs in about 50% of SSc patients and can manifest as pulmonary fibrosis or pulmonary arterial hypertension (PAH). While pulmonary fibrosis is more common in dcSSc patients, PAH is more frequently found in lcSSc patients (48). In general, lung involvement – present as pulmonary fibrosis or as PAH - is a severe complication of SSc and the most common cause of SSc-related death (49, 50).

1.4.2. Pathomechanisms of SSc

Several cell types are involved in the pathological changes of lung remodelling in SSc. Repeated injury of alveolar epithelial cells (AECs) is a crucial factor in the development of pulmonary fibrosis (51). Depending on the microenvironment AECs can undergo apoptosis or acquire a phenotype similar to mesenchymal cells, which is termed epithelial-to-mesenchymal transition. During this process, AECs lose their polarity and increase migratory capacity, apoptosis-resistance and extracellular matrix production (51). EMT has been implicated in the development of pulmonary fibrosis associated with SSc (52), however this concept is debatable, as other studies have shown that several cell types contribute to pulmonary fibrosis and did not find indications for EMT (53).

Another crucial cell type in the development of fibrosis is the myofibroblast. These cells can arise from resident fibroblasts, circulating fibrocytes or by transdifferentiation of other cell types (54). Current concepts on the development of myofibroblasts are depicted in Figure 4.

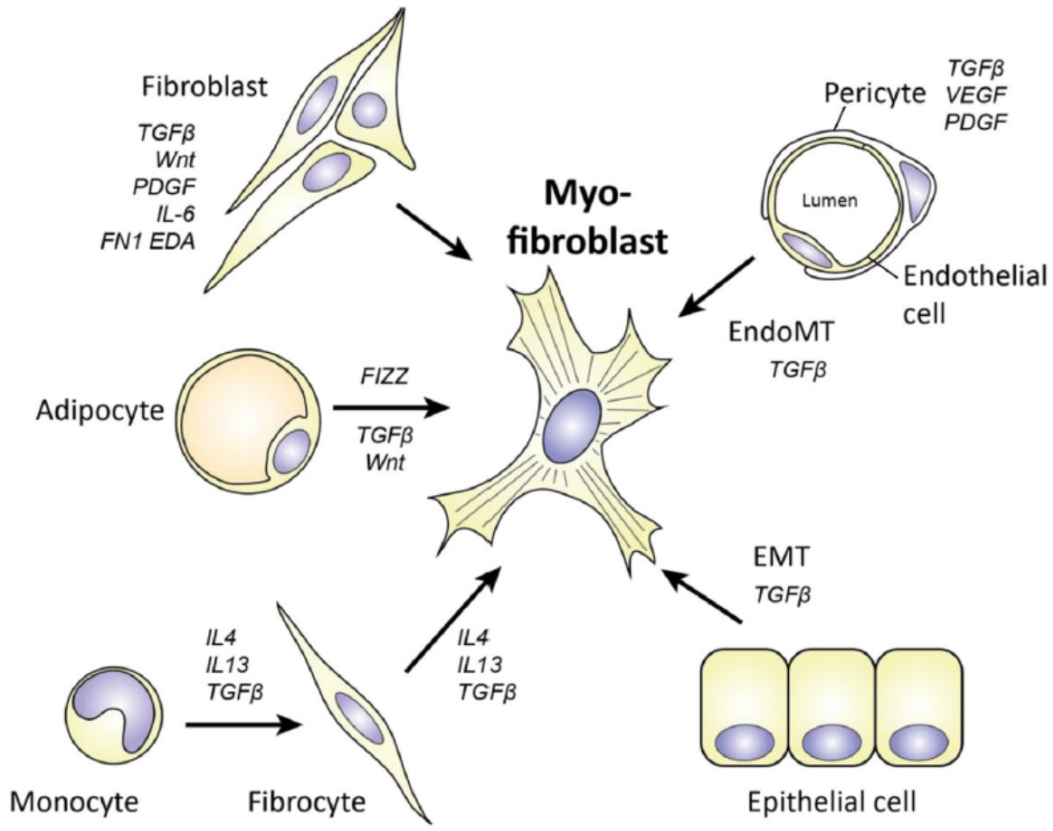

Figure 4: Current concepts on the cellular origins of myofibroblasts. Cell types and key mediators leading to the formation of myofibroblasts are depicted. (Figure from (54)).

Due to their contractile and ECM-producing properties, myofibroblasts are crucial in wound healing processes, but can contribute and lead to the development of tissue fibrosis if not tightly regulated (reviewed in (54)). They not only produce high amounts of ECM proteins, but also express and secrete several ECM-maturation enzymes such as transglutaminase-2 and lysyl oxidases (LOX) which post-translationally covalently crosslink collagen, thereby increasing the strength of collagen networks and the ECM structure (55).

SSc patients at risk for pulmonary involvement are mostly identified by the presence of inflammation in the lung. Increased levels of neutrophils and eosinophils can be found in the bronchoalveolar lavage fluid of SSc patients with lung involvement compared to healthy controls (56, 57). SSc patients with pulmonary inflammation further had a worse prognosis. However, risk stratification of patients was not possible as the presence/severity of pulmonary inflammation did not correlate with disease deterioration (57). Furthermore, end-stage lung disease can present

completely without pulmonary inflammation solely as severe fibrosis and remodelling of the lung.

One of the major cell types seen in inflammatory infiltrates in SSc lungs are alveolar macrophages, which undergo alternative activation and produce high amounts of pro-fibrotic cytokines and growth factors, and can stimulate collagen production by fibroblasts (58). Increased numbers of alternatively activated macrophages have been reported in patients with SSc (59) as well as in the Fra2 TG mouse (60).They further can produce IL-13 and activate Th2 cells which in turn produce pro-fibrotic cytokines such as IL-4 (61-64). In addition to Th2 cells, CD8+ memory T-cells can be found in lungs of SSc patients. In SSc patients, these cells are more prone to produce pro-fibrotic factors IL-4 and IL-5 compared to cells from healthy controls and increased numbers are associated with more severe pulmonary fibrosis (65). In addition to macrophages and T-cells, mast cells are implicated in the development of pulmonary fibrosis in SSc. Their numbers are elevated in the bronchoalveolar lavage fluid (BALF) of SSc patients, especially in those patients who have interstitial fibrosis (66). Mast cells can stimulate collagen production by fibroblasts via the release of CCL2, also known as monocyte-chemotactic protein (MCP)-1 (67), enhance fibroblast proliferation through histamin production (68) and contribute to elevated levels of IL-4 (69). In fibrotic lung tissue of SSc patients, increased degranulation of eosinophils can be observed, leading to high levels of eosinophil-derived major basic protein. Increased levels of this protein as well as eosinophil numbers in the BALF are associated with decreased lung function and more fibrosis, respectively (70, 71). Additionally, eosinophils can adhere to fibroblasts, thereby stimulating fibroblast proliferation and collagen production and contributing to pulmonary fibrosis (72).

1.4.3. Growth factors and inflammatory mediators associated with SSc lung involvement

Growth factors

Transforming growth factor β (TGFβ) has long been associated with fibrosis development in SSc (73). It is produced by a variety of cell types, including inflammatory cells such as macrophages and lymphocytes as well as structural cells as fibroblasts, endothelial and epithelial cells. TGFβ is a potent activator of ECM

production stimulating the expression of collagens, fibronectin, fibrillin and proteoglycans (74, 75) and drives the development of fibroblasts into myofibroblasts (54).

Connective tissue growth factor (CTGF) can be induced and acts downstream of TGFβ. It induces proliferation of fibroblasts and expression of ECM proteins such as collagen and fibronectin (76). CTGF levels in the sera of SSc patients are elevated and correlate with the extent of fibrotic skin and the severity of pulmonary fibrosis (77).

In the BAL fluid of SSc patients, elevated levels of platelet-derived growth factor (PDGF)-AA and PDGF-BB can be found (78). Similar to TGFβ, PDGF induces ECM production in fibroblasts, and may additionally contribute to fibrosis development by stimulation expression of the pro-fibrotic chemokine monocyte chemoattractant protein (MCP)-1 (79).

Pro-inflammatory cytokines

The interleukin (IL)-1 family members IL-1α and IL-1β are strongly increased in the serum of SSc patients (80, 81). IL-1β levels are further increased in the bronchoalveolar lavage fluid (BALF) of SSc patients and negatively correlate with lung function (80). Fibroblasts isolated from SSc patients constitutively express IL-1α leading to increased levels of PDGF-A and IL-6 thereby contributing to the development of fibrosis (82). IL-1 does not stimulate the production of extracellular matrix, however it increases fibroblast proliferation (83).

Similarly to IL-1, tumour necrosis factor α (TNFα) stimulates fibroblast chemotaxis, while inhibiting collagen production (84). However, in rats lung-specific overexpression of TNFα led to inflammation followed as well as fibrosis due to the upregulation of TGFβ (85). In SSc patients, TNFα levels in the serum are elevated and correlate with pulmonary fibrosis and decreased lung function (86).

Macrophages, T-cells and also fibroblasts are a source of cytokines of the IL-6 family, such as IL-6 or oncostatin M (OSM). Upon stimulation with OSM, fibroblasts increase proliferation and extracellular matrix production (87, 88). The pro-fibrotic properties of IL-6 in SSc have been well documented, as not only its plasma levels

are elevated in patients (89), but also several animal studies highlight its crucial role in the development of pulmonary fibrosis (90).

Type 1 and type 2 cytokines

Activated T helper cells can be categorized into 3 main categories (reviewed in (91)): 1) Th1 cells, which protect against intracellular pathogens, produce high levels of interferon γ (Ifnγ) and lead to the activation of phagocytes and the production of opsonizing antibodies. 2) Th2 cells, which are the first line of defence against extracellular parasites such as helminths and crucial in allergic reactions. They produce large amounts of IL-4 and IL-13, cytokines inducing the class switch in B-cells enabling mast cell and basophil sensitization, and IL-5, a mediator that stimulates eosinophil activation, recruitment and proliferation. 3) Th17 cells that lead to recruitment and activation of neutrophils and produce IL-17 (IL-17A and IL-17F), IL-8, IL-21 and IL22. Th17 responses are involved in the clearance of extracellular pathogens, especially fungi. The differentiation of T-helper cells is defined by specific sets of transcription factors that are activated in response to the cytokine microenvironment during the antigen-mediated activation of naïve T-cells. Whereas Th2 immunity is typically involved in allergic responses, Th1 and Th17 immune responses are more often associated with autoimmune disorders (91).

Studies on the balance of type 1/type 2 inflammation in SSc lung disease are controversial (reviewed in (92)), however it was reported that a shift towards type 2 inflammation is associated with a decline in lung function (65). Whereas interferon γ (IFNγ), the hallmark cytokine of the type 1 immune response, inhibits fibroblast proliferation and collagen production, type 2 cytokines such as IL-4, IL-13 and IL-10 are mostly exerting pro-fibrotic effects (93). For example, IL-4 and IL-13 stimulate proliferation of fibroblasts and their differentiation towards myofibroblasts (94). IL-4 itself has a potent pro-fibrotic effect (95, 96) and its levels are significantly increased in the serum of SSc patients (97). In addition to the direct pro-fibrotic effects, IL-4 can lead to alternative activation of macrophages which are in turn involved in the development of fibrosis (98) and stimulate TGFβ as well as CTGF production by fibroblasts (99, 100).

Chemokines

Chemokines play an important role in immune cell homeostasis as well as in infection and inflammatory diseases, and can actively contribute to the accumulation of extracellular matrix. They are critical for the function of the innate immunity as they control migration and positioning of inflammatory cells through their chemotactic properties. Several chemokines such as the CC-motif Chemokines: CCL2, CCL3 or CCL5 are elevated in SSc patients (101). CCL2 (also known as MCP-1) also exerts direct pro-fibrotic effects on fibroblasts. It can be found in increased levels in the BAL fluid of SSc patients (63) and upregulates collagen production in lung fibroblasts (102). Elevated CCL2 serum levels are linked to the presence of pulmonary fibrosis in SSc patients (103).

1.5. Asthma bronchiale

Asthma bronchiale, in short asthma, is one of the most common chronic inflammatory diseases and is in the vast majority of cases caused by airway inflammation. Its symptoms are acute dyspnoea, coughing, chest tightness and wheezing and are usually caused by triggers such as allergens, common colds or exercise (104). Asthma affects all age groups and has a global prevalence ranging from 1% to 21% with over 300 million people worldwide being affected (104). It is a very heterogeneous disease with several phenotypes that were originally defined by clinical characteristics. Recent advances have tried to link the underlying pathobiology to the phenotype (105). Most asthma patients suffer from allergic/atopic asthma, with a strong Th2-driven inflammation, however there are also asthma phenotypes with little or no Th2 inflammation (105). Elevated levels of eosinophils, T-cells and the Th2 cytokines, interleukin (IL)-4, IL-5 and IL-13, cause remodelling and bronchoconstriction (106), and aberrant mucus production (107), leading to hyperresponsiveness of the airways, and to obstruction and severe airflow limitation (104). While most patients respond to non-specific anti-inflammatory drugs, such as corticosteroids, some patients with very high Th2 or neutrophilic inflammation display steroid-refractory asthma. These severe and poorly controlled asthma phenotypes remain a crucial unmet medical need (105).

Several studies indicate involvement of AP-1 in the development of asthma (108-110) and even highlight its potential as a therapeutic target for the treatment of asthma and allergic airway disease (109, 111). Another study showed increased DNA-binding activity of AP-1 in peripheral blood mononuclear cells of steroid refractory patients (112). Concomitantly there was a decreased interaction of the glucocorticoid receptor (GR) and AP-1 indicating that this might be the cause for the altered response to glucocorticoids and thus steroid refractory asthma (112). However, studies on the role of AP-1 and especially its specific subunits in the development of asthma are scarce. Further investigations might therefore help to identify new therapeutic applications for the treatment of severe asthma.

1.6. Rationale of this study

The complex interplay between different inflammatory and structural cells, as well as signalling mediators such as growth factors, cytokines and chemokines indicate that the pro-fibrotic network leading to pulmonary fibrosis in SSc patients is very complex and still requires further investigations. Very few drugs successfully tested in animal models of pulmonary fibrosis translated into clinical trials with beneficial patient outcome (113). This might be due to limited comparability of human disease and attempts to reproduce disease mechanisms in animal models. A better/detailed understanding of pathomechanisms in human as well as in disease models is crucial to better predict the potential beneficial effects of specific compounds in clinical trials (113).

We hypothesised that a thorough characterisation of the time-dependent Fra2-induced pulmonary inflammation and phenotype in mice will delineate the role of specific cytokines in the development of pulmonary fibrosis associated with systemic sclerosis and their potential as therapeutic targets. A detailed characterization of the inflammatory profile in the lung interstitial and alveolar space of Fra2 TG mice over a time period of 3 months was performed. This profiling was corroborated by thorough assessment of pulmonary remodelling and lung function testing to get a comprehensive understanding of the time-dependent lung pathology.

First results led to the hypothesis, that increased Th2 cytokines and eosinophilia leads to an asthmatic phenotype of Fra2 TG mice. This hypothesis was tested in the

second part of the thesis. Further, the impact of Th2 cytokines, in specific IL-13, signalling and the effect of systemic anti-inflammatory treatment using glucocorticoids on the Fra2 induced lung phenotype was characterized.

2. Material and Methods

2.1. Animal experiments

2.1.1. Animal strains, breeding and housing

All animal experiments met the EU guidelines 2010/63/EU and were approved by the local authorities (Austrian Ministry of Education, Science and Culture, BMWF-66.010/0086-11/3b/2012, BMWF-66.010/0138-II/3b/2013, BMWFW-66.010/0067-WF/V/3b/2016, BMWFW-66.010/0069-WF/V/3b/2016).

Fra2 TG mice (Tg(H2-K-Fosl2,EGFP)13Wag; Mouse Genome Informatics - MGI:3813493) were obtained from Prof. Erwin Wagner at the Institute for Molecular Pathology Vienna. The strain of origin, with a mixed C57BL/6 x CBA background, was backcrossed with C57BL/6, without altering the phenotype (42). Mice were kept under specific pathogen free (SPF) conditions in the animal facility of the Medical University of Graz (Biomedical Research). Fra-2 transgenic (TG) mice and wild-type (WT) littermates were maintained in isolated and ventilated cages with 12-hour light/dark cycles. Water and chow were supplied ad libitum. Animals were looked after daily by experienced personnel. To assure animal well-being cages were supplied with nesting material and tunnels. Further, to evade stress it was avoided to keep single mice alone in cages and mice were transferred to the experimental animal facility a minimum of three days prior to the start of an experiment. All measures were taken to keep animal suffering to a minimum.

2.1.2. Baseline lung function measurements

Lung function of mice was measured *in vivo* using the FlexiVent FX Module 1 (SciReq, Inc., Montreal, PQ, Canada) (114). The mice were anaesthetized via *intraperitoneal* injection of 0.05 ml Ketanest (150mg/ml Ketamin, Parke-Davis, Berlin) and Rompun (2% Xylazinhydrochlorid, Bayer Leverkusen) in a ratio of 1:1. Thereby animals were sedated, relaxed and analgised to allow tracheotomy. A suture was pulled below the trachea and a small incision was made above the suture. A canula was inserted into the trachea and fixed with the suture before attaching the mouse to the FlexiVent module. Mice were mechanically ventilated at a frequency of 150 breaths/min with a tidal volume of 10 ml/kg and a positive end expiratory pressure of two cmH_2O. During different lung function manoeuvres

mechanical ventilation was paused and either pressure- or volume-driven waveforms, called pertubations, were applied to the lungs. Throughout these manoeuvres, pressure, flow and volume were constantly recorded. Lung function measurements were performed using deep inflation, single frequency and broadband forced oscillation techniques, and pressure-volume loops (Figure 5).

Pertubation name	Typical paramters
Deep inflation (recruitment manoever)	- IC: inspiratory capacity
SnapShot-150 (single frequency forced oscillation)	Single Compartment Model parameters: - R: resistance of the respiratory system - E: elastance of the respiratory system - C: dynamic compliance
Quick Prime-3 Prime-8 (broadband frequency forced oscillation)	Constant Phase Model parameters: - Rn: Newtonian resistance (resistance of the airways) - G: Tissue damping (related to tissue resistance) - H: Tissue elastance - η: ration of G/H
Pressure-Volume curve	- Pressure-volume curve - Cst: quasi-static compliance - Area: Area between the inspiratory and expiratory limb of the pressure-volume curve - Salazar-Knowles parameter A: estimate of inspiratory capacity - Salazar-Knowles parameter K: curvature of the upper portion of the expiratory limb of the P-V curve.
NPFE (negative pressure-driven forced expiration)	- flow-volume curve - FEV0.1: forced expired volume in 0.1 s - FVC: forced vital capacity - PEF: peak expiratory flow

Figure 5: Overview of perturbations used for lung function measurements and calculated parameters.

The deep inflation manoeuvre (Figure 6A) which gradually inflates the lung to the total capacity (defined as a pressure of 30 cmH_2O) enables to measure the inspiratory capacity (IC) of mouse lungs. Furthermore, this manoeuvre was used to open closed areas of the lung and restore normal lung volume in between different doses during dose response measurements of airway hyperresponsiveness. Airway resistance (Rrs), compliance (Crs) and elastance (Ers) were obtained in a single frequency forced oscillation manoeuvre (Figure 6B). A signal containing a wide range of frequencies, both below and above the range of breathing frequency (broadband forced oscillation, Figure 6C), was applied to obtain respiratory system

input impedance, which was further analysed using a constant phase model (115). This model enables a parametric distinction between tissue and airway mechanics. The obtained parameters are as follows: The newtonian resistance (Rn), representing the resistance of the central or conducting airways, tissue damping (G), a parameter closely related to tissue resistance, and tissue elastance (H), a parameter reflecting the energy conservation in the alveoli.

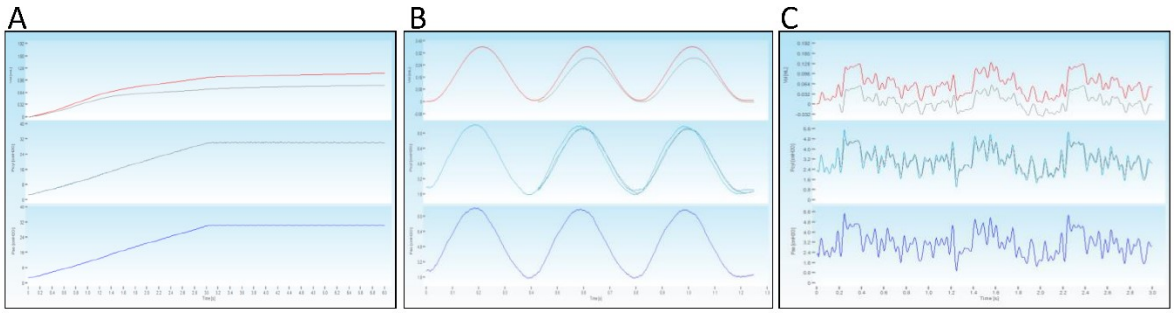

Figure 6: Deep inflation, single and broadband forced oscillation manoeuvres performed for lung function measurements. A) Deep inflation, B) single frequency and C) broadband forced oscillation manoeuvres with constant measurement of volume (upper panel; red line: volume displaced by the piston of the ventilator; grey line: volume delivered to the lung), cylinder pressure (middle panel; green line) and airway opening pressure (lower panel; blue line).

Pressure-volume-loops, keeping the pressure constant (Figure 7A,B), were performed to obtain the quasi-static mechanical properties of the lung. The Salazar-Knowles-equation was fit to the expiratory part of the PV-loop (red line, Figure 7A) and the quasi-static compliance (Cst) of the respiratory system was calculated. Further, the parameter A, an estimate of inspiratory capacity, the parameter K, a shape parameter indicating the curvature of the upper portion of the expiratory branch, also known as elasticity index (116), and the area enclosed by the pressure-volume-loop, indicating the amount of airspace closure before the loop manoeuvre, were calculated.

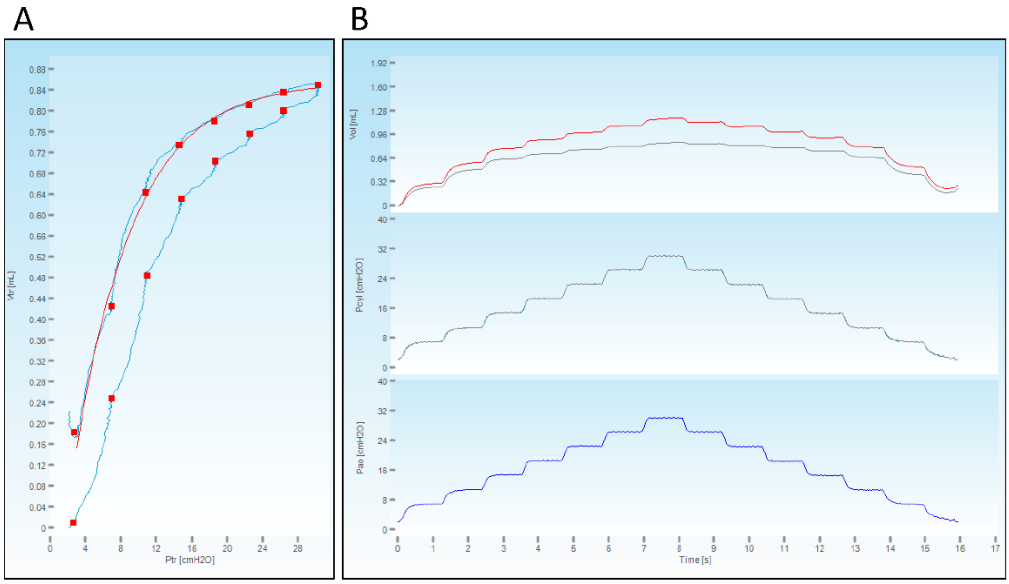

Figure 7: Pressure-volume loop (PV-loop) performed during lung function measurement. A) The PV-loop manoeuvre plotted as pressure (x-axis) versus volume (y-axis). B) The PV-loop manoeuvre over time measuring volume (upper panel; red line: volume displaced by the piston of the ventilator; grey line: volume delivered to the lung), cylinder pressure (middle panel; green line) and airway opening pressure (lower panel; blue line).

2.1.3. Assessment of airway hyperresponsiveness

Airway hyperresponsiveness was measured as a response to increasing concentrations of methacholine (0, 1, 3, 10, 30 and 100 mg/ml, Sigma Aldrich). Different doses of methacholine were nebulized using the Aeroneb adapter of the flexiVent directly before lung function measurements. At one concentration 12 single frequency and broadband forced oscillation measurements were performed over a three-minute period following the methacholine dose. Before each set of repeated measurements, two deep inflation manoeuvres were performed to re-open closed airspace areas and normalise lung volume.

2.1.4. Bronchoalveolar lavage

To lavage the bronchial and alveolar compartment of the lung, one mL of sterile PBS supplemented with 2 mM EDTA and protease inhibitors (Sigma) was injected to the lung via a tracheal incision with a steady flow and carefully retrieved again. The obtained bronchoalveolar lavage (BAL) was kept on ice until further use.

The BAL was centrifuged for 5 min at 500 g at 4°C. The supernatant, further on referred to as bronchoalveolar lavage fluid (BALF), was collected and stored

at -80°C until further use. The cell pellet was resuspended in 500 µl of 1% BSA in PBS and live cells were counted. 25,000 cells were used for cytospins, the rest of the cells were fixed in 1% PFA in PBS for 20 min, washed with MACS buffer and stored at 4°C for further staining and flow cytometric analysis.

2.1.5. Organ collection

Following lung function measurements, the thorax was opened and mice were exsanguinated by collecting the maximum amount of blood from the right ventricle. Blood was collected in tubes supplemented with 30µl of 3.6% sodium citrate for the collection of plasma. In the next step, the lung was lavaged as described in the previous section. Following lavage, an incision was made into the left atrium and the lung was flushed with PBS through the right ventricle until it obtained a white colour. A suture was inserted below the right lung lobes and the lobes were tied off. The middle right lobe was collected in medium and stored on ice to further process for single cell lung homogenate preparation and flow cytometric analysis, the other lobes of the right lung were shock frozen in liquid nitrogen and stored at -80°C until further use.

The left lung was inflated with formalin, to obtain the physiological structure during processing, removed from the thorax, separated from the heart and stored in formalin for fixation for 24 hours, before embedding in paraffin.

2.1.6. Isolation of mouse ASMC

Airway smooth muscle cells (ASMC) were isolated as described in (117): The trachea of eight week old Fra2 TG or WT mice was isolated, cleared from surrounding adipose and connective tissue and cut into two to three mm^2 pieces. The tissue pieces were put into 6-well culture plates and kept in DMEM-F12 culture medium supplemented with 10% FCS, 1% glutamine and antibiotics/antimycotics (ThermoFisher Scientific) until outgrowth of smooth muscle cells (approximately two weeks). Cells and tissue pieces were detached using trypsin and put through a 100 µm cell strainer to remove tissue pieces. The quality of ASMC isolation and purity was confirmed by IF staining for smooth muscle cells, fibroblast and epithelial cell markers (117).

2.1.7. Single cell lung tissue homogenates

After perfusion, a medium-sized lobe of the right lung was collected in 1 ml of RPMI medium supplemented with 10% FCS, 2 mM L-Glutamin and 1% penicillin/streptomycin (RPMI complete). The tubes with medium were weighed before and after lung collection to calculate lung weight used for analysis. The lung lobe was cut into small pieces approximately 1 mm^3 in size using two scalpels. Obtained tissue pieces were transferred into a 1.5 ml tube. The dish used for cutting was flushed twice with 500 µl RPMI complete medium and medium was transferred into the same tube. The lung tissue was digested with 0.7 mg/ml collagenase and 30 µg/ml DNase in RPMI complete medium at 37°C for 40 min while shaking.

Following digestions, tubes were transferred on ice, lung fragments were resuspended and screened through a 100 µm cell strainer using the plug of a 5 ml syringe. The empty tube and cell strainer were washed with three to five ml of RPMI complete medium and cells were centrifuged at 4°C at 300 g. The supernatant was discarded, and the pellet was resuspended in 1 ml 1x ammonium chloride erythrolysis buffer, incubated on a roller for five minutes at room temperature and washed with 25 ml of RPMI complete medium. After centrifugation at 300 g for 10 min at 4°C, the pellet was resuspended in 1 ml medium and cell number was counted.

Cells were fixed using 2 ml of 1% PFA, incubated on ice for 20 min, centrifuged as described before and resuspended in 500 µl of MACS buffer. The fixed cells were stored at 4°C until staining and flow cytometric analysis.

2.2. Flow cytometry

Flow cyometric analysis of inflammatory cells was performed in cooperation with the translational platform of the LBI Lung Vascular Research with the help of Dr. Leigh Marsh and Eva Grasmann. Approximately 200.000 cells of the BAL or of single cell lung homogenates were used for staining. To block Fc-receptors, cells were pre-incubated with CD16/CD32 (Clone 93, eBioscience/Thermo Fisher Scientific) in a dilution of 1:100, followed by a 20 minute incubation period at 4°C with the corresponding antibody panel for staining. Antibodies used to analyse lymphoid and

myeloid cell populations are shown in table 1. After incubation, cells were washed three times with MACS buffer and analysed on a LSRII flow cytometer (BD Biosciences). Cell singlets were initially gated on CD45 positivity and further defined as follows: CD11b+, CD11c−, Gr-1+ for neutrophils; CD11b low, CD11c+, Siglec-F+ for macrophages; CD11b+, CD11c+,MHC-II high for dendritic cells; CD11b+, CD11c-, Siglec F+ for eosinophils; CD3+, CD4+ for T helper cells; CD3+, CD8+ for cytotoxic T cells; and CD19+ for B-cells.

Table 1: Antibodies used for flow cytometry analysis of single cell lung homogenates and bronchoalveolar lavage of Fra2 TG and WT mice.

Antigen	Label	Company	Clone	Isotype	Dilution Factor
CD3	FITC	eBioscience	145-2C11	Hamster IgG	1:20
CD4	APC	Biolegend	GK1.5	Rat IgG2b, κ	1:100
CD8	PE	Biolegend	53-6.7	Rat IgG2a, κ	1:200
CD11b	V500	BD Bioscience	M1/70	Rat IgG2b, κ	1:50
CD11c	ef450	eBioscience	N418	Hamster IgG	1:50
CD19	AF700	Biolegend	6D5	Rat IgG2a, κ	1:100
CD45	PerCP-Cy5.5	eBioscience	30-F11	Rat IgG2b, κ	1:200
CD45	FITC	Biolegend	30-F11	Rat IgG2b, κ	1:200
Gr-1	PE-Cy7	Biolegend	RB6-8C5	Rat IgG2b, κ	1:800
MHC-II	APC-Cy7	Biolegend	M5/114.15.2	Rat IgG2b, κ	1:400
Siglec F	PE	BD Bioscience	E50-2440	Rat IgG2a, κ	1:20

2.3. Histological analysis

For histological analysis, formalin-fixed paraffin embedded tissue slices with a thickness of 2.5 µm were used. The paraffin was removed by overnight incubation at 60°C followed by two washes in Xylol, 10 min each. Tissue slices were rehydrated by an ethanol-gradient starting from 100%, to 90%, 70% and 50% ethanol. Slides were washed in water prior to subsequent staining procedures.

If not otherwise indicated, slides were dehydrated following different staining procedures using the reverse ethanol gradient as described for rehydration and mounted with xylol based mounting medium. Images were taken using an Olympus VS120 slide scanning microscope at 40x magnification.

2.3.1. Haematoxylin and Eosin staining

Rehydrated tissue slides were placed in Mayer's haematoxylin solution (Gatt-Koller) for two minutes and rinsed in running warm tab water for approximately three to five minutes. Tissue was counterstained for one minute in eosin final staining solution (Gatt-Koller) and washed in distilled water for five minutes, dehydrated and mounted as described in the previous section.

2.3.1. Masson's trichrome staining

Masson's trichrome staining was used to visualise collagen fibres in blue, nuclei in black and other tissue (such as muscle or cell cytoplasm) in pink/red. Slides were placed in Bouin's solution (Gatt-Koller) at 60°C for one hour and rinsed in running tap water until no colour was dissolving any more. Nuclei were stained in Weigert's iron haematoxylin solution (Gatt-Koller) for ten minutes and blackened under hot running tap water for approximately ten minutes to stain nuclei. Tissue was counterstained in Biebrich-scarlet-acid fuchsin solution for 10 to 25 minutes. Staining time was determined by microscopic control of staining intensity. Following a washing step in distilled water, tissue staining was differentiated in phosphomolybdic-phosphotungstic acid solution until collagen fibres lost all staining (approximately 10 to 15 minutes). Slides were directly transferred to aniline blue solution (2.5% aniline blue w/v in 2% acetic acid solution) for 10 to 20 minutes, until collagen fibres were stained blue. Slides were shortly differentiated (approximately 30 seconds) in 1% acetic acid solution, washed in distilled water and directly dehydrated and mounted. Staining and differentiation efficiency was controlled under the microscope at every step and incubation times were accordingly adapted to achieve optimal staining quality.

2.3.2. Sirius red staining

For the morphological assessment of collagen deposition in the lungs, collagen was visualised using picrosirius red staining. Slides were treated with freshly prepared 0.2% phosphomyolybdic acid for 4 minutes, stained with Sirius red solution for 30 to 35 min and washed for 3 minutes in 0.5% acetic acid before dehydration and mounting.

2.3.3. Periodic acid-Schiff staining

Mucus production in the airways was investigated by periodic acid-Schiff staining for glycogen and mucin. For that, rehydrated tissue slides were oxidized in 0.5% periodic acid solution (Gatt-Koller) for five minutes, rinsed in distilled water for one minute and incubated in Schiff's reagent (Merck) for 15 minutes. Slides were washed in lukewarm tap water for five minutes, counterstained for 45 seconds in Mayer's haematoxylin solution and rinsed with warm tap water for five minutes before dehydration and mounting.

2.4. Immunohistochemistry and immunofluorescence stainings

2.4.1. Immunohistochemical staining

Immunohistochemical and immunofluorescence staining was performed on deparaffinised and rehydrated formalin-fixed, paraffin embedded human and mouse lung tissue sections with 2.5 µm thickness. Heat-induced antigen retrieval was done using Citrate (pH6) or Tris-EDTA (pH9) buffer (both DAKO). The optimal antigen retrieval was tested together with the best dilutions for each antibody on trial sections. Slides were incubated in pre-heated antigen retrieval buffer in a 95°C water bath for 20 min. After cooling of the antigen retrieval buffer to room temperature, slides were removed and washed in PBS. Endogenous peroxidase activity in the tissue was blocked by incubating the slides in 3% H_2O_2 in methanol. After washing twice in distilled water and twice in PBS, a hydrophobic barrier was drawn around the tissue sections using DAKO pen to reduce volumes needed for the following incubation steps. Unspecific binding sites on the tissue were blocked for 60 min at room temperature using 3% BSA in PBS, followed by 20 min serumblock using 2.5% normal horse serum (ImmPress Kit, Vector Laboratories). Primary antibodies were diluted in 3% BSA in PBS and the slides were incubated overnight at 4°C. Antibody dilutions used for immunohistochemical stainings are listed in table 2. The next day, slides were washed with PBS for approximately one to two hours exchanging the buffer every 15 to 20 minutes and incubated with secondary antibody conjugated to peroxidase (ImmPRESS reagent peroxidase) for 30 min at room temperature. Following secondary antibody incubation, slides were washed, and staining was developed using the NovaRed substrate as described in

the manufacturer's recommendations (Vector Laboratories). The colour reaction was stopped in distilled water and nuclear counterstain was performed for 45 s in haematoxylin. Slides were blackened under running warm tap water, dehydrated and mounted as described in the previous section. Stained slides were scanned using an Olympus VS120 slide scanning microscope (Olympus, Germany).

2.4.2. Immunofluorescence staining

Immunofluorescence staining was done following the same protocol with omission of the endogenous peroxidase block. Primary antibodies used for immunofluorescence stainings are listed in table 2. Following overnight incubation with the primary antibody and washing, the slides were incubated with Alexa Fluor (AF)488, AF555 or AF647-labelled secondary antibodies (ThermoFisher Scientific) for one hour at room temperature. Following a short wash in PBS the slides were mounted with aqueous DAPI containing mounting medium (Vectashield, Vector Laboratories) and the cover glass was sealed with transparent nail polish. Fluorescence images were taken with the Nikon A1R Ultra-Fast Spectral Scanning Confocal Microscope with a CFI Plan Apochromat Lambda 60x/1.4 oil immersion objective.

Table 2: Antibodies and dilutions used for immunohistochemistry and immunofluorescence staining of mouse lung tissue.

Antigen	*application*	*Company*	*catalogue number*	*dilution*
aSMA	IHC	Sigma Aldrich	A2547	1:3000
VWF	IHC	DAKO/Agilent	A0082	1:900
CD45	IHC	Abcam	ab10558	1:250
pSTAT6	IHC	Cell Signaling	#9361S	1:100
MUC5AC	IF	Abcam	ab212636	1:100
CLCA1	IF	Abcam	ab180851	1:1000

2.5. Morphological assessment of lung remodelling

2.5.1. Quantification of vascular muscularisation

Muscularisation of pulmonary vessels ranging from 10 to 250 µm in size was quantified using lung slides stained with the endothelial cell marker von Willebrand

factor (vWF) and the smooth muscle cell marker α-smooth muscle actin (α-SMA; Figure 8A) as previously described (118). Muscularisation was quantified using the visiopharm image analysis software (VIS version 5.2.). First, identification of vessels was performed automatically using vWF staining to identify circular structures and vessels were marked as regions of interest (ROI; Figure 8B). Vessel ROIs were controlled manually and incomplete vessels were removed. In a second step, automated colour recognition was used to identify endothelial cell and smooth muscle cell areas (Figure 8C). The length of α-SMA staining relative to the vessel circumference was calculated. Vessels were categorized as non-muscularised, partially muscularised and fully muscularised depending on their ration of muscularisation.

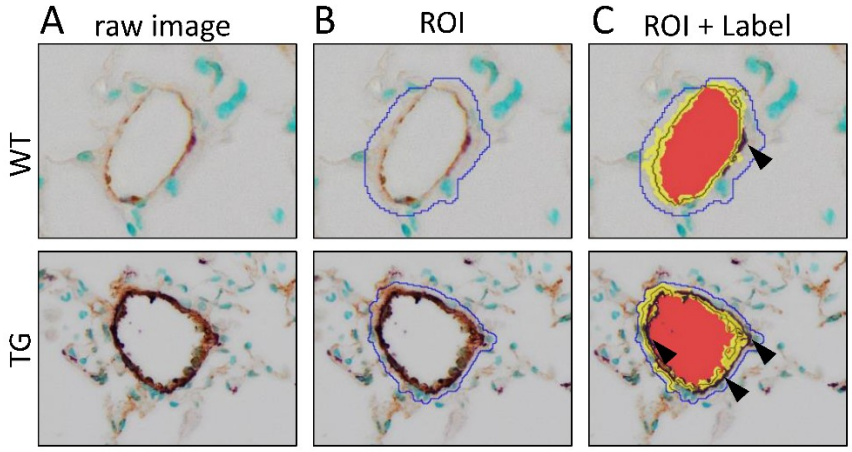

Figure 8: Quantification of vascular muscularisation in Fra2 WT and TG mice. A) Lung slides were stained with von Willebrand-factor (light brown) and α-smooth muscle actin (purple) and muscularisation was quantified using automated colour recognition with the visiopharm integrated software. B) Vessels were marked as regions of interest (ROI). C) Endothelial (yellow) and smooth muscle cell (dark purple; arrowheads) staining was automatically labelled and analysed. The vessel lumen is shown in red.

2.5.2. Quantification of parenchymal collagen deposition

Due to less background and counterstaining, the sensitivity of collagen quantification using Sirius red stained lung sections is increased compared to using Masson's trichrome staining. Therefore, parenchymal collagen deposition was measured on whole lung sections stained with Sirius red. To avoid bias due to different cutting depths within the tissue blocks and the concomitant variation of vessel numbers, all bronchi and vasculature >80 µm and their surrounding collagen

were excluded from the analysis. Furthermore, the pleura was excluded from the analysed Region of interest.

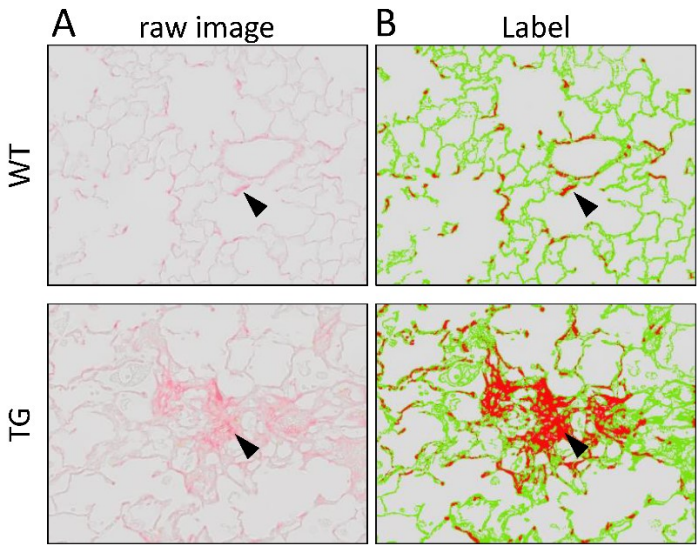

Figure 9. Quantification of parenchymal collagen deposition in the lungs of Fra2 WT and TG mice. A) Raw image of Sirius red stained lung sections. B) Analysed image after automated colour recognition. Green label: tissue; red label: collagen. Arrows highlight Areas of collagen deposition.

2.5.3. Quantification of airway remodelling

Quantification of remodelling was performed as described in (117): Goblet cells and mucus volume were quantified on automatically selected, random regions of the 40x scanned sections stained with PAS, using the NewCast software (Visiopharm, Hoersholm, Denmark). Goblet and epithelial cells intersecting the airway basement membrane (Figure 10A) were counted and the percentage of goblet cells per mm basement membrane was calculated. Mucus volume in the airways determined by point counts was compared to the surface area of the airway basement membrane as determined by line probe intersections (119, 120).

Peribronchial collagen deposition and airway smooth muscle thickness was analysed on Sirius red or α-SMA stained sections, respectively. For each animal 13 ± 7.8 bronchi, between 50 and 300 µm in size were analysed per slide using the Visiopharm image analysis software. For both protocols, bronchi were outlined to define regions of interest, and collagen or smooth muscle staining was marked by automated colour recognition (Figure 10B, C). Stained areas were skeletonized and

the width of peribronchial collagen or the bronchial smooth muscle layer was calculated as follows: $Width = \frac{Area\ of\ staining}{\frac{interface\ length}{2}}$

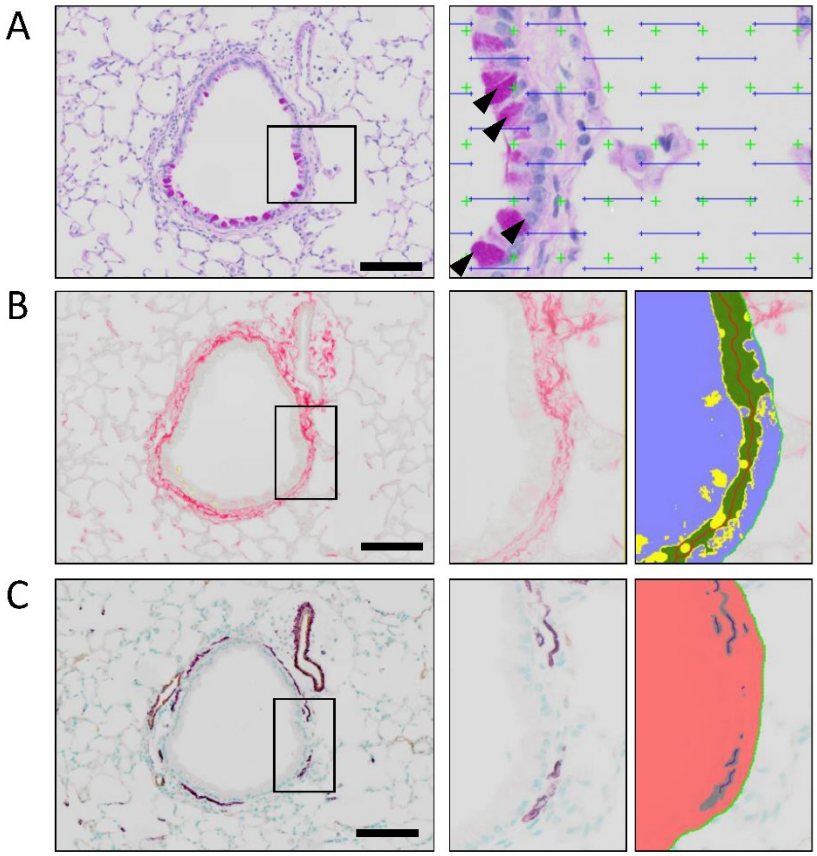

Figure 10: Quantification of goblet cells, peribronchial collagen and airway smooth muscle thickness. A) Goblet cells (purple; black arrowheads) and epithelial cells (no PAS staining) intersecting the airways were counted. B, C) Representative images of automated colour recognition and image analysis to determine peribronchial collagen (B) and airway smooth muscle thickness (C). Image adapted from (117).

2.6. Cell culture

2.6.1. Culturing of cells

Mouse airway smooth muscle cells (ASMC) were grown in DMEM-F12 medium (Gibco) supplemented with 10% FCS, 1% glutamine and 0.2% penicillin/streptomycin in an 37°C incubator with 5% CO_2. Cells were detached with trypsin (Gibco) before reaching confluency. Trypsin was neutralised with full medium and the cell number was determined by counting using a Neubauer chamber.

2.6.2. Cell proliferation

For the measurement of proliferation, 5000 ASMC per well were seeded in a 96-well plate. On the second day, the medium was changed to basal medium (DMEM-F12 supplemented with 0.2% penicillin/streptomycin, without FCS or L-Glutamine) and cells were starved overnight. The following day, cells were trested ^{3}H-labelled thymidine (1 µCi/ml, BIOTREND Chemikalien, Germany) diluted in basal medium. Cell proliferation was measured after 24 hours as follows: Cells were harvested onto a 96-well filter plate. After letting the filter plate dry, 25 µl Beta Plate scintillation cocktail (Perkin Elmer, Waltham, MA) per well were added and radioactivity was counted on a Microbeta Trilux (PerkinElmer).

2.7. RNA isolation and real-time PCR

Total RNA was isolated from lung homogenate samples or cells using a peqGOLD Total RNA Kit (Peqlab, Erlangen, Germany) and reverse transcribed using the iScript™ cDNA Synthesis kit (Bio-Rad Laboratories, Hercules, CA, USA). qRT-PCR reaction was set up by applying the QuantiFast® SYBR® Green PCR kit (Qiagen, Hilden, Germany) and run on LightCycler® 480 System (Roche Applied Science, Wien, Austria). The cycling conditions were as follows: 5 minutes at 95°C followed by 40 cycles of 5 seconds at 95°C, 5 seconds at 60°C, and 10 seconds at 72°C. Due to the nonselective double-strand DNA binding of the SYBR® Green I dye, melting curve analysis and gel electrophoresis were performed to confirm the specific amplification of the expected PCR products. Primers and their respective sequences are listed in table 3. Hydroxymethylbilane synthase (HMBS/PBGD) and beta-2-microglobulin (B2M) were used as the reference genes. The difference in threshold cycle (Ct) values was calculated as follows: ΔCt = meanCt reference genes – Ct target gene. ΔCt values of WT and TG mice following treatment were normalised to the mean expression of untreated WT control mice (ΔΔCt): ΔΔCt = ΔCt – mean ΔCt of all WT mice.

Table 3: Sequences of primers used for real-time PCR on mouse lung homogenates.

Gene	*Forward (5'-3')*	*Reverse (5'-3')*
Il1a	CGAAGACTACAGTTCTGCCATT	GACGTTTCAGAGGTTCTCAGAG

Il1b	GCCACCTTTTGACAGTGATGAG	GACAGCCCAGGTCAAAGGTT
Col1a1	AATGGCACGGCTGTGTGCGA	AACGGGTCCCCTTGGGCCTT
Acta2	CAGCCAGTCGCTGTCAGGAACC	CCAGCGAAGCCGGCCTTACA
Il4	ATGGATGTGCCAAACGTCCT	TGCAGCTCCATGAGAACACT
Il13	GCCAAGATCTGTGTCTCTCCC	CCAGGTCCACACTCCATACC
I17	AGGACGCGCAAACATGAGTC	GGACACGCTGAGCTTTGAGG
Il12a (p35)	GACCCTGTGCCTTGGTAGCATC	TGCTTCTCCCACAGGAGGTTTC
Ifng	CAGCAACAGCAAGGCGAAAAAGG	TTTCCGCTTCCTGAGGCTGGAT
Hmbs	GCCAGAGAAAAGTGCCGTGGG	TCCGGAGGCGGGTGTTGAGG
β2m	CGGCCTGTATGCTATCCAGAAAACC	TGTGAGGCGGGTGGAACTGTG
Mmp12	TGATGCAGCTGTCTTTGACC	GTGGAAATCAGCTTGGGGTA
Tnfa	CATCTTCTCAAAATTCGAGTGACAA	TGGGAGTAGACAAGGTACAACCC
Il6	ACAACCACGGCCTTCCCTACTT	CACGATTTCCCAGAGAACATGTG
Il5	AAGCAATGAGACGATGAGGCT	CCCCACGGACAGTTTGATTCT
Tbx21	CAACAACCCCTTTGCCAAAG	TCCCCCAAGCAGTTGACAGT
Gata3	AGAACCGGCCCCTTATCAA	AGTTCGCGCAGGATGTCC
Il10	AGGCGCTGTCATCGATTTCT	ATGGCCTTGTAGACACCTTGG
Tgfb	GTGGACCGCAACAACGCCATCT	GCAATGGGGGTTCGGGCACT

2.8. Protein isolation and western blotting

Proteins were isolated from lung homogenate samples using RIPA buffer (Sigma), separated by SDS-PAGE (8-12% polyacrylamide, depending on the size of the target protein) at 120 V for 1.5 hours, and transferred to PVDF membranes (GE Healthcare, Vienna, Austria) at 320 mA, 1.5 hours, 4°C. Following incubation with primary and secondary antibodies (table 4) membranes were incubated with ECL prime developing solution (GE Healthcare) and signal detection was done using a ChemiDoc TM Touch Imaging System (Bio-Rad).

Table 4: Antibodies and their respective dilutions used for western blotting.

Antigen	***Company***	***catalogue number***	***dilution***
Collagen I	Southern Biotech	1310-01	1:1000
aSMA	Everest Biotech	EB06450	1:1000
a-Tubulin	Cell Signaling	#2125S	1:5000
STAT6	Santa cruz	#621	1:1000
pSTAT6	Cell Signaling	#9361S	1:1000
Fra2	Atlas Antibodies	HPA004817	1:1000

2.9. ELISA and multiplex assay

Protein levels of cytokines in BAL fluid and lung homogenates of mice were analysed using FlowCytomix Multiple Analyte Detection (for TNFα, IL-6, IL-1α, IL-1β, IFNγ, IL-17, IL-4, IL-5, IL-13, IL10; ThermoFisher Scientific) according to the manufacturer's instructions and measured on a LSRII Flow Cytometer (BD Bioscicens). Enzyme-linked immunosorbent assays (ELISA; ThermoFisher Scientific) were used to measure eotaxin levels and for determination of IL-13 in BALF, lung homogenate and plasma levels after administration of an IL-13 neutralising antibody to Fra2 TG mice. ELISAs were performed as described in the manual and measured using a SpectraMax Plus 384 spectrophotometer (ThermoFisher Scientific).

2.10. Micro array analysis

Micro array analysis was performed by the collaboration partner Dr. Jochen Wilhelm, at the Justus-Liebig-University in Gießen as described previously in detail (121). In short, RNA was isolated with the RNeasy Mini Kit (Peqlab, Erlangen, Germany) from lung tissue of Fra2 TG mice 16 weeks of age and WT littermate controls. Eight animals for each group were used. Using the Low-input QuickAmp Kit (Agilent Technology, Santa Clara, CA), 200 ng RNA were pre-amplified and labelled with Cy5 according to manufacturer's protocol. Hybridizations on Agilent 6x80K mouse microarrays were performed in Agilent hybridization chambers for 18 h at 42°C. Data analysis was performed with the limma package in R and intensity values were background-corrected and quantile normalized. Using moderated t-statistics, differential expression was estimated. Genes with a fold change >2 and a significance of $p<0.05$ were defined as regulated. A screening of gene names or corresponding aliases together with the search terms "asthma" and "airway disease" was conducted using PubMed or UniProt Knowledgebase to find associations of regulated with asthma.

2.11. *In silico* transcription factor binding site analysis

In silico investigation of putative AP-1 binding sites was done with the ConTra v3 web server (as described in (122)). Promoter regions 1000 base pairs upstream of the transcription start site were analysed using the mouse (*mus musculus*) genome as a reference sequence. The V$AP1_CM00199 positional weight matrix (TRANScription FACtor database) was selected for visualization with a core stringency of 0.90 and similarity stringency of 0.75. A graphical representation (sequence logo) of the positional weight matrix motif V$AP1_CM00199 is shown in Figure 11).

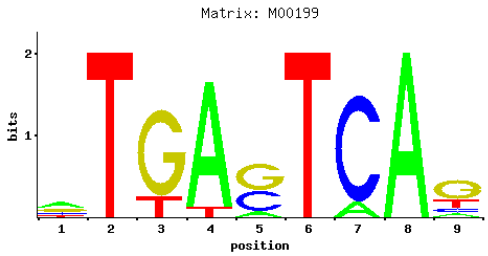

Figure 11: Sequence logo of the positional weight matrix motif V$AP1_CM00199 (TRANScription FACtor database) used for the *in silico* transcription factor binding site analysis.

2.12. Statistics

Statistical analysis was performed in R or Graphpad Prism 5 software (Graph Pad Software Inc., USA). Data are shown as single data points with lines indicating the mean or as scatterplots with a boxplot overlay showing median and interquartile range, if not indicated otherwise. Two groups with same variance, calculated using an F test to compare variances assuming normal distribution, were compared using unpaired, two-tailed Student's t-test. For two groups with different variance a non-parametric Mann-Whitney test was used. Comparison of more than two groups was done using One-way analysis of variance (ANOVA) with Bonferroni's *post hoc* test for the comparison of selected groups. Dose response curves were analysed using two-way ANOVA with Bonferroni's *post hoc* test to test for significance differences between WT and TG groups upon Methacholine treatment.

3. Results

3.1. Development of pulmonary remodelling in Fra2 TG mice

Mice with ectopic overexpression of Fra2 develop a phenotype resembling systemic sclerosis with fibrotic thickening of the skin (26, 43) and pulmonary fibrosis (42) without any second trigger necessary for disease induction. Fra2 TG mice spontaneously develop inflammation and fibrotic disease, making it a good model to study early phases of disease development and progression. To investigate these pathomechanisms, we conducted a detailed profiling of pulmonary histology, inflammation and function in Fra2 TG mice over a period of three months.

3.1.1. Parenchymal remodelling starts at approximately 16 weeks and increases with age in Fra2 TG mice

Histologic assessment of the lung (Figure 12) did not show any overt phenotype in eight-week-old Fra2 TG mice compared to the lungs of WT control mice. At 16 weeks of age, increased perivascular cell infiltrates (black arrowheads) and collagen deposition (white arrowheads) around the pulmonary vasculature as well as around the bronchi was observed. In mice older than 20 weeks of age, severe vascular and interstitial remodelling could be observed with cellular infiltrates and collagen deposition (white arrowheads, Figure 12) in the lung parenchyma and a concomitant loss of alveolar space. Further, vascular remodelling developed with an increased vessel wall thickness and collagen deposition within the vessel wall (grey arrowhead).

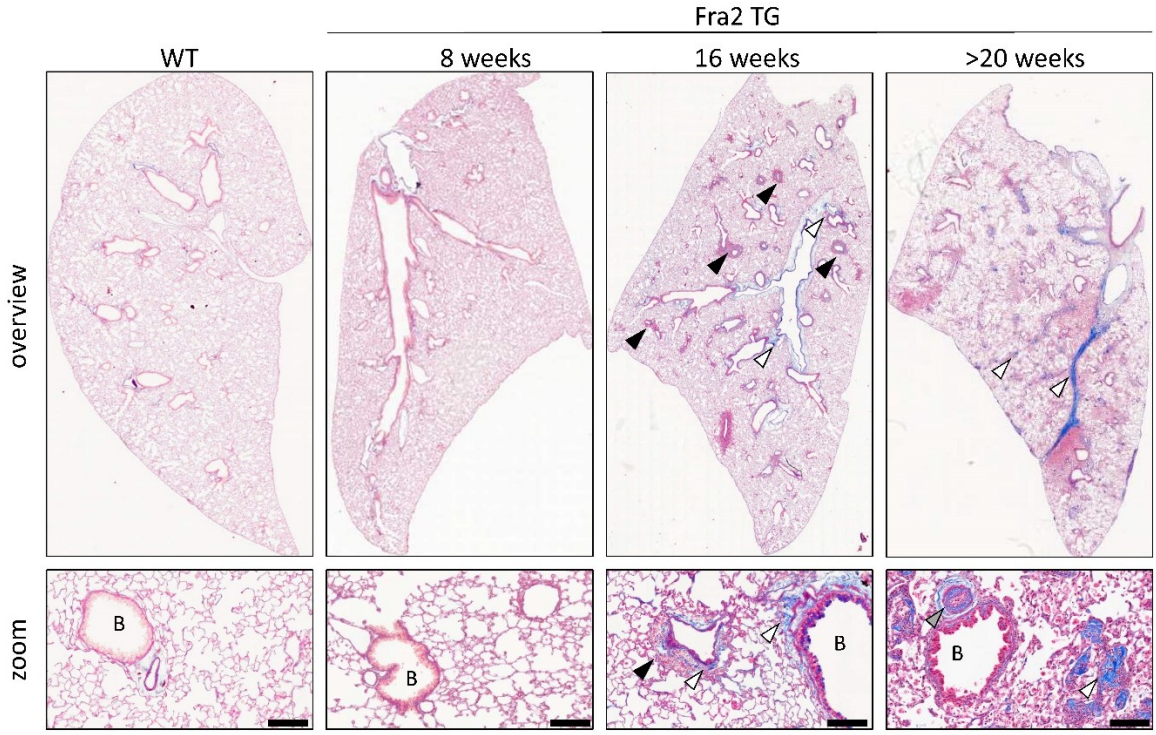

Figure 12: Pulmonary histology of Fra2 TG mice compared to WT littermates. Representative images of the whole left lung lobe of Fra2 TG mice at 8, 16 or >20 weeks of age and WT littermate control (16 weeks) stained with Masson's Trichrome (collagen in blue). B: bronchus; black arrowheads: perivascular cell infiltrates; white arrowheads: collagen deposition; grey arrowhead: collagen deposition in the vessel wall; scalebars: 100 µm.

To investigate whether the observed perivascular infiltrates and increased perivascular collagen in 16-week-old Fra2 TG mice (Figure 12) were accompanied by changes in the lung parenchyma, the amount of collagen fibres specifically in the lung parenchyma was analysed. Increased collagen deposition in the lung parenchyma of TG mice 16 weeks or older was quantified on Sirius red stained sections of the left lung using the using the Visiopharm image analysis software. Wild-type sex- and age-matched littermate controls were used as control group. Of note, due to inter-batch variability of staining intensity, WT mice at 16 or >20 weeks show different baseline collagen levels and collagen quantifications are not comparable. Therefore, two separate graphs for the different time-points are shown. At 16 weeks of age, Fra2 TG showed increased perivascular collagen (Figure 13A), without elevated levels of parenchymal collagen deposition (Figure 13B), whereas in 20-week-old (or older) Fra2 TG mice, the collagen deposition in the parenchyma was significantly augmented (Figure 13A, C).

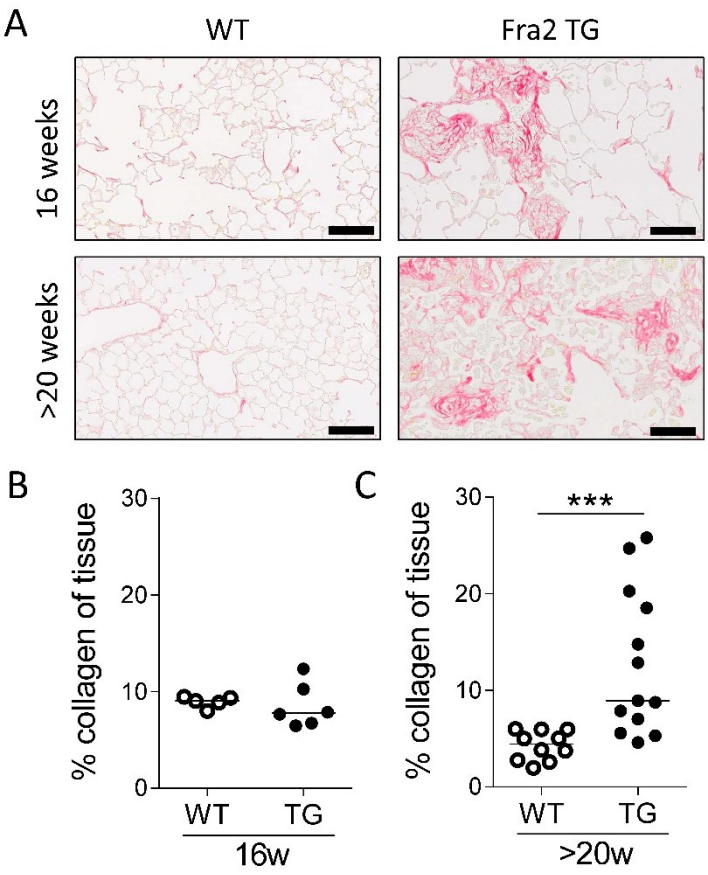

Figure 13: Increased collagen deposition in the lungs of Fra2 TG mice. A) Representative images of Sirius red stained lung sections of 16 and >20-week-old Fra2 TG mice and age- and sex-matched WT littermate control mice. Collagen fibres are stained in red. Scalebars: 100 µm. B, C) Quantification of collagen deposition in the lung of 16-week-old (B) and >20-week-old (C) Fra2 TG and WT mice. Each dot represents one animal. Significance of differences were determined using Mann Whitney test; ***p<0.001.

The gradual development of fibrosis in Fra2 TG mice was further assessed by expression analysis of collagen 1 (Col1a1) in the lung homogenates of Fra2 TG compared to WT mice (Figure 14). In 16-week-old Fra2 TG mice a slight but insignificant increase in collagen expression was observed, whereas in >20-week-old or older mice Col1a1 mRNA levels were elevated (Figure 14A), confirming the results of the parenchymal collagen quantification on Sirius red stained lung sections (Figure 13). mRNA levels of the smooth muscle cell and myofibroblast marker α-smooth muscle actin were unaltered (Figure 14B). Expressional changes of Col1a1 and Acta2 mRNA levels were confirmed on the protein level using western blot analysis (Figure 14C) and showed similar regulation: Col1 was slightly

increased at 16 weeks and strongly upregulated in older mice (>20 weeks; Figure 14C). α-Sma protein levels were unaltered in all time-points (Figure 14D).

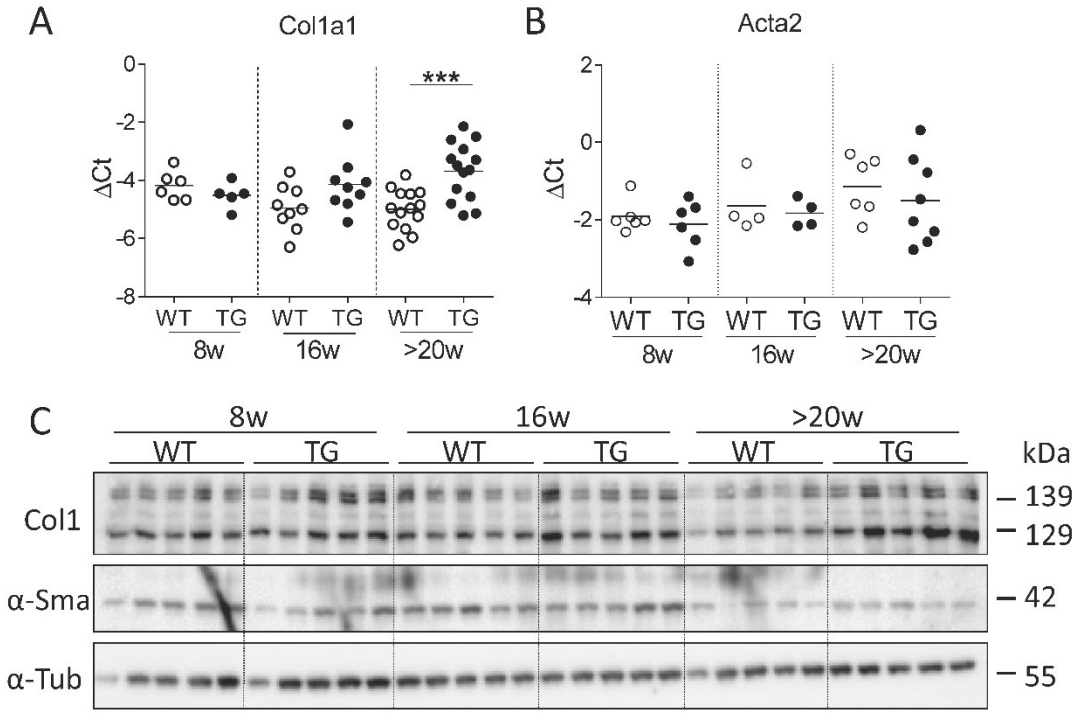

Figure 14: Elevated expression of Collagen I in lungs of Fra2 TG mice compared to WT littermate controls. A,B) mRNA expression levels of Col1a1 (A) and Acta2 (α-Sma) (B) in lung homogenates as assessed by qRT-PCR. C) Western blot analysis of Col1 and α-SMA protein levels in Fra2 TG and WT lung homogenates. α-tubulin (α-Tub) was used as loading control. Each dot represents one animal. Significance of differences were determined using unpaired t-test; **p<0.01, ***p<0.001.

This contrasts with immunohistochemical stainings against α-Sma in mouse lungs, where α-Sma positive cells outside the vessel walls were observed in 16-week-old and accumulated in >20-week-old Fra2 TG mice (Figure 15). At 16 weeks, α-Sma positive cells appeared in close proximity of inflammatory infiltrates around small parenchymal vessels and further spread throughout across remodelled lung areas in TG mice older than 20 weeks, indicating myofibroblast formation and accumulation in the lung parenchyma (Figure15). These results differ to those obtained by the expression level analysis in total lung homogenates. The observed unaltered mRNA and protein levels could be due to the concomitant increase of other cell types, such as infiltrating inflammatory cells, which evens out the increase of α-Sma expressing cells in total lung homogenates.

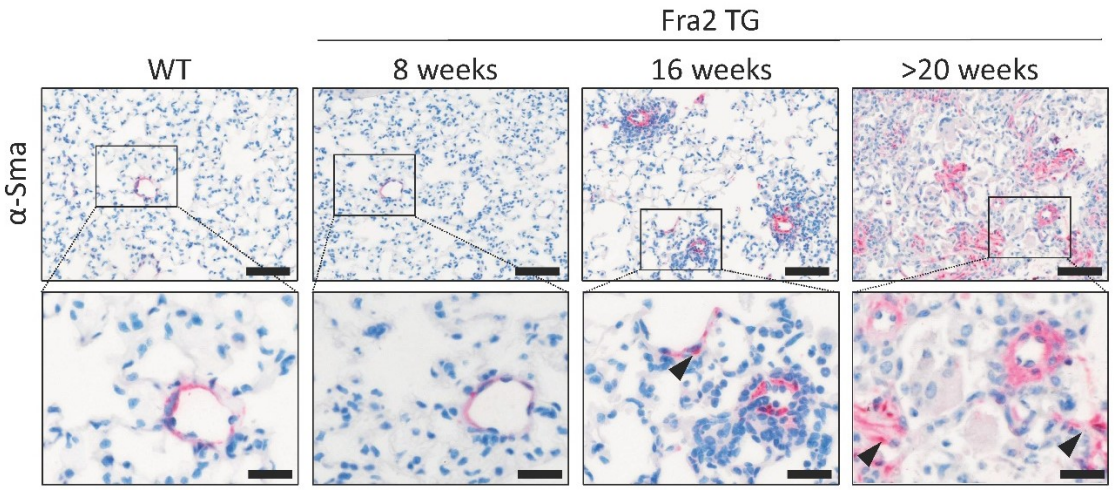

Figure 15: Fra2 TG mice have parenchymal α-Smooth muscle actin (α-Sma) immunoreactivity starting from 16 weeks of age. Representative overview and high magnification images of the lungs of Fra2 TG mice at 8, 16 or >20 weeks of age and WT littermate control (16 weeks) stained with antibodies against α-Sma. Black Arrowheads indicate non-vascular α-Sma-positive cells. Scalebars: 50 µm (upper panel), 20 µm (higher magnification of insets, lower panel).

3.1.2. Lung function is restricted in Fra2 TG mice

To assess whether increased collagen deposition in the lungs is reflected as a decrease in respiratory capacity, we measured lung function of 8-, 16- or over 20-week-old-mice using the flexiVent FX Module 1. The inspiratory capacity of mice older than 20 weeks was tendentially decreased, although no statistical difference was observed (Figure 16A). Following the same trend, the parameter A, an estimate of the inspiratory capacity as assessed by the Salazar-Knowles equation (116), was significantly lower in >20-week-old mice (Figure 16B), indicating a decreased lung volume in old mice with established pulmonary fibrosis. In line with this, the quasi-static compliance of the lung was decreased in older (>20 weeks) mice (Figure 16C) and the area within the pressure-volume loop was decreased (Figure 16D) indicating higher levels of airspace closure.

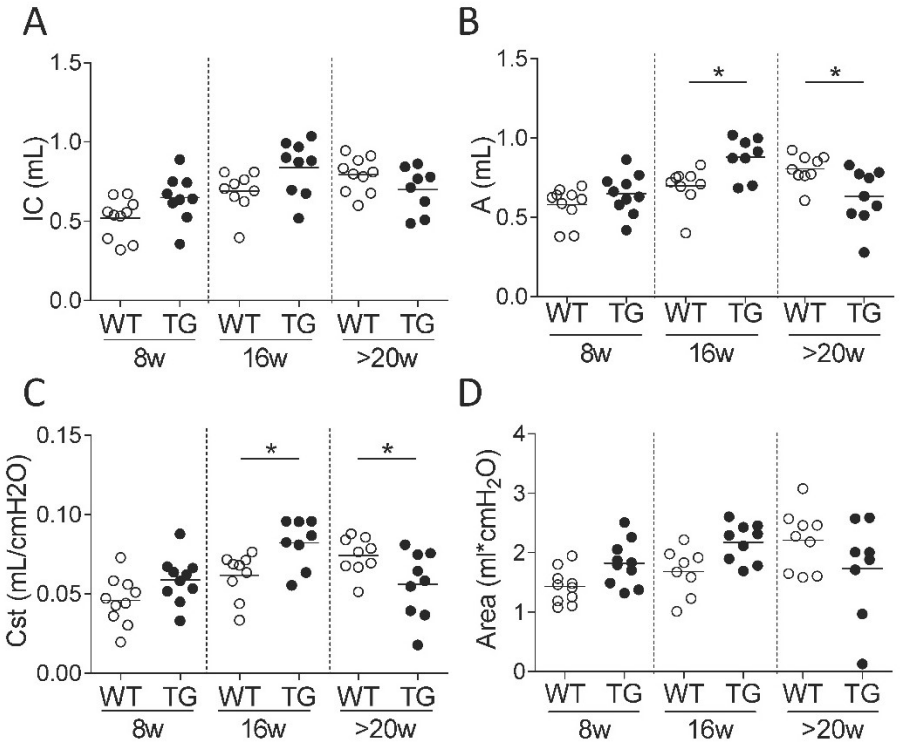

Figure 16: Decreased lung volume and quasi-static compliance of the lung in 20-week-old Fra2 TG mice. A) The inspiratory capacity (IC) in Fra2 TG and WT mice was assessed by deep inflation manoeuvres. Pressure-volume loops with constant pressure were used to assess B) the parameter A, C) the quasi static compliance (Cst) and D) the area within the pressure-volume loops (Area). Each dot represents the mean of three repeated measurements of one animal. Significance of differences were determined using unpaired t-test; *p<0.05.

Interestingly, at 16 weeks of age, inspiratory capacity/A and quasi-static compliance were increased, indicating a loss of elastic tissue and an emphysema-like phenotype. The same tendency was observed in 8-week-old Fra2 TG mice, but did not reach statistical significance (Figure 16B, C).

Using single frequency forced oscillation, mechanics the overall elastic properties of the respiratory system including lung, airways and chest wall were measured. In contrast to the parameters obtained by performing pressure-volume-loops, significant differences were only observed in Fra2 TG mice 20 weeks of age or older. These mice had increased elastic stiffness and constriction of the lungs as shown by a decreased compliance (Figure 17A), and increased elastance and resistance of the lungs (Figure 17B, C).

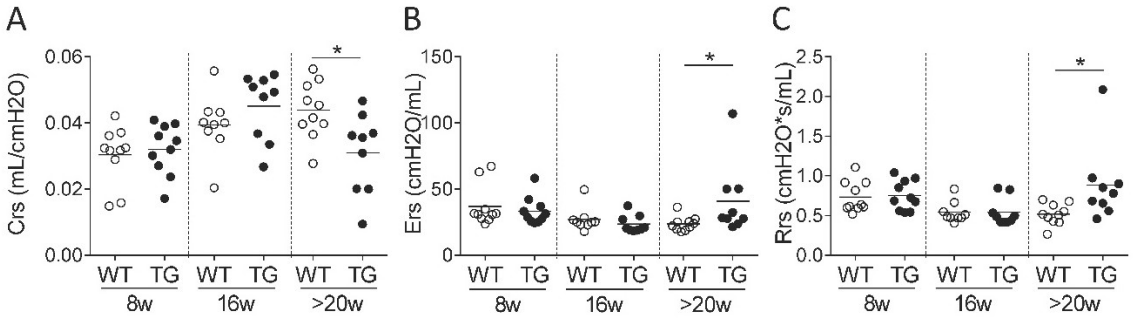

Figure 17: Decreased compliance and increased elastance and resistance of the respiratory system in 20-week-old Fra2 TG mice. Compliance (Crs; A), elastance (Ers; B) and resistance (Rrs; C) of the respiratory system were measured using the single frequency forced oscillation technique. Each dot represents the mean of three repeated measurements of one animal. Significance of differences were determined using unpaired Mann Whitney test; *p<0.05.

Further perturbations applying a wide range of frequencies (broadband forced oscillation) were used to calculate tissue and airway mechanics as previously described (115). Neither the resistance of the central/conducting airways (Newtonian resistance, Figure 18A), tissue resistance (tissue damping, Figure 18B) nor tissue elastance (Figure 18C) were significantly altered in Fra2 TG mice compared to age-matched WT littermate control mice. Nevertheless, a trend towards increased resistance of the airways as well as of the tissue was observed in older Fra2 TG mice (>20 weeks of age). In line, tissue elastance was slightly increased in old Fra2 TG mice (Figure 18A-C).

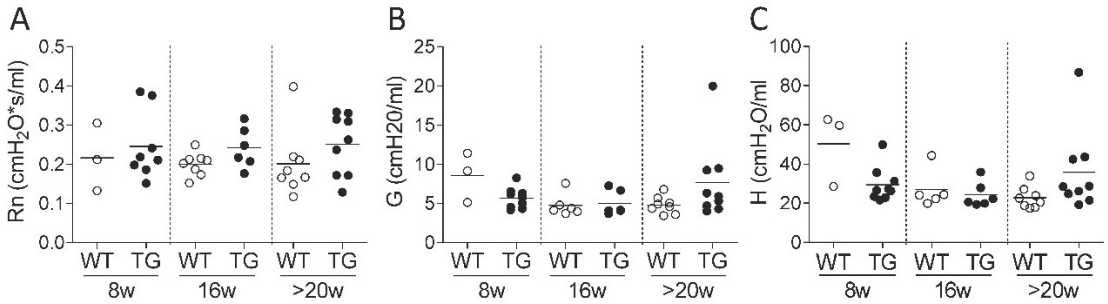

Figure 18: Airway and tissue mechanics of 8-, 16- and >20-week-old Fra2 TG compared to WT control mice. A) Newtonian resistance (Rn), B) tissue damping (G) and C) tissue elastance (H) were obtained using broadband frequency forced oscillation perturbations.

It was shown that in patients with SSc, Matrix metalloproteinase 12 (MMP-12) levels in serum and tissue (skin and lung) are increased and that serum levels correlate

with the severity of lung malfunction (123). Furthermore, MMP-12 gene polymorphisms may contribute to SSc susceptibility and lung involvement/interstitial lung disease in SSc (124). Interestingly, MMP-12 was highly upregulated in all investigated time-points in Fra2 TG mice (Figure 19), indicating pathomechanisms similar to human disease.

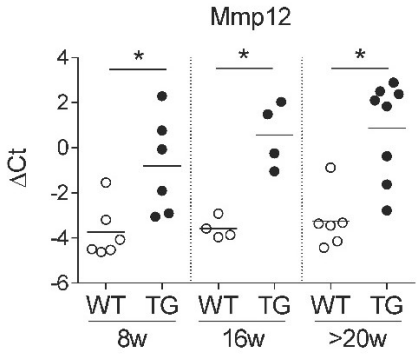

Figure 19: Fra2 TG mice have increased expression levels of Mmp12. mRNA levels of matrix metalloproteinase 12 (Mmp12) were measured in lung homogenates of Fra2 TG and WT littermate control mice. Significance of differences were determined using unpaired t-test; *p<0.05.

In conclusion, Fra2 TG mice do not show overt differences in lung function at eight weeks of age, but exhibit changes resembling emphysema at 16 weeks of age. In later stages of the disease (>20 weeks of age), increased ECM production and collagen deposition lead to restrictive lung function with decreased lung volume, pulmonary compliance and a concomitant increase of pulmonary elastance and resistance.

3.1.3. Vascular remodelling precedes parenchymal remodelling in Fra2 TG mice

Fra2 TG mice have an increased number of α-smooth muscle actin positive vessels in the parenchyma (16). To quantify the degree of neo-muscularisation of small vessels in the lungs of Fra2 TG mice, we performed immunohistochemical double staining with the endothelial cell marker von Willebrand factor (vWF, brown staining) and the smooth muscle cell marker α-smooth muscle actin (α-Sma, purple staining; Figure 20A). Automated vessel recognition was based on vWF staining and the percentage of muscularisation for each vessel was calculated. Vessels were classified as non-muscularised, partially muscularised or fully muscularised.

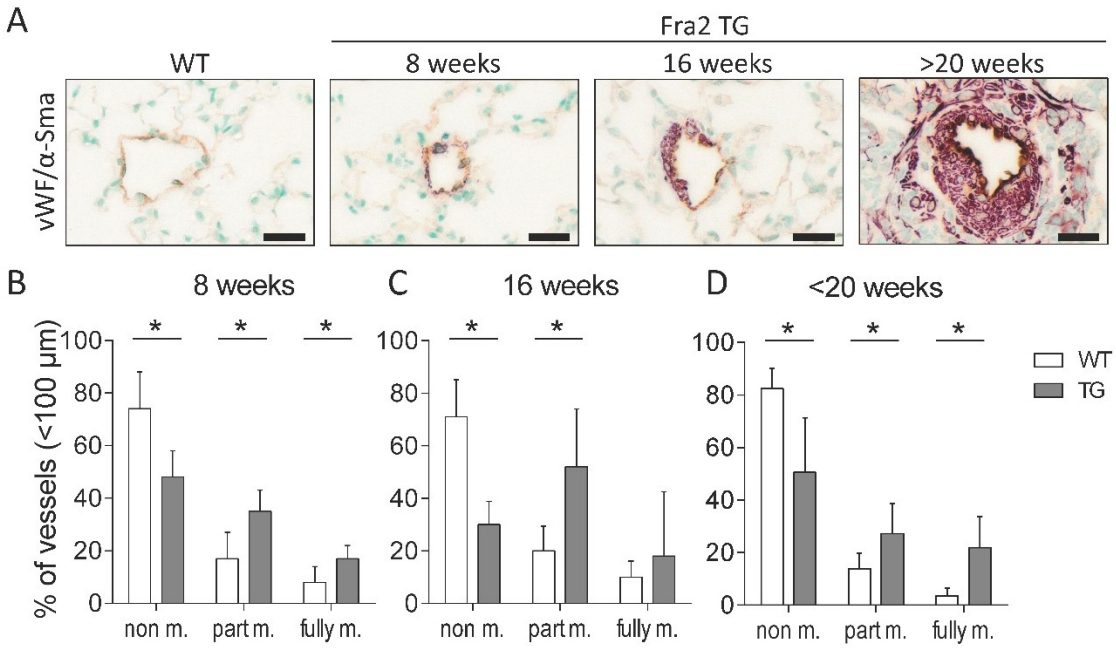

Figure 20: Fra2 TG mice have a higher percentage of fully muscularised small lung vessels. A) Lung sections of 8-, 16- or >20-week-old Fra2 TG and WT mice were stained with antibodies against the endothelial cell marker von Willebrand Factor (vWF; brown) and the smooth muscle cell marker α-Smooth muscle actin (α-SMA; purple). One representative staining of a 16-week-old WT mouse is shown. Scalebars: 20 µm. B-D) Quantification of (neo-)muscularisation of pulmonary vessels smaller than 100 µm for Fra2 TG (grey bars) and WT (white bars) control mice 8 (B), 16 (C) and >20 (D) weeks of age. Vessels were classified as non-muscularised (non m.), partially muscularized (part m) or fully muscularized (fully m.). Significance of differences were determined using unpaired t-test; *p<0.05.

Starting at 8 weeks of age, Fra2 TG mice showed increased muscularisation of normally not muscularised small pulmonary vessels (Figure 20A). The extent of vascular remodelling increased with age and led to severe remodelling and muscularisation of small vessels in Fra2 TG mice older than 20 weeks. Quantification of vascular muscularisation (of vessels with a diameter smaller than 100 µm) showed a significant decrease of the proportion of non-muscularised vessels, with a concomitant increase of partially and fully muscularised vessels. These changes were already apparent in eight-week-old mice (Figure 20B) and became more prominent in older mice (Figure 20C, D). These results are in line with previous reports showing increased right ventricular systolic pressure (RVSP) in eight-week-old Fra2 TG mice (16) and indicate that vascular remodelling precedes the onset of parenchymal fibrotic changes in Fra TG mice.

3.2. Inflammatory profiles of Fra2 TG mice in distinct stages of pulmonary remodelling

As described in Figure 12, the first apparent changes in the lungs of Fra2 TG mice are cellular infiltrates around bronchi and pulmonary vessels. Immunohistochemical staining with the inflammatory cell marker CD45 showed that these infiltrates predominantly consist of CD45+ inflammatory cells (Figure 21): In WT and in 8-week-old Fra2 TG mice, only single alveolar macrophages (back arrowheads) were CD45-positive, whereas in 16-week-old mice strong CD45-positivity of the perivascular cell infiltrates could be observed. In older mice (>20 weeks of age), inflammatory cell infiltrates were more pronounced and spread towards the lung parenchyma (Figures 21).

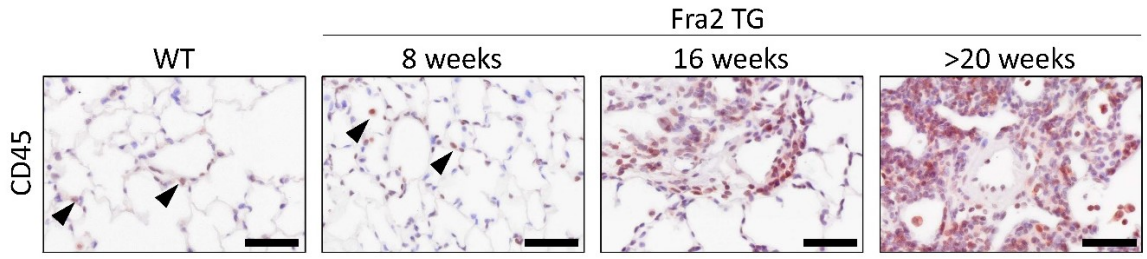

Figure 21: Inflammatory cell infiltrates around small vessels in Fra2 TG mice. Lung sections of 8-, 16- or >20-week-old Fra2 TG and WT mice were stained with an antibody directed against the inflammatory cell marker CD45 (brown). One representative staining of a 16-week-old WT mouse is shown. Arrowheads: alveolar macrophages. Scalebars: 50 µm.

3.2.1. Fra2 TG mice have increased expression of pro-inflammatory cytokines

Pulmonary fibrosis in connective tissue diseases such as SSc is strongly associated with increased activation of the immune system and elevated levels of pro-inflammatory and pro-fibrotic cytokines and mediators such as TGFβ, IL-1 or cytokines produced by Th2 cells (92). In SSc, both vascular and parenchymal remodelling correlated with increased cytokine levels. We thoroughly assessed the inflammatory profile of Fra2 TG mice throughout different phases of disease development. With this approach we aimed to delineate the role of different cytokines in distinct phases of pulmonary remodelling.

In a first step, expression levels of key pro-inflammatory and pro-fibrotic cytokines were measured in lung homogenates of Fra2 TG mice compared to age- and sex-matched WT control mice. When investigating pro-inflammatory cytokines of the innate immunity, we found that tumour necrosis factor α (Tnfα) levels were unaltered (Figure 22A), whereas interleukin 6 (IL-6) levels were increased in 16-week-old Fra2 TG mice (Figure 22B). Interestingly, mRNA levels of IL-1α were already elevated in young mice, 8 weeks of age (Figure 22C), prior to any histologically apparent inflammation in the lung. Expression levels of IL-1β, another potent pro-inflammatory mediator of the IL-1 family of cytokines, did not change (Figure 22D). In line with mRNA levels, Tnfα protein levels did not change in lung homogenates of Fra2 TG mice, whereas IL-6 levels were elevated in 16-week-old mice and tendentially increased in >20-week-old Fra2 TG mice (Figure 23A, B). In contrast to the mRNA levels, IL-1α protein levels were not altered in 8-week-old, but highly elevated in 16-week-old and older Fra2 TG mice compared to WT littermate control mice (Figure 23C). Due to technical difficulties, IL-1β protein levels were not obtained in lung homogenates but were measured in the BAL fluid. IL-1β protein levels were unaltered in Fra2 TG mice at all time-points (Figure 23D).

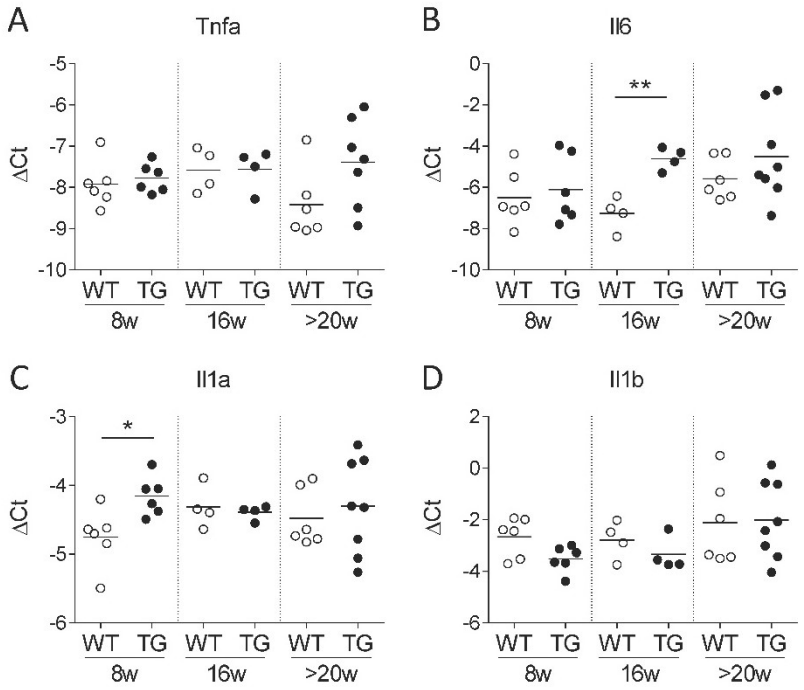

Figure 22: Fra2 TG mice have and early increase of IL-1α, followed by elevated IL-6 expression. mRNA levels of the pro-inflammatory cytokines A) tumor necrosis factor α (Tnfa), B) Interleukin 6 (Il6), C) Interleukin 1α (Il1a) and D) IL-1β (Il1b) were assessed by quantitative

real-time PCR in lung homogenates of 8-, 16- or >20-week-old Fra2 TG and WT mice. Significance of differences were determined using unpaired t-test; p<0.05, **p<0.01.

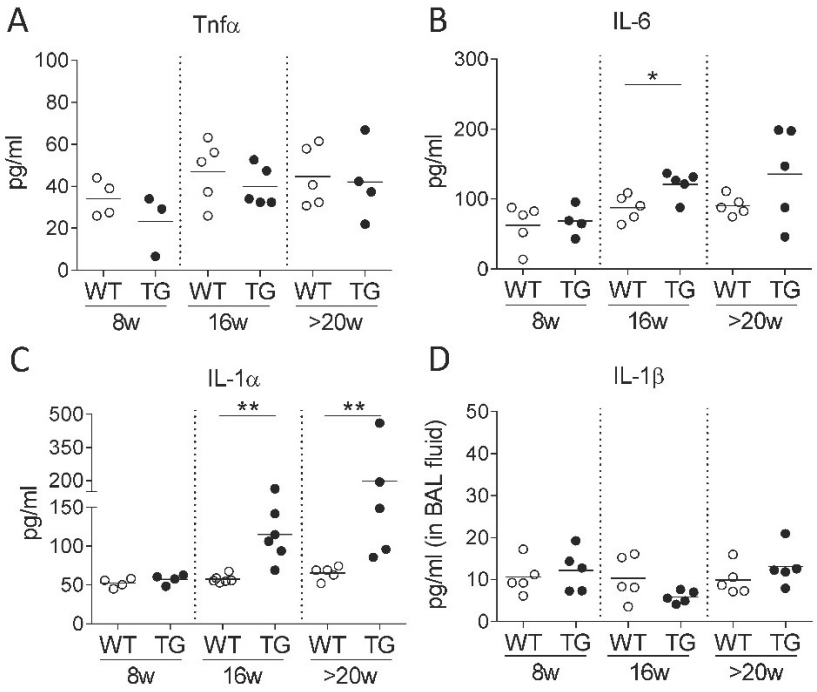

Figure 23: IL-6 and IL-1α protein levels are elevated in Fra2 TG mice. Protein levels of A) tumour necrosis factor α (Tnfα), B) Interleukin 6 (IL-6), C) Interleukin 1α (IL-1α) and D) IL-1β were assessed in lung homogenates (A-C) or bronchoalveolar (BAL) fluid (D) of 8-, 16- or >20-week-old Fra2 TG and WT mice. Significance of differences were determined using unpaired t-test (IL-6) or Mann Whitney test (IL-1α); p<0.05, **p<0.01.

3.2.2. Th2 cytokine production is increased in Fra2 TG mice

Pulmonary fibrosis is not only influenced by pro-inflammatory cytokines of the acute phase or innate immunity, but also by adaptive immune responses. We therefore investigated cytokine levels which are produced by activated T-helper cells (Th cells).

The expression levels of the classical Th1 cytokine interferon γ (Ifnγ) were unaltered in Fra2 TG mice in all time-points (Figure 24A). IL-12A, a cytokine produced by cells of the innate immunity and critically involved in the differentiation of naïve T-cells to Th1 cells, was also unchanged (Figure 24B).

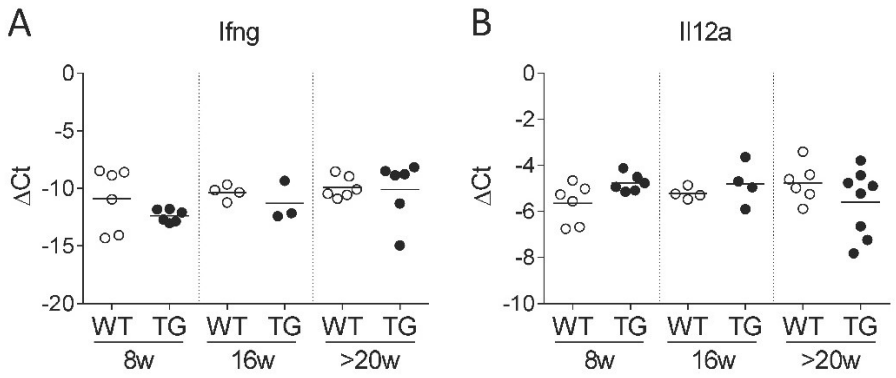

Figure 24: Expression levels of Th1 cytokine IFNγ and IL-12 are unaltered in Fra2 TG mice. mRNA levels of the Th1 cytokines A) interferon γ (Ifng) and B) Interleukin 12 (Il12a) were assessed by quantitative real-time PCR in lung homogenates of 8-, 16- or >20-week-old Fra2 TG and WT mice.

Corresponding to Ifnγ mRNA levels, protein levels were not altered in lung homogenates of Fra2 TG mice, although a trend towards higher Ifnγ protein concentration could be observed in mice older than 20 weeks (Figure 25). Overall this indicates that Th1 immune responses do not play a role in early disease development of Fra2 TG mice.

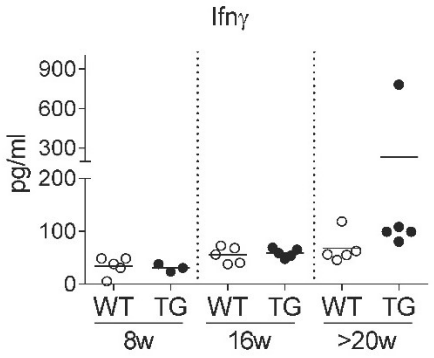

Figure 25: Interferon γ is unaltered in Fra2 TG mice. Protein levels of IFNγ were assessed in lung homogenates of 8-, 16- or >20-week-old Fra2 TG and WT mice.

mRNA and protein levels of IL-17, the main cytokine produced by Th17 cells, were not changed in any of the investigated time-points in Fra2 TG mice (Figure 26A, B).

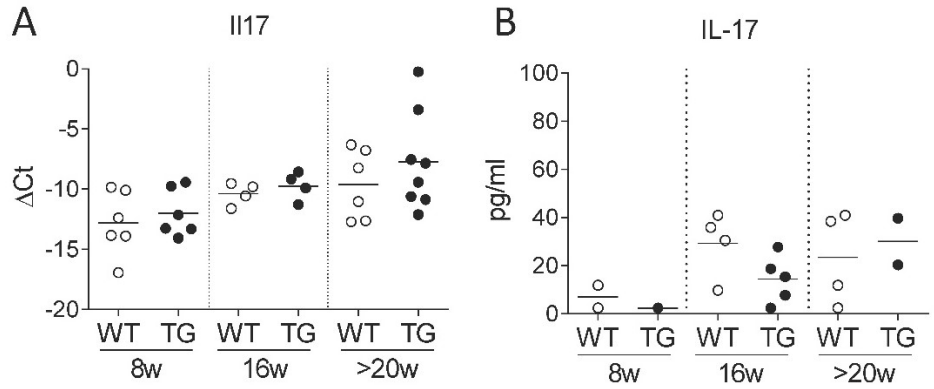

Figure 26: Interleukin 17 levels are unaltered in Fra2 TG mice. A) mRNA levels of interleukin 17 (Il17) assessed by quantitative real-time PCR and B) protein levels in lung homogenates of 8-, 16- or >20-week-old Fra2 TG and WT mice. (Parts of this data have been published in (117).)

In contrast, cytokines produced by Th2 cells were elevated in Fra2 TG mice. mRNA levels of IL-4 and IL-13, two cytokines which can signal through a common receptor, were unaltered in 8-week-old Fra2 TG mice but were elevated in 16-week-old mice (Figure 27A, B). In Fra2 TG mice older than 20 weeks, there was a trend towards heightened IL-4 and IL-13 levels, although no statistically significant differences were observed, probably due to low sample size and high variability, respectively. The potent eosinophil activator and stimulator of eosinophil proliferation IL-5 was significantly elevated only in older mice (>20 weeks), but already tendentially increased in 8- and 16-week-old Fra2 TG mice (Figure 27C).

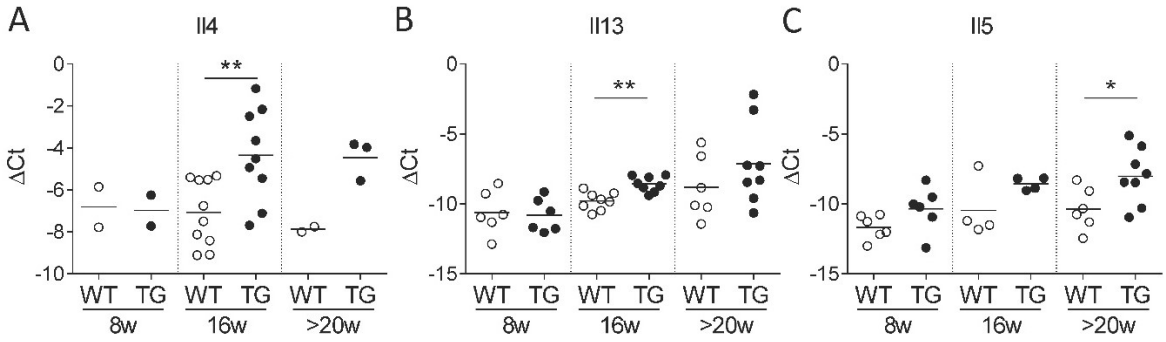

Figure 27: Th2 cytokine expression is increased in Fra2 TG mice. mRNA levels of the Th2 cytokines A) interleukin 4 (Il4), B) interleukin 13 (il13) and C) interleukin 5 (Il5) were assessed by quantitative real-time PCR in of 8-, 16- or >20-week-old Fra2 TG and WT mice. Significance of differences were determined using unpaired t-test; $p<0.05$, $**p<0.01$. (Parts of this data have been published in (117).)

IL-4 protein levels in lung homogenates of Fra2 TG mice were not significantly altered at 16 weeks, but increased in at 20 weeks as compared to WT control mice (Figure 28A). IL-13 levels were already significantly increased in 16-week-old mice and even higher in >20-week-old mice, whereas IL-5 protein levels were not significantly altered (Figure 28B, C).

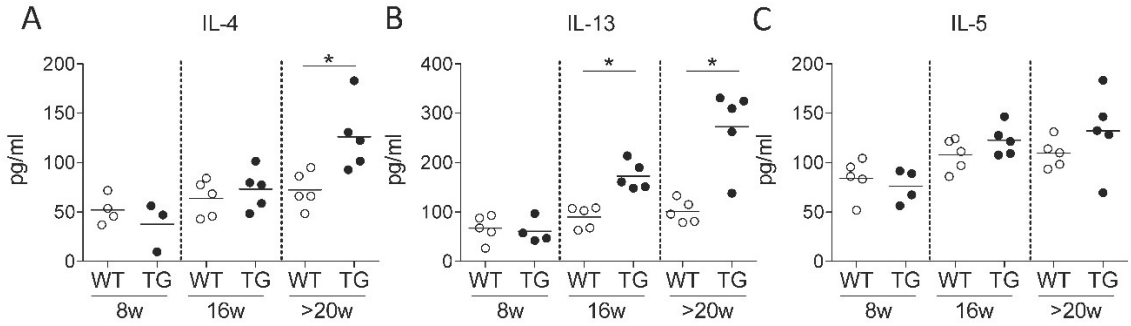

Figure 28: Th2 cytokine levels are elevated in Fra2 TG mice. Protein levels of A) IL-4, B) IL-13 and C) IL-5 were assessed in lung homogenates of 8-, 16- or >20-week-old Fra2 TG and WT mice. Significance of differences were determined using unpaired t-test; *p<0.05.

We further investigated the expression levels of the transcription factors T-box 21 (Tbx21) and GATA binding protein 3 (Gata3). Tbx21 and Gata3 are crucial regulators of Th differentiation towards Th1 and Th2 cells, respectively. We observed a clear decrease of Tbx21 expression in Fra2 TG mice at all time-points (Figure 29A), whereas Gata3 expression levels did not change (Figure 29B). This is in line with the observed predominance of Th2 cytokines, indicating a Th2 driven inflammation in Fra2 TG mice.

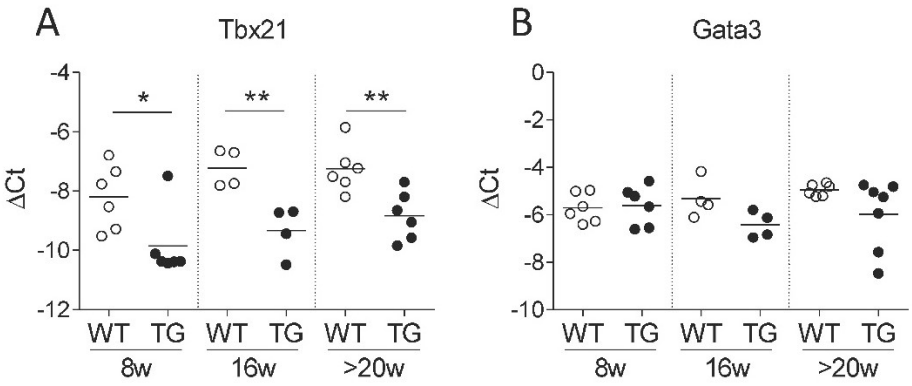

Figure 29: Expression levels of transcription factors involved in T helper cell differentiation are changed in Fra2 TG mice. mRNA levels of the transcription factors A) T-box 21 (Tbx21) and B) GATA binding protein 3 (Gata3) were assessed by quantitative real-time PCR in of 8-,

16- or >20-week-old Fra2 TG and WT mice. Significance of differences were determined using unpaired t-test; p<0.05, **p<0.01.

3.2.3. Anti-inflammatory cytokines are unchanged in Fra2 TG mice

Interleukin 10 (IL-10) is a cytokine produced by Th2 cells as well as by monocytes. IL-10 was originally described as a factor inhibiting cytokine production and has potent anti-inflammatory effects (125). In line with increased production of other Th2 cytokines in 16-week-old Fra2 TG mice (Figure 27 and Figure 28), IL-10 expression was increased at this time-point (Figure 30A).

We further assessed the expression levels of transforming growth factor β (Tgfβ), an anti-inflammatory, but pro-fibrotic cytokine that stimulates collagen production in a variety of cells and leads to transdifferentiation of fibroblasts to myofibroblasts (reviewed in (54)). Despite the prominent role of Tgfβ in the development of fibrosis, we did not observe a change of Tgfβ expression in any of the investigated time-points (Figure 30B), indicating that the role of Tgfβ in this mouse model of fibrosis might be limited.

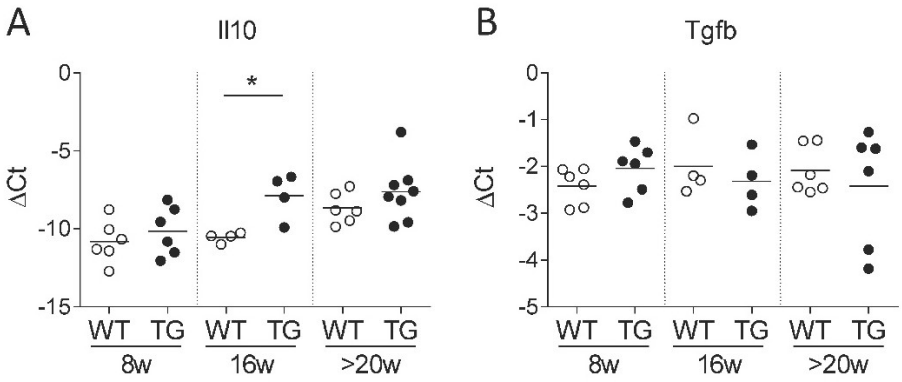

Figure 30: Expression of anti-inflammatory cytokines in Fra2 TG mice. mRNA levels of A) interleukin 10 (Il10) and B) transforming growth factor β (Tgfb) were assessed by quantitative real-time PCR in of 8-, 16- or >20-week-old Fra2 TG and WT mice. Significance of differences were determined using unpaired t-test; *p<0.05.

Although levels of IL-10 mRNA (Figure 30A) were increased in Fra2 TG mice compared to WT mice at 16 weeks, no change in the protein levels of IL-10 could be observed in lung homogenates of Fra2 TG mice at any time-point (Figure 31).

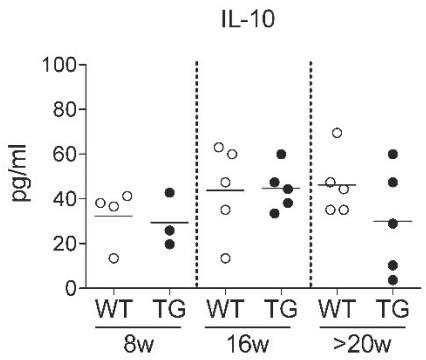

Figure 31: Interleukin-10 (IL-10) is unaltered in Fra2 TG mice. Protein levels of IL-10 were assessed in lung homogenates of 8-, 16- or >20-week-old Fra2 TG and WT mice.

3.2.4. Pro-fibrotic and eosinophil-attracting chemokines are elevated in Fra2 TG mice

Chemokines are a protein family with a major role in leukocyte activation, chemoattraction and angiogenesis. Ccl2, a chemokine which recruits monocytes and T-cells and stimulates collagen production in lung fibroblasts (100), was elevated in Fra2 TG mice at all time-points with a significant increase at 16 and >20 weeks of age (Figure 32A). Ccl5 expression was downregulated in 8-week-old Fra2 TG compared to WT mice and normalised at later time-points (Figure 32B).

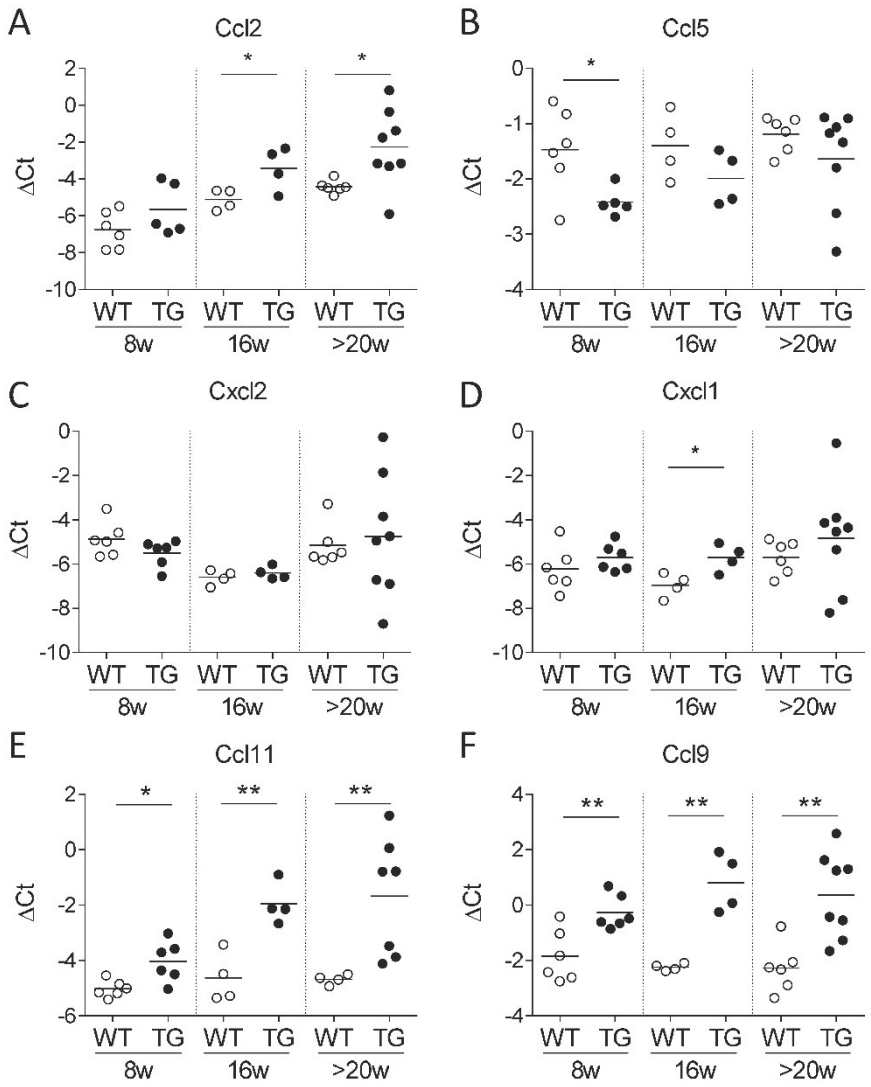

Figure 32: Chemokine expression in Fra2 TG mice. mRNA levels of A) Ccl2, B) Ccl5, C) Cxcl2, D) Cxcl1, E) Ccl11 (eotaxin-1) and F) Ccl9 were assessed by quantitative real-time PCR in of 8-, 16- or >20-week-old Fra2 TG and WT mice. Significance of differences were determined using unpaired t-test or Mann Whitney test; *p<0.05, **p<0.01.

Expression levels of the C-X-C motif chemokines Cxcl1 and Cxcl2, two powerful chemoattractants for neutrophils were mostly unaltered, with a slight increase of Cxcl1 in 16-week-old Fra2 TG mice (Figure 32C, D). In contrast, the eosinophil-selective chemoattractant Ccl11, also termed eotaxin-1 (126), was significantly increased in Fra2 TG mice of all ages (Figure 32E). Similarly, Ccl9 which can be produced in vast amounts by activated eosinophils (127), was highly upregulated in all time-points (Figure 32F). Together this indicates that eosinophil homing and activation might play an important role in the lung phenotype of Fra2 TG mice.

3.2.5. Inflammatory infiltrates in the lung of Fra2 TG mice predominately consist of eosinophils and T-cells

Altered expression and production of key inflammatory cytokines visible already at 8 weeks, as well as the inflammatory infiltrates apparent in the lungs of 16-week-old Fra2 TG mice indicate that inflammation is a major contributor to pulmonary disease in this mouse model. To assess how altered cytokine levels contribute to the recruitment of diverse inflammatory cells to the lung, inflammatory cell populations were analysed using flow cytometry in 16- and >20-week-old Fra2 TG mice compared to age- and sex-matched littermate control WT mice. Lung perfusion and bronchoalveolar lavage enabled to distinguish between inflammatory cell populations present in the lung tissue (interstitium) and the alveolar space, respectively, avoiding cross-contamination with circulating inflammatory cells from the blood stream. Inflammatory cells in single cell lung homogenates were identified by positivity for the surface marker CD45.

Corresponding to the increased levels of pro-inflammatory cytokines, the amount of inflammatory cells in the BAL (Figure 33A) and in the lung homogenate (Figure 33B) of Fra2 TG mice was increased in 16- and in >20-week-old mice.

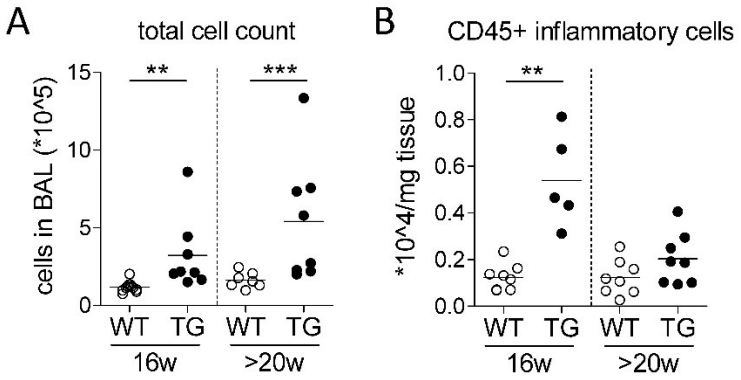

Figure 33: The number of inflammatory cells in the bronchoalveolar lavage (BAL) and the lung tissue of Fra2 TG mice is increased. A) Total number of cells in the BAL and B) number of CD45+ inflammatory cells detected in single cell lung homogenates were analysed in 16- and >20-week-old Fra2 TG and WT control mice. Significance of differences were determined using unpaired Mann Whitney test; **p<0.01, ***p<0.001.

The number of alveolar macrophages significantly diminished in the BAL of >20-week old Fra2 TG mice, whereas interstitial macrophages in the lung tissue slightly

increased (Figure 34A, B). These data indicate macrophage infiltration from the alveolar into the interstitial space.

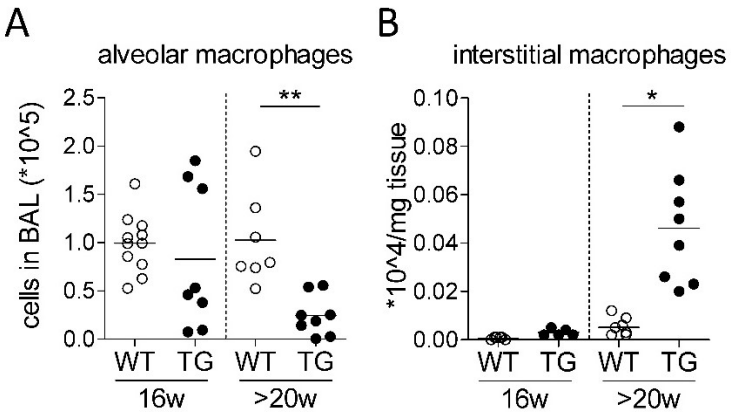

Figure 34: Macrophages infiltrate the lung tissue in Fra2 TG mice. Alveolar (A) and interstitial (B) macrophages were assessed A) in the bronchoalveolar lavage (BAL) and B) in the lung tissue of 16- and >20-week-old Fra2 TG and WT control mice. Significance of differences were determined using unpaired Mann Whitney test; *p<0.05, **p<0.01.

The number of neutrophils in the BAL of Fra2 TG mice was slightly elevated, although no significant differences were observed at any time-point (Figure 35A). The number of dendritic cells significantly increased in Fra2 TG mice of both age groups, however, the major change was observed in eosinophils, which made up approximately 70-80% of the total BAL cell count (Figure 35A). In the lung tissue, the amount of neutrophils was unaltered, whereas dendritic cells increased. Similar to the BAL, the vast majority of inflammatory cells were eosinophils, which were highly increased in Fra2 TG mice at 16 weeks as well as in >20 weeks (Figure 35B).

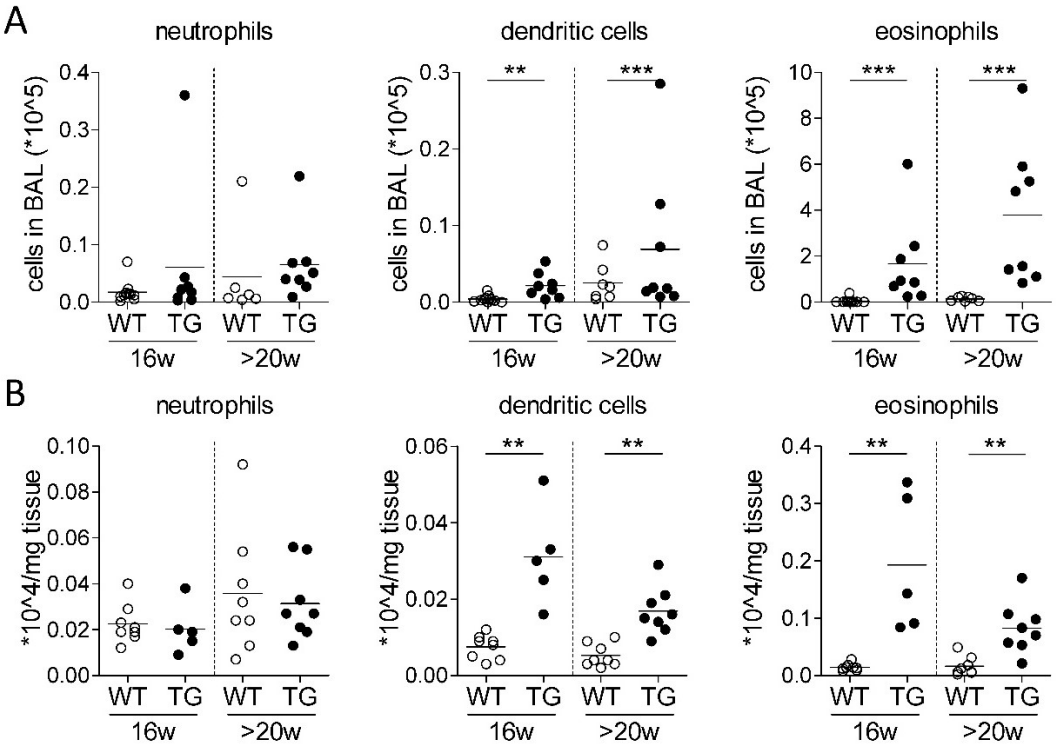

Figure 35: Pulmonary inflammation in Fra2 TG mice is characterized by severe eosinophilia. Numbers of neutrophils, dendritic cells and eosinophils were assessed A) in the bronchoalveolar lavage (BAL) and B) in the lung tissue of 16- and >20-week-old Fra2 TG and WT control mice. Significance of differences were determined using unpaired Mann Whitney test; **p<0.01, ***p<0.001.

Not only cells of the innate immunity were enriched in the lungs of Fra2 TG mice, but also T- and B-lymphocytes. At 16, as well as >20 weeks, Fra2 TG mice had increased amounts of T-helper cells (identified by the expression of the surface marker CD4), effector T-cells (identified by CD8 expression) and B-cells in the BAL (Figure 36 A). These changes were less pronounced in the lung tissue, where CD4+ T-cells were only increased at 16 weeks of age and CD8+ effector cells were unaltered at both time-points (Figure 36B). However, there was a clear infiltration of B-cells in the lung tissue of Fra2 TG mice compared to WT controls(Figure 36 B).

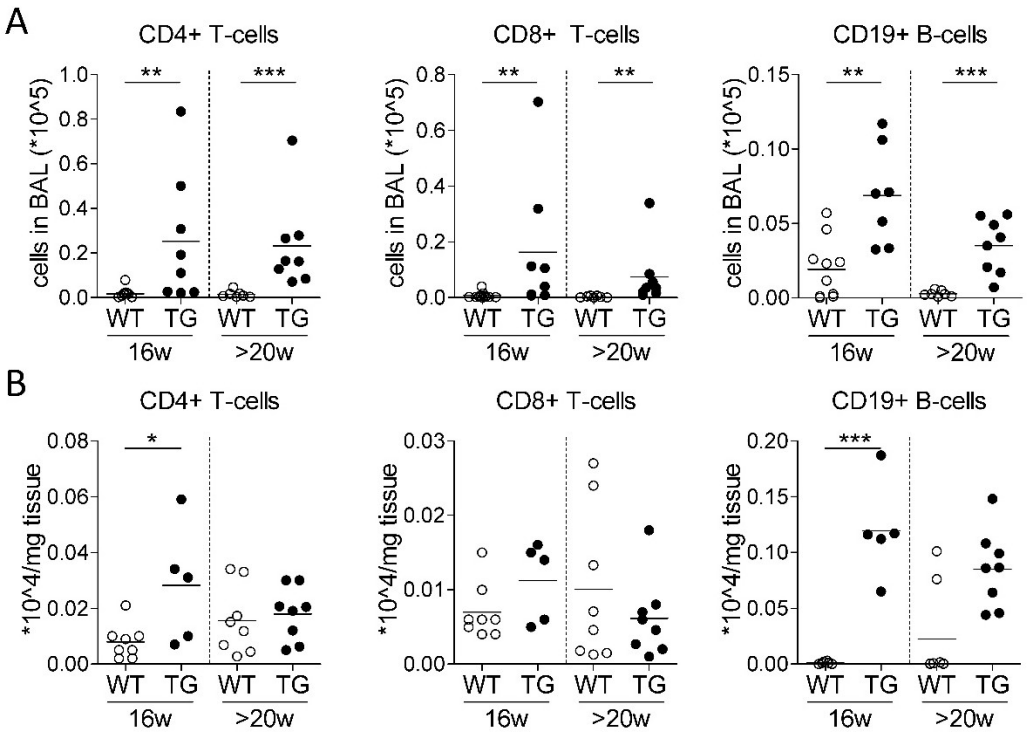

Figure 36: Fra2 TG mice exhibit increased lymphocyte infiltration in the lung. CD4+ T-helper cells, CD8+ effector T-cells and CD19+ B-lymphocytes were assessed A) in the bronchoalveolar lavage (BAL) and B) in the lung tissue of 16- and >20-week-old Fra2 TG and WT control mice. Significance of differences were determined using unpaired Mann Whitney test; *p>0.05, **p<0.01, ***p<0.001.

In conclusion, Fra overexpression in mice leads to a time-dependent increase of inflammation in the lung, characterized by the expression of pro-inflammatory cytokines, such as IL-1, IL-6 or the Th2 cytokines IL-4 and IL-13, and inflammatory cell infiltrates, predominately consisting of eosinophils, into the lung tissue and the alveolar space.

3.2.6. Increased IL-4/IL-13 downstream signalling in Fra2 TG mice

As previously mentioned, we measured increased levels of IL-4 and IL-13 in the lungs of Fra2 TG mice. IL-4 can bind and activate the IL-4 type I receptor which is consisting of IL-4Rα and γδ chains. Furthermore, both IL-4 and IL-13 can act on the IL-4 type II receptor, also named IL-13Rα1, a dimer consisting of an IL-4Rα and an IL-13Rα1 chain (128). Both cytokines lead to phosphorylation and thereby activation of the signal transducer and activator of transcription 6 (STAT6) transcription factor (129). To explore the impact of Th2 cytokine signalling in the Fra2 TG mouse model,

protein levels of STAT6 and phosphorylated (p) STAT6 were investigated by Western blot (Figure 37A).

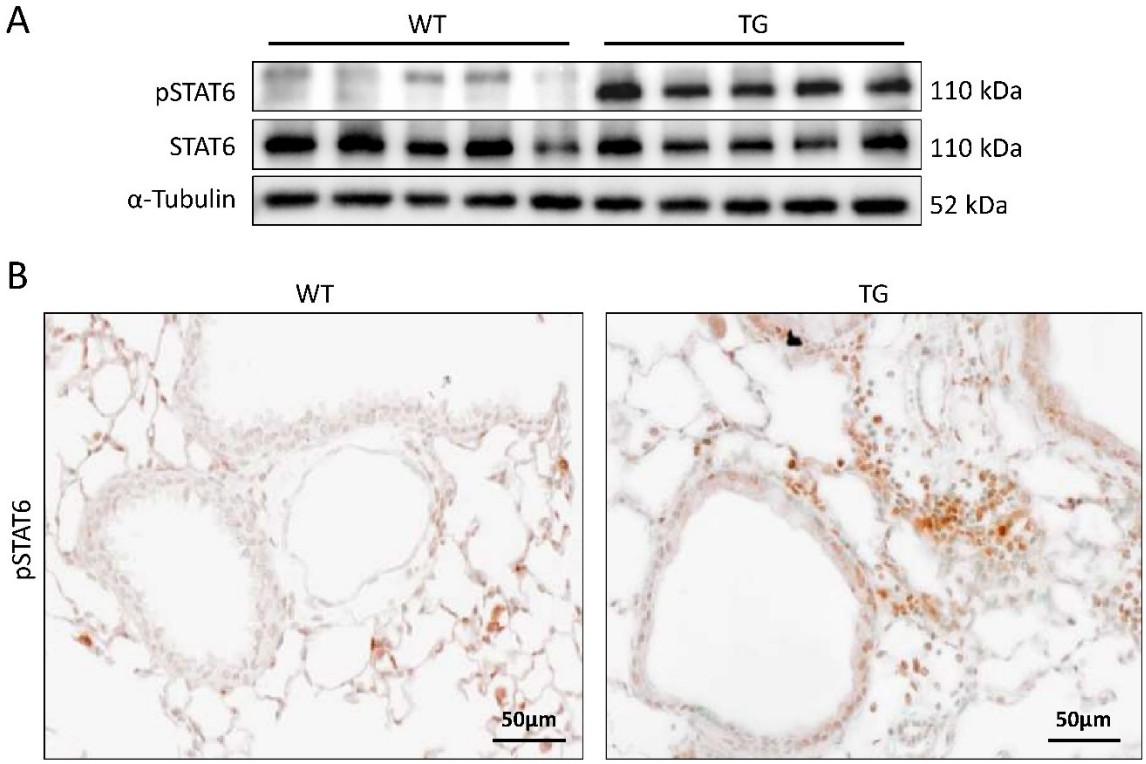

Figure 37: IL-4/IL-13 downstream signalling is activated in Fra2 TG mice. A) Levels of phosphorylated signal transducer and activator of transcription 6 (pSTAT6) and total STAT6 levels in the lung homogenates of 16-week-old Fra2 TG mice were investigated by western blotting and compared to WT control mice. α-Tubulin was used as loading control. B) Immunohistochemical staining on the lungs of 16-week-old WT and Fra2 TG mice was performed using an antibody against phosphorylated STAT6. The tissue was counterstained using methylgreen. (Figure adapted from (117))

Although total protein levels of STAT6 were unaltered in Fra2 TG compared to WT mouse lung homogenates, phosphorylation of STAT6 was highly increased. Furthermore, pSTAT6 immunoreactivity was increased in the lungs of Fra2 TG mice (Figure 37B). Strong nuclear staining of pSTAT6 was mostly observed in bronchial epithelial cells and in inflammatory cell infiltrates around the bronchi and vessels of Fra2 TG mice. These data show that the lung in Fra2 TG mice is not only a producer of Th2 cytokines, but that they act locally inducing IL-4/IL-13 downstream signalling as indicated by phosphorylated STAT6.

3.3. Fra2 TG mice develop experimental asthma

Profiling of inflammatory cell populations and cytokines revealed increased Th2 and eosinophilic inflammation in Fra2 TG mice compared to WT littermate control mice at already 16-weeks of age, prior to the onset of pulmonary fibrosis. Th2 driven, eosinophilic inflammation is a hallmark of asthma and airway hyperresponsiveness/allergic airway disease, therefore we hypothesised that Fra2 TG mice exhibit a phenotype similar to asthma, prior to the development of pulmonary fibrosis.

3.3.1. Fra2 TG mice exhibit differential expression of asthma-associated genes

Gene expression profiling of the lungs of 16-week old Fra2 TG and WT mice, performed by our collaboration partner at the Justus-Liebig University in Giessen, was analysed and regulated genes were screened for associations with chronic airway disease and asthma. A total of 775 genes were differentially regulated (443 up- and 342 downregulated). Several of the highest regulated genes, for example Clca1 (chloride channel accessory 1) and Retnla (resistin like alpha, Relma/Fizz) (Figure 38) were strongly associated with asthma (119, 130).

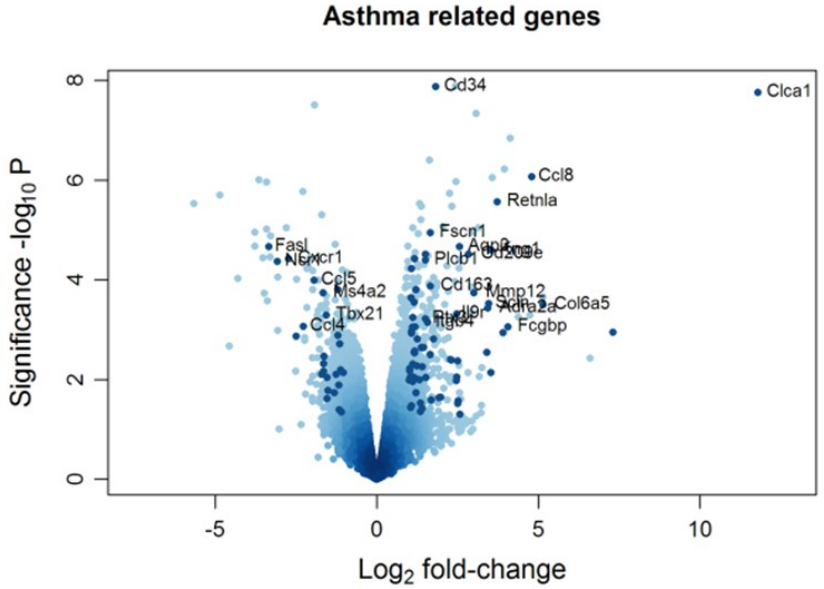

Figure 38: A high proportion of regulated genes in Fra2 TG mice is associated with asthma. Differential gene expression was assessed in 16-week-old Fra2 TG versus WT mice. Dark points indicate genes related to chronic airway disease. (Figure adapted from (117))

Furthermore, a lot of genes related to inflammatory responses – sub-classified into eosinophilic inflammation, immunoregulatory, pro-inflammatory and Th2 response genes - (Figure 39A), asthma susceptibility (Figure 39B) and remodelling processes – sub-classified into airway remodelling, bronchoconstriction, ECM production and mucus production and secretion genes – (Figure 39C) were identified.

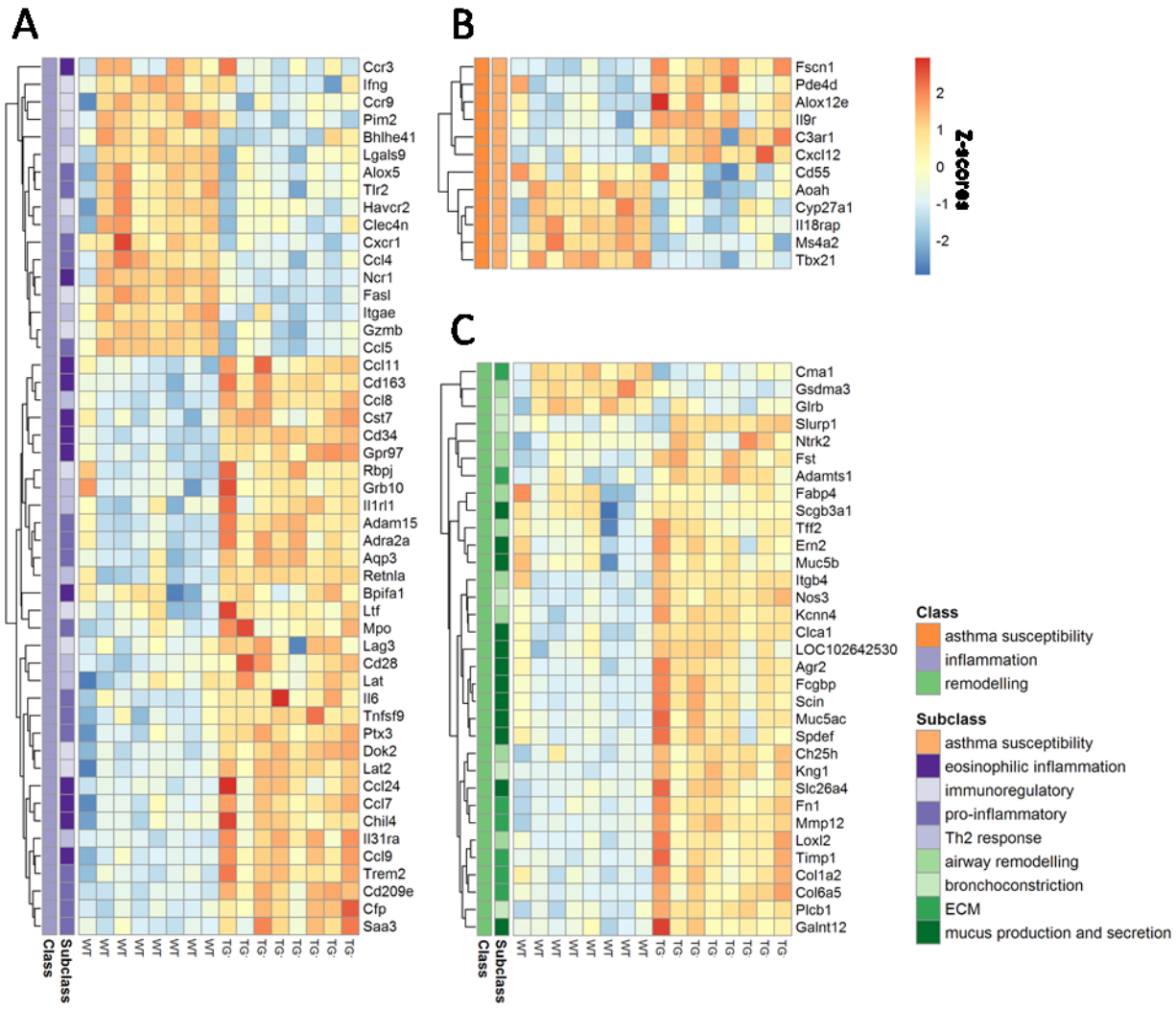

Figure 39: Regulated genes in Fra2 TG mice associated with asthma. Heatmap representation of asthma-related genes classified according to their association with A) inflammation (purple), B) asthma susceptibility (orange) and C) remodelling processes (green). Z-scores are shown. (Figure adapted from (117))

In total, 12% of all regulated genes could be linked to chronic airway disease and asthma, strengthening the hypothesis that Fra 2 TG mice exhibit an asthmatic phenotype with airway remodeling, inflammation and airway hyperresponsiveness.

3.3.2. Increased mucus production and secretion in Fra2 TG mice

Nine of the fifteen highest regulated asthma associated genes were linked to mucus production and secretion, rendering the question if Fra2 might be directly involved in the transcriptional regulation of these genes. *In silico* transcription factor binding site analysis of the proximal promoter regions revealed multiple putative AP-1 binding sites in 83% (10 out of 12) in the promoter regions of the analysed genes (Figure 40), indicating that Fra2 might indeed be directly responsible for increased gene expression.

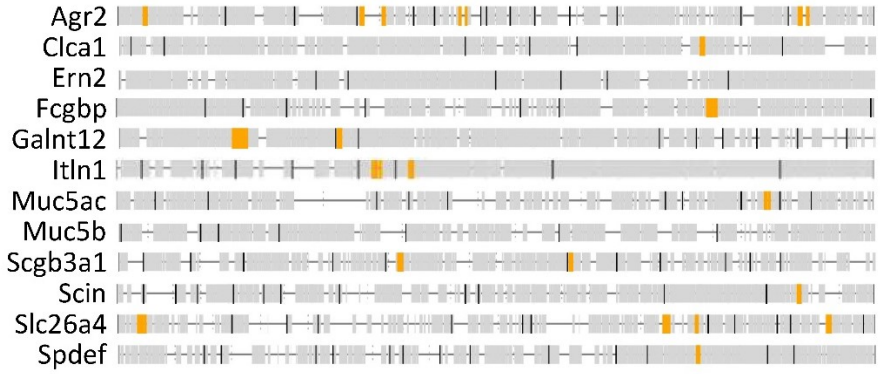

Figure 40: *In silico* transcription factor binding site analysis revealed multiple putative AP-1 binding sites in the promoter of differentially regulated genes associated with mucus production and secretion. The proximal promoter regions including 1 kb upstream of the start codon were analysed. Putative AP-1 binding sites are marked yellow. (Figure adapted from (117))

Increased expression of *Clca1* (chloride channel accessory 1) and of the mucus genes *Muc5ac* and *Muc5b* was verified using an independent mouse cohort (Figure 41A). *Clca1* is crucial for the correct secretion and hydration of mucus and was confirmed to be highly elevated in Fra2 TG mice. Of the two main airway mucus genes *Muc5ac* and Muc5b only the first was confirmed to be upregulated, whereas no significant changes could be observed in the latter (Figure 41A). However, increased expression of CLCA1 and MUC5AC was confirmed on the protein level, using immunofluorescence staining. While no staining was detected in healthy lung tissue of WT mice, a strong immunoreactivity was observed in the bronchial epithelium of Fra2 TG mice (Figure 41B).

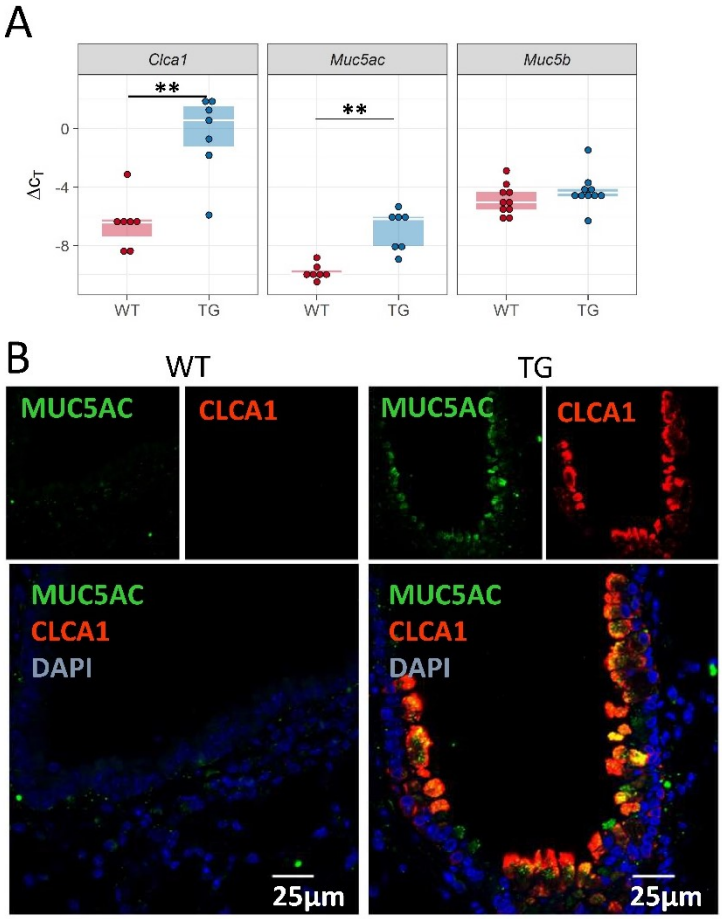

Figure 41: Increased mucus production and secretion in Fra2 TG mice. A) Gene expression of *Clca1*, *Muc5ac* and *Muc5b* was assessed by quantitative real-time PCR in 16-week-old Fra2 TG and WT mice. Significance of differences were determined using unpaired t-test; **p>0.01. B) Representative immunofluorescence staining of MUC5AC (green) and CLCA1 (red) in the lung of Fra2 TG and WT mice (n=3 each). (Figure adapted from (117))

Further, we investigated the expression of *Spdef* (SAM Pointed Domain containing ETS Transcription Factor) and *Foxa3* (Forkhead Box A3), two transcription factors regulating goblet cell differentiation and mucus production. *Spdef* expression was only slightly elevated, whereas *Foxa3* expression significantly increased, indicating higher levels of mucus producing goblet cells (Figure 42).

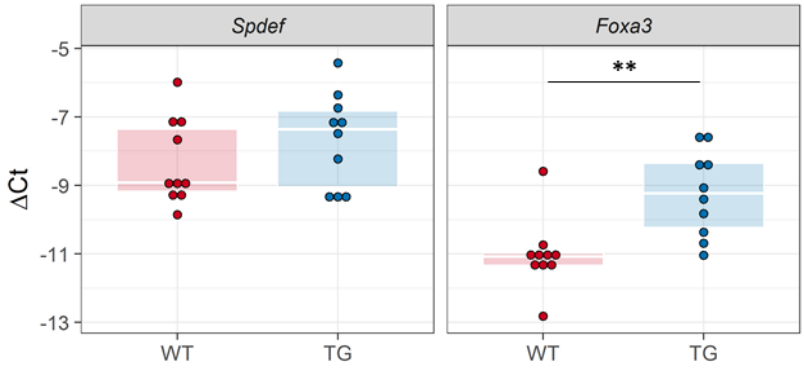

Figure 42: Transcription factors involved in goblet cell differentiation and mucus production are elevated in Fra2 TG mice. mRNA levels of *Spdef* and *Foxa3* were assessed by quantitative real-time PCR in lung homogenates of 16-week-old Fra2 TG and WT mice. Significance of differences were determined using unpaired Mann Whitney test; **p<0.01. (Figure adapted from (117))

3.3.3. Increased airway remodelling and hyperresponsiveness in Fra2 TG mice

Next to increased mucus production, collagen deposition around the airways and thickening of the airway smooth muscle layer are key features of bronchial remodelling. Mucus volume as well as the amount of goblet cells in the airways were significantly increased upon Fra2 overexpression in mice (Figure 43), in line with the gene expression data showing pronounced levels of transcription factors relevant for goblet cell differentiation and genes related to mucus production and secretion.

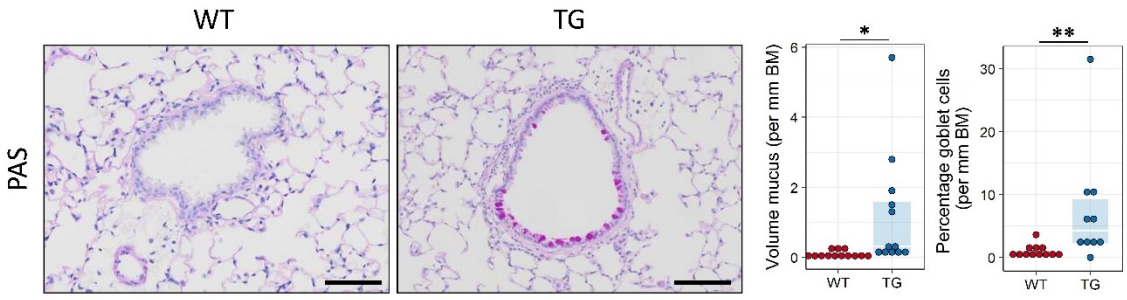

Figure 43: Goblet cells differentiation and mucus production is increased in Fra2 TG mice. Stereologic assessment of mucus volume in the airways and percentage of goblet cells per mm basement membrane (BM) was performed on periodic acid-Schiff (PAS) stained lung section of 16-week old Fra2 TG and WT mice. Scalebar: 75 µm; Significance of differences were determined using unpaired Mann Whitney test; *p>0.05, **p>0.01. (Figure adapted from (117))

Additionally to these cellular changes within the airways of Fra2 TG mice, collagen deposition around the bronchi was increased (Figure 44A) and the smooth muscle layer was thickened (Figure 44B).

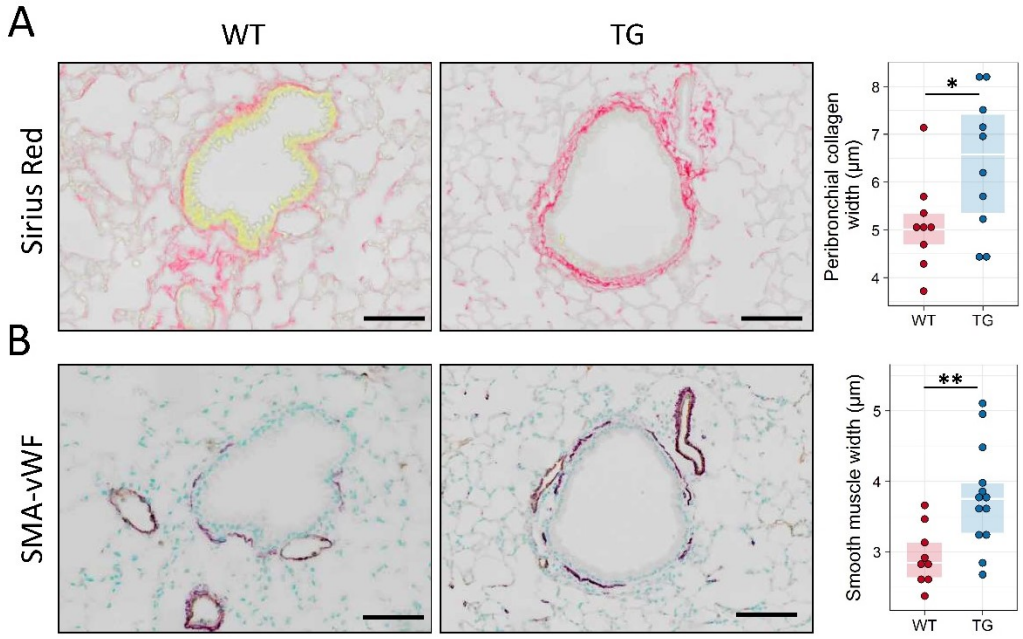

Figure 44: Bronchial remodelling in Fra2 TG mice. A) Peribronchial collagen deposition was analysed on Sirius Red stained lung sections of 16-week-old Fra2 TG and WT mice. B) Airway smooth muscle thickness was quantified using double immunohistochemical staining of smooth muscle actin (SMA) and von Willebrand factor (vWF) on lung sections of 16-week-old Fra2 TG and WT mice. Scalebar: 75 µm, Significance of differences were determined using unpaired Mann Whitney test; *p>0.05; **p>0.01. (Figure adapted from (117))

Augmented proliferation of airway smooth muscle cells isolated from Fra2 TG mice (Figure 45) compared to those from WT mice, indicated that the increased thickness of airway smooth muscle is a direct consequence of ASMC growth due to Fra2 overexpression.

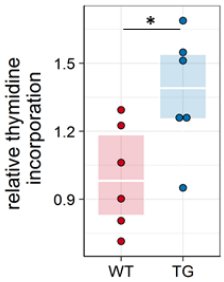

Figure 45: Fra2 overexpression leads to increased proliferation of airways smooth muscle cells (ASMC). Proliferation of ASMC isolated from Fra2 TG or WT mice was assessed by

measuring the incorporation of ^{3}H-labelled thymidine after 24 hours. Significance of differences were determined using unpaired Mann Whitney test; *p>0.05. (Figure adapted from (117))

To assess whether these structural changes lead to functional alterations, the airway response to increasing doses of methacholine was measured. Fra2 TG mice showed significantly higher resistance and elastance of the airways at high doses of methacholine. At the same time airway compliance declined (Figure 46).

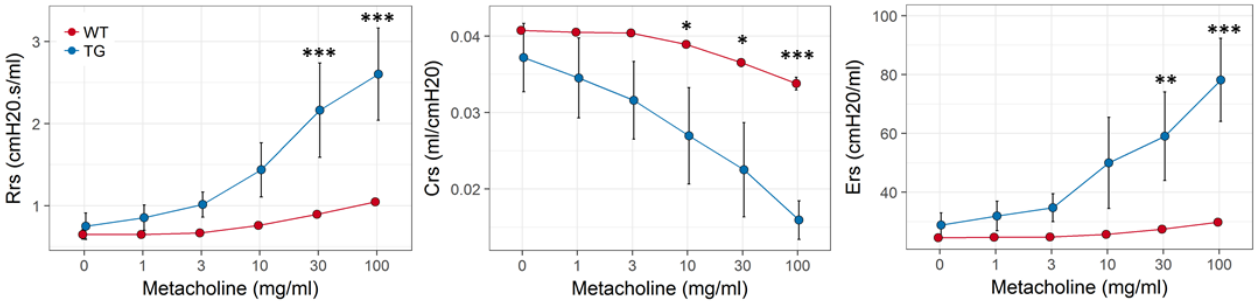

Figure 46: Fra2 TG mice have increased airway hyperresponsiveness (AHR). Lung function in response to increasing doses of methacholine was assessed in Fra2 TG (n=5) and WT (n=7) mice to determine changes in airway resistance (Rrs), compliance (Crs) and elastance (Ers). Significance of differences were determined using two-way ANOVA with Bonferroni's *post hoc* test; *p>0.05, **p>0.01, ***p>0.001. (Figure adapted from (117))

In summary, we show that 16-week-old Fra2 TG mice develop all major features of chronic airway disease, namely airway inflammation, remodelling and hyperresponsiveness, prior to any apparent fibrotic histological changes.

3.4. Experimental asthma in Fra2 TG mice is dependent on IL-13 signalling and can be ameliorated by glucocorticoid treatment

In Fra2 TG mice, pulmonary inflammation is characterized by vast amounts of eosinophils and increased levels of the Th2 cytokines IL-4 and IL-13. Both IL-4 and IL-13 bind and activate the IL-13R type I (comprised of the IL-4Rα and the IL-13Rα1 chain), nevertheless, their functional role in mediating allergic asthma *in vivo* are very distinct. While IL-4 is responsible for the initiation of allergic responses by stimulating Th2 differentiation and proliferation, as well as IgE class switching in B-cells, IL-13 is crucial for the effector phase (119, 120). IL-13 stimulates mucus

hypersecretion by regulating the expression of several transcription factors important for the differentiation of club (Clara) cells to goblet cells (such as *Spdef*), and additionally regulates mucus production and secretion by inducing genes such as *Muc5ac* and *Clca1* (119, 131, 132).

3.4.1. Blockade of IL-13 improves the Fra2 TG phenotype

We therefore wanted to elucidate the importance of IL-13 in the Fra2-induced asthmatic phenotype and the therapeutic potential of blocking IL-13 signalling in these mice. For this purpose, Fra2 TG mice were treated twice a week with a neutralizing antibody directed against IL-13. Treatment was started at 10 weeks of age and continued until mice were 16 weeks old (Figure 47).

Figure 47: Schematic representation of the treatment with IL-13 blocking antibodies (anti-IL13) or isotype control antibodies (IgG). Fra2 TG and WT mice (n=5-8) were treated twice a week intraperitoneal (i.p.) with anti-IL13 or IgG control antibodies. (Figure adapted from (117))

Anti-IL13 treatment clearly decreased IL-13 downstream signalling in the lung, as seen by diminished levels of phosphorylated STAT6 (Figure 48). In comparison, the total amount of STAT6 was unaltered by the treatment of Fra2 TG mice, showing a successful blockade of IL-13 signalling in the lung.

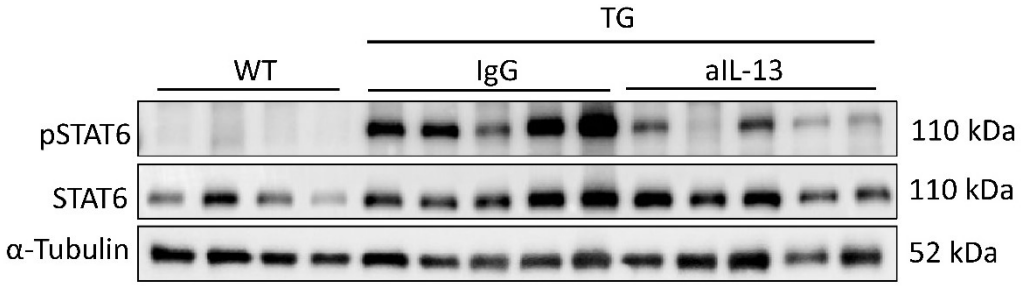

Figure 48: IL-13 downstream signalling is decreased In Fra2 TG mice upon blockade of IL-13. IL-13 signalling was assessed by western blot analysis of phosphorylated (p) levels of STAT6 in the lung homogenates of 16-week-old WT and Fra2 TG mice treated with control isotype (IgG) or IL-13 blocking antibodies (aIL-13). α-Tubulin served as loading control. (Figure adapted from (117))

Blockade of IL-13 reduced the production of MUC5AC and CLCA1 indicating diminished mucus production and secretion in the airways of Fra2 TG mice (Figure 49). This finding was substantiated by the quantitative assessment of mucus production and goblet cell differentiation: Treatment with IL-13 neutralizing antibodies significantly diminished the percentage of goblet cells within the epithelial lining of the airways in Fra2 TG mice (Figure 50). Together, these data show that IL-13 plays an important role in the differentiation of goblet cells and the production and secretion of mucus in the airways of Fra2 TG mice.

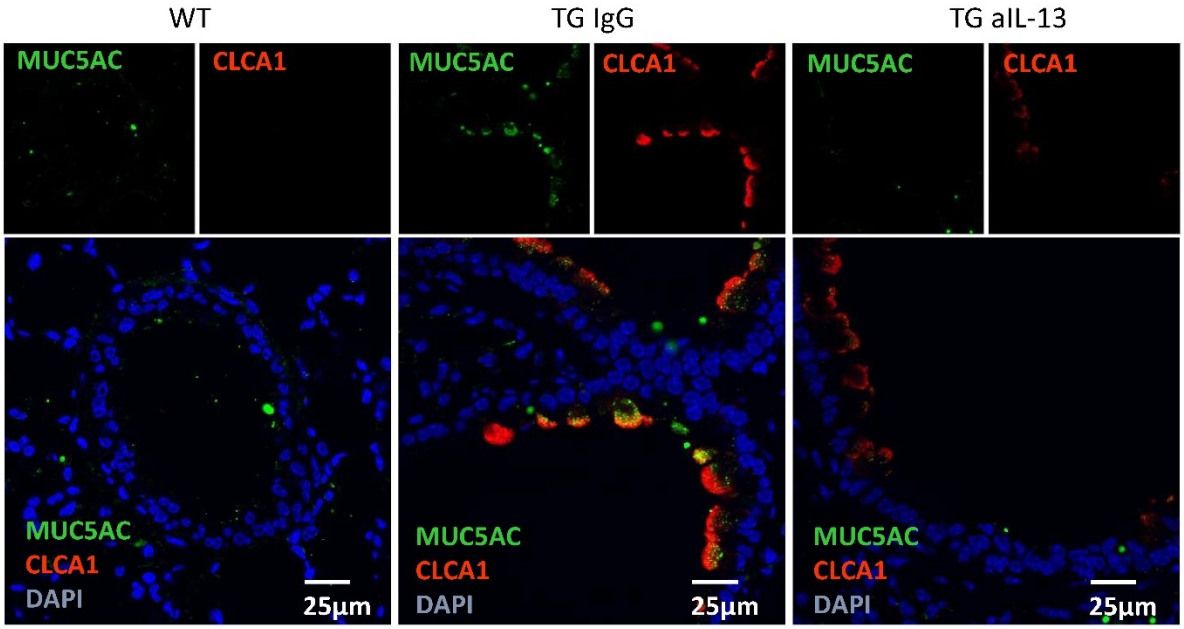

Figure 49: IL-13 blockade diminishes mucus production and secretion in Fra2 TG mice. Representative immunofluorescence images (from n=3) of MUC5AC (green) and CLCA1 (red) in the lungs of WT and Fra2 TG mice treated with control IgG or anti-IL-13 neutralising antibodies. (Figure adapted from (117))

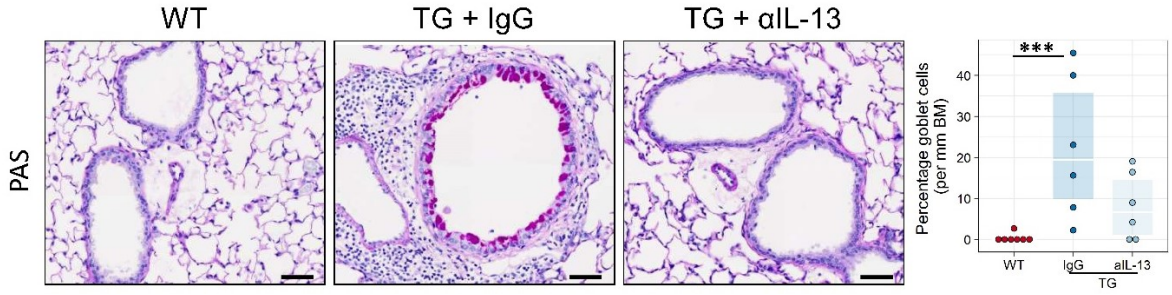

Figure 50: Increased goblet cells differentiation and mucus production in Fra2 TG mice is ameliorated upon IL-13 blockade. Stereological assessment of the percentage of goblet cells per mm basement membrane (BM) was performed on periodic acid-Schiff (PAS) stained lung section of 16-week old WT and Fra2 TG treated with control isotype (IgG) and IL-13

neutralizing (αIL-13) antibodies. Scalebar: 50 µm; Significance of differences were determined using unpaired Mann Whitney test; ***p>0.001. (Figure adapted from (117))

However, peribronchial collagen deposition was not influenced by blockade of IL-13 and was still significantly increased in Fra TG mice treated with IL-13 neutralizing antibodies compared to WT mice (Figure 51A), possibly due to the direct influence of Fra2 on collagen expression (26). Smooth muscle thickness around the bronchi slightly diminished upon treatment, although changes did not reach significance (Figure 51B).

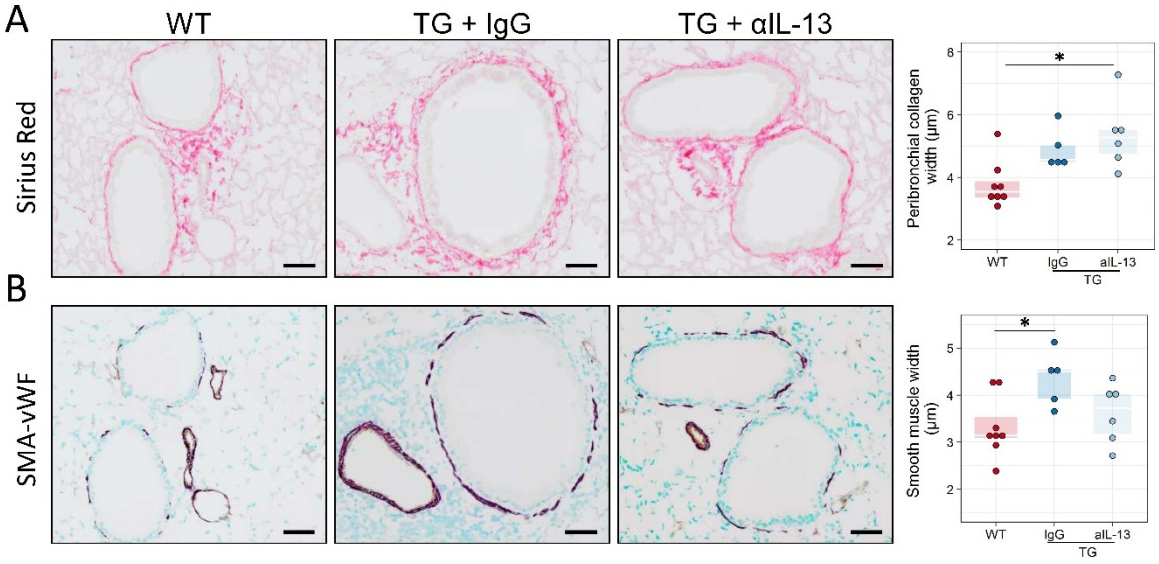

Figure 51: Bronchial remodelling is not significantly improved in Fra2 TG mice upon IL-13 blockade. Representative images and subsequent quantification of A) Sirius red staining for peribronchial collagen width and B) double immunohistochemistry for von Willebrand-factor (vWF, brown) and a-smooth muscle actin (SMA, purple) for airway smooth muscle thickness. Remodelling was assessed in 16-week old WT and Fra2 TG treated with control isotype (IgG) and IL-13 neutralizing (αIL-13) antibodies. Scalebar: 50 µm; Significance of differences were determined using unpaired Mann Whitney test; *p>0.05. (Figure adapted from (117))

Neutralisation of IL-13 in Fra2 TG mice improved AHR. While Fra2 TG mice treated with control IgG had significantly higher airway resistance, elastance and decreased airway compliance especially at high doses of metacholine, αIL-13 treated Fra2 TG mice showed significantly improved lung function (Figure 52). However, treatment did not completely restore the phenotype and αIL-13 treated Fra2 TG mice still had elevated airway resistance compared to WT mice (Figure 52).

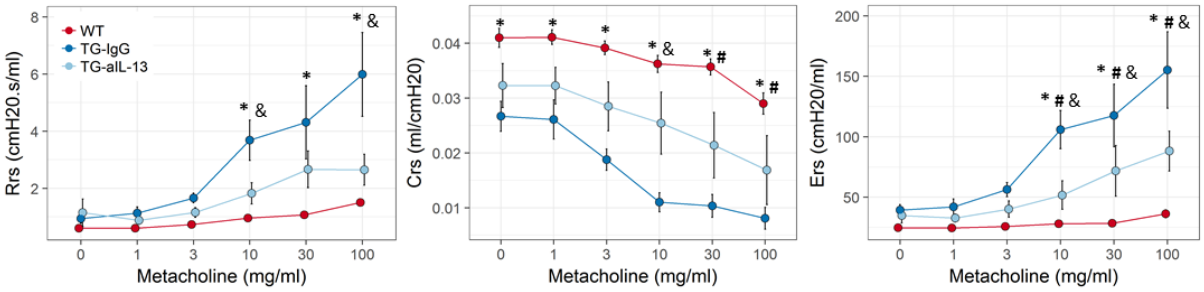

Figure 52: Airway hyperresponsiveness (AHR) is improved after IL-13 blockade in Fra2 TG mice. Lung function testing upon increasing doses of Methacholine was performed to determine changes in airway resistance (Rrs), compliance (Crs) and elastance (Ers) in WT mice (n= 8) and Fra2 TG mice treated with isotype control (IgG, n = 5) or anti-IL-13 antibodies (n = 6). Significance of differences were determined using two-way ANOVA with Bonferroni's *post hoc* test; *p < 0.05 WT vs. TG-IgG, #p < 0.05 WT vs. TG-aIL-13, &p < 0.05 TG-IgG vs. TG-aIL-13. (Figure adapted from (117))

Analysis of pulmonary inflammation in Fra2 TG mice with and without treatment revealed that blocking IL-13 significantly decreased the amount of inflammatory cells in the BAL of Fra2 TG mice (Figure 53). Especially the high numbers of eosinophils and T-cells significantly decreased to levels similar as in WT mice and the alveolar macrophage population was restored. The numbers of CD19+ B-cells, which were significantly increased in control IgG treated TG mice compared to healthy WT mice, declined only slightly and was still significantly higher compared to WT (Figure 53).

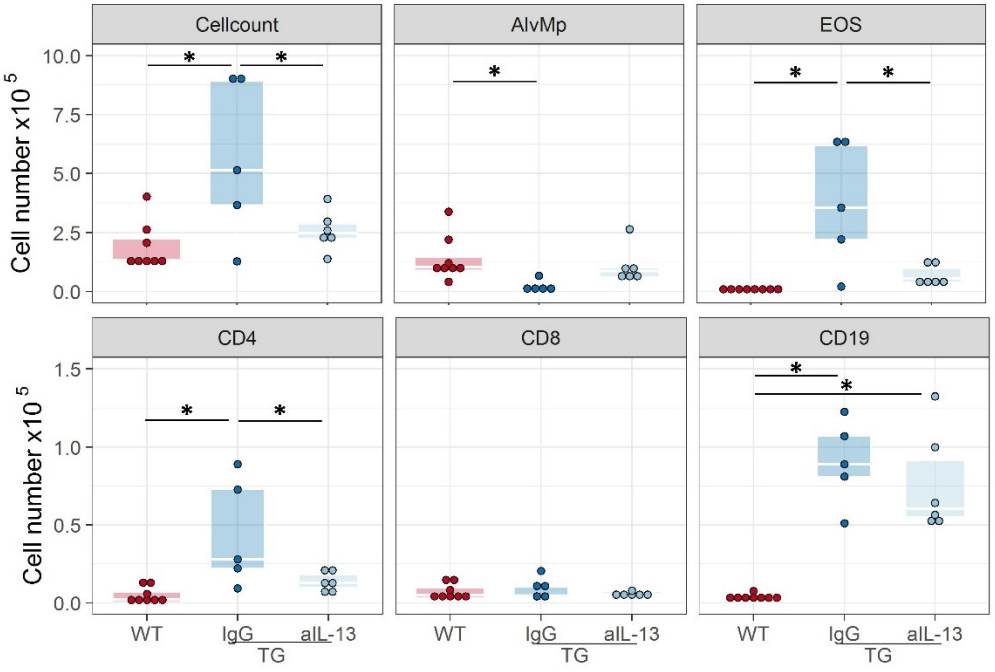

Figure 53: Blocking IL-13 signalling reduced inflammation in Fra2 TG mice. Flow cytometric analysis of inflammatory cells in the bronchoalveolar lavage of WT or Fra2 TG mice treated with IL-13 neutralising (aIL-13) or isotype (IgG) antibodies. Significance of differences were determined using unpaired Mann Whitney test; *p>0.05. (Figure adapted from (117))

Expression of the Th2 cytokines IL-4, IL-5 and IL-13 itself was not altered upon blockade of IL-13 (Figure 54). Interestingly, the levels of IL-17 slightly increased in treated Fra2 TG mice, however not significantly. This is in line with reports showing that IL-13 negatively regulates IL-17 production (133). Blockade of IL-13 might therefore have not only have beneficial effects, but could lead to increased IL-17-driven inflammation.

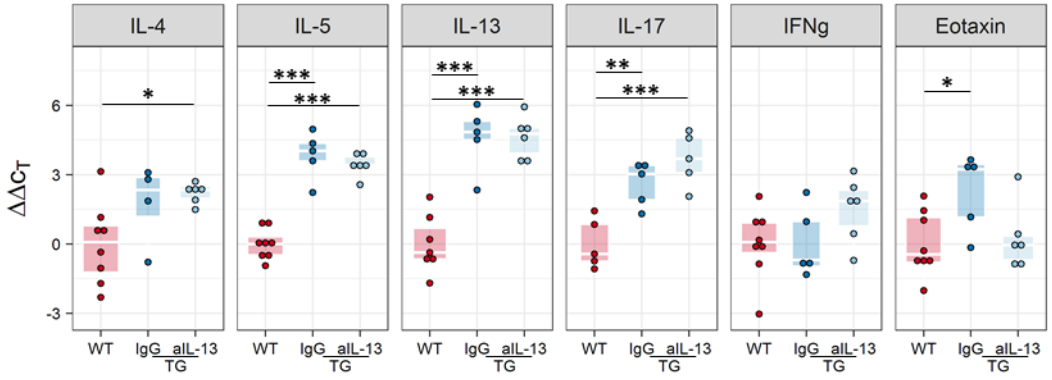

Figure 54: Blockade of IL-13 alters the expression of key inflammatory cytokines. mRNA levels of interleukin (IL)-4, IL-5, IL-13, IL-17, interferon γ (IFNg) and eotaxin were assessed by quantitative real-time PCR in 16--week-old WT mice and Fra2 TG mice treated with IL-13 neutralising (aIL-13) or isotype (IgG) antibodies. Significance of differences were determined using unpaired Mann Whitney test; *p>0.05, **p>0.01, ***p>0.001. (Figure adapted from (117))

Interestingly, Blockade of IL-13 led to decreased levels of IL-13 in the BAL fluid and in the lung tissue of Fra2 TG mice. In contrast, circulating IL-13 in the plasma was highly increased in Fra2 TG mice treated with IL-13 blocking antibodies (Figure 55). This effect might be caused by an inability to internalise IL-13 bound to the blocking antibody and therefore disturbed clearance of IL-13 from the circulation (134).

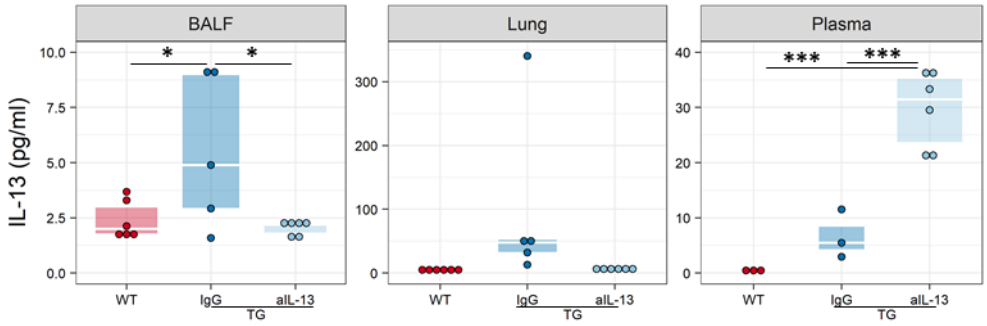

Figure 55: Treatment with IL-13 neutralising antibodies leads to a decrease of IL-13 in the bronchoalveolar lavage fluid (BALF) of Fra2 TG mice, while increasing the circulating IL-13 levels. Using enzyme-linked immunosorbent assay, IL-13 protein levels were measured in the lung homogenate, BALF and plasma of WT and Fra2 TG mice treated with isotype control (IgG) or IL-13 neutralising (aIL-13) antibodies. Significance of differences were determined using unpaired Mann Whitney test; *p < 0.05, *** p < 0.001. (Figure adapted from (117))

3.4.2. Anti-inflammatory treatment using budesonide

Glucocorticoids, by activating the glucocorticoid receptor (GR), block several inflammatory pathways by interacting and thereby inhibiting inflammation associated transcription factors such as STATs, NF-κB and also AP-1 (135). Furthermore they induce the expression of anti-inflammatory mediators. Therefore, we wanted to assess whether a general suppression of inflammation using the glucocorticoid budesonide would improve the asthmatic phenotype induced by overexpression of Fra2. To this end, Fra2 TG mice were treated with budesonide twice a week intranasally (Figure 56).

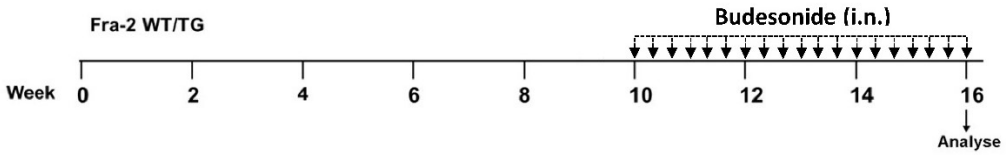

Figure 56: Schematic representation of budesonide treatment. Fra2 TG and WT mice (n=5-7) were treated twice a week intranasally (i.n.) with budesonide. (Figure adapted from (117))

As previously shown, Fra2 TG mice had increased numbers of goblet cells in the airways which were significantly reduced by the treatment with budesonide and almost comparable to healthy control WT mice (Figure 57).

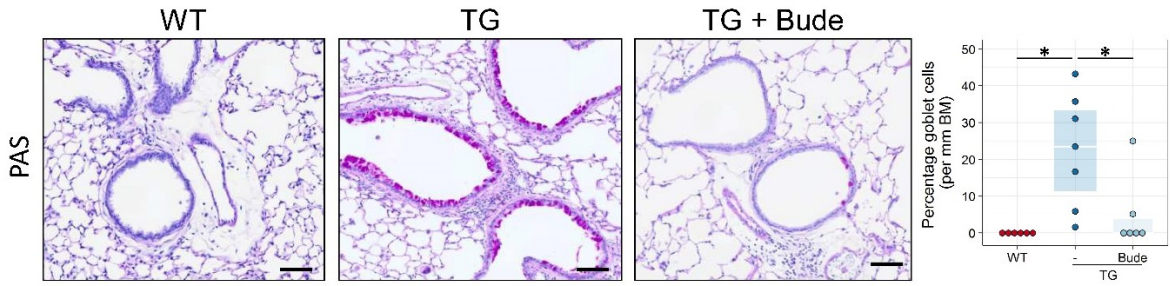

Figure 57: Budesonide treatment lessens goblet cells differentiation and mucus production in Fra2 TG mice. Stereological assessment of the percentage of goblet cells per mm basement membrane (BM) was performed on periodic acid-Schiff (PAS) stained lung section of 16-week old WT and Fra2 TG with or without budesonide (Bude) treatment. Scalebar: 50 µm; Significance of differences were determined using unpaired Mann Whitney test; *p>0.05. (Figure adapted from (117))

In contrast to IL-13 blockade, budesonide led to an improvement of bronchial remodelling in Fra2 TG mice, with decreased deposition of peribronchial collagen (Figure 58A) and considerably less smooth muscle thickening (Figure 58B) compared to untreated mice.

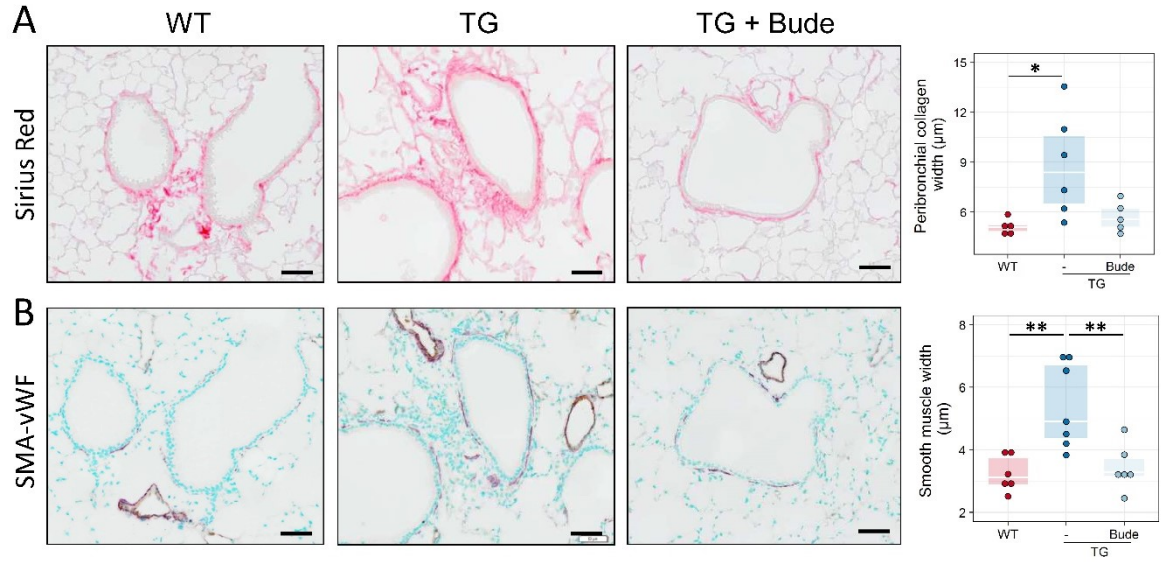

Figure 58: Budesonide reduces bronchial remodelling in Fra2 TG mice. Representative images and subsequent quantification of A) Sirius red staining for peribronchial collagen width and B) double immunohistochemistry for von Willebrand-factor (vWF, brown) and a-smooth muscle actin (SMA, purple) for airway smooth muscle thickness. Remodelling was assessed in 16-week old WT and Fra2 TG with or without budesonide (Bude) treatment. Scalebar: 50 µm; Significance of differences were determined using unpaired Mann Whitney test; *p>0.05, **p>0.01. (Figure adapted from (117))

Corresponding to the improved bronchial remodelling, Fra2 TG mice treated with budesonide had significantly less AHR (Figure 59). Interestingly, already at baseline improved compliance of the respiratory system (Crs, Figure 59) could be observed, indicating that not only hyperresponsiveness, but lung function of Fra2 TG mice in general benefits from budesonide treatment.

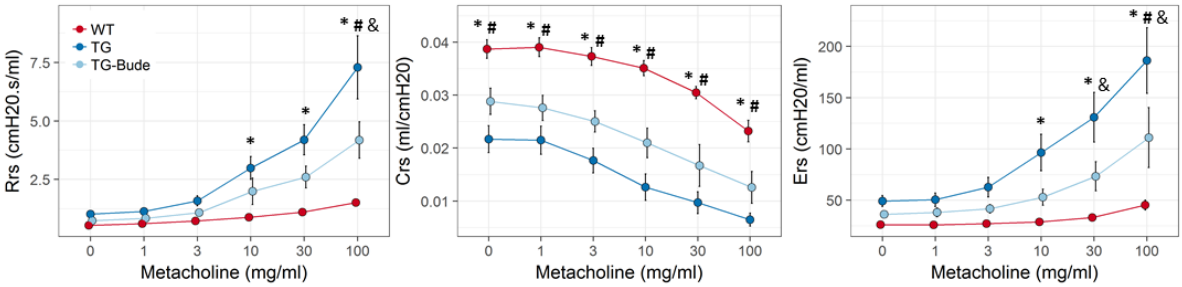

Figure 59: Airway hyperresponsiveness (AHR) in Fra2 TG mice is improved after budesonide treatment. Lung function testing upon increasing doses of Methacholine was performed to determine changes in airway resistance (Rrs), compliance (Crs) and elastance (Ers) in WT mice and Fra2 TG mice with or without budesonide (Bude) treatment (n = 6 per goup). Significance of differences were determined using two-way ANOVA with Bonferroni's *post hoc* test; *p < 0.05 WT vs. TG, #p < 0.05 WT vs. TG-Bude, & p < 0.05 TG vs. TG-Bude. (Figure adapted from (117))

As expected, budesonide significantly decreased the inflammation in the lungs of Fra2 TG mice (Figure 60). The amount of CD45+ inflammatory cells per mg lung tissue significantly declined upon treatment. Further, eosinophil numbers were decreased. Although no significant changes of CD4+ T-cells or B-cells (CD19+) were observed within the groups, there was a clear trend towards increased levels of these cell types in Fra2 TG mice, which was reversed upon treatment with budesonide (Figure 60).

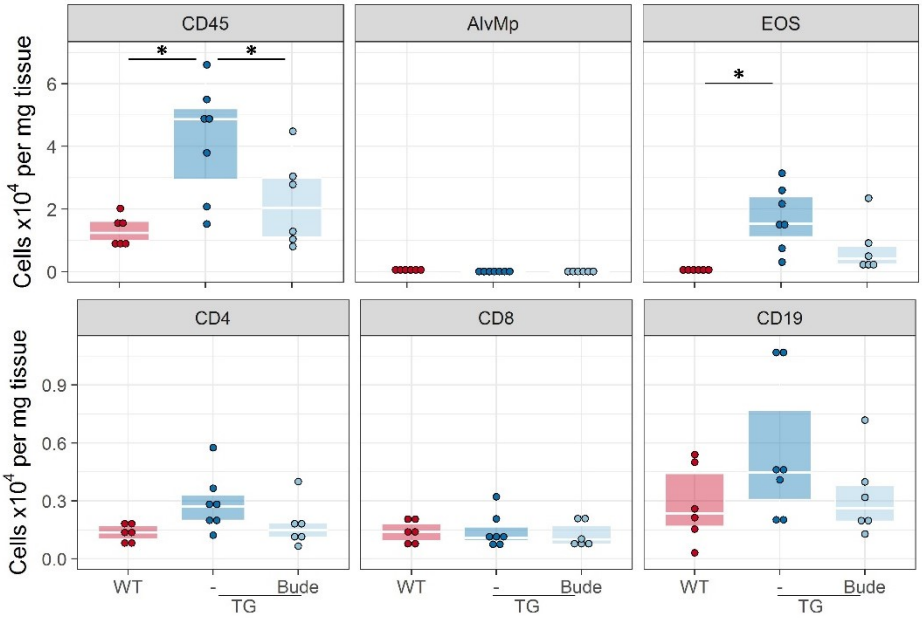

Figure 60: Inflammation in the lung tissue of Fra2 TG mice is decreased upon treatment with budesonide. Flow cytometric analysis of inflammatory cells in single cell lung homogenates of WT or Fra2 TG mice treated with or without budesonide (Bude). Significance of differences were determined using unpaired Mann Whitney test; *p>0.05. (Figure adapted from (117))

Of note, due to technical difficulties, flow cytometry data of the BAL cells did not meet the quality criteria and could not be analysed. However, as shown previously in section 3.2.5, inflammatory cell population changes in the lung tissue mirror the changes observed in the BAL. Therefore, one can assume that the differences in the lung tissue shown in Figure 60, reflect changes of inflammatory cell populations in the BAL of Fra2 TG mice.

The expression levels of Th2 cytokines IL-4, IL-5 and IL-13, as well as IL-17 were slightly decreased in Fra2 TG mice treated with budesonide. However, all cytokines, including IFNγ and eotaxin were still significantly elevated in budesonide treated Fra2 TG mice when compared to WT mice (Figure 61), indicating that budesonide does not efficiently block cytokine production, but acts rather on downstream signalling pathways.

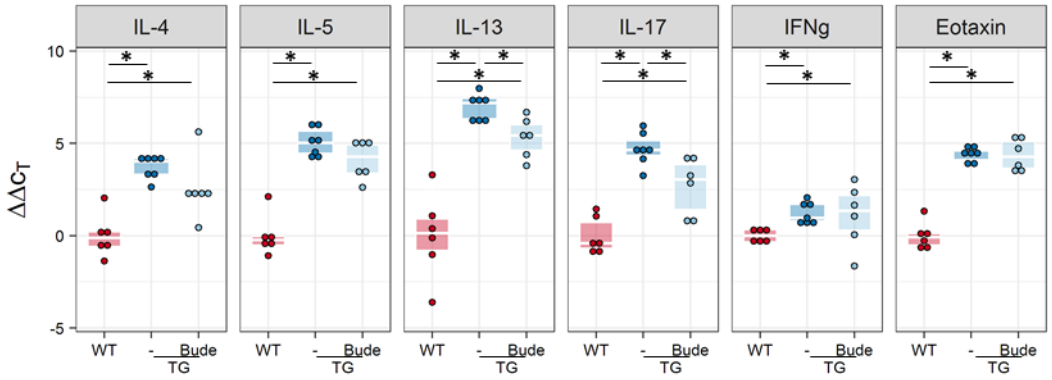

Figure 61: Expression of pro-inflammatory cytokines is decreased in Fra2 TG mice treated with budesonide. mRNA levels of interleukin (IL)-4, IL-5, IL-13, IL-17, interferon γ (IFNg) and eotaxin were assessed by quantitative real-time PCR in 16-week-old WT mice and Fra2 TG mice with or without budesonide (Bude) treatment. Significance of differences were determined using unpaired Mann Whitney test; *p>0.05. (Figure adapted from (117))

This hypothesis was corroborated by the fact that budesonide efficiently blocked phosphorylation and thereby activation of STAT6 (Figure 62). This observed effect could be due to the direct interaction of STAT6 with the glucocorticoid receptor, as it was previously shown that they physically and functionally interact (136).

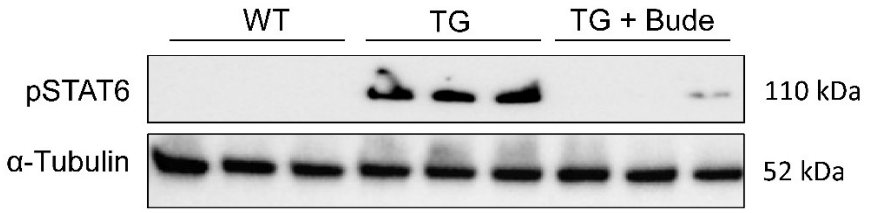

Figure 62: Activation of STAT6 is decreased in Fra2 TG mice after treatment with budesonide. Levels of phosphorylated signal transducer and activator of transcription 6 (pSTAT6) and total STAT6 levels in the lung homogenates of 16-week-old WT and Fra2 TG mice with or without budesonide (Bude) treatment were investigated by western blotting. One representative of two western blots is shown. α-Tubulin was used as loading control. (Figure adapted from (117))

3.4.3. Protein levels of Fra2 are decreased upon effective anti-inflammatory treatment

As AP-1/Fra2 is a potent inflammation induced transcription factor that can be downstream of several pro-inflammatory cytokines, such as IL-13, we measured the amount of Fra2 in the lung homogenates of Fra2 TG mice, after successful anti-

inflammatory treatment using IL-13 neutralizing antibodies or the glucocorticosteroid budesonide.

In Fra2 TG mice, ectopic expression of Fra2 was observed by increased band thickness and the appearance of higher molecular weight bands, indicating increased phosphorylation of Fra2 (Figure 63A, B). Interestingly, Fra2 levels decreased after blockade of IL-13 as well as treatment with budesonide (Figure 63A, B).

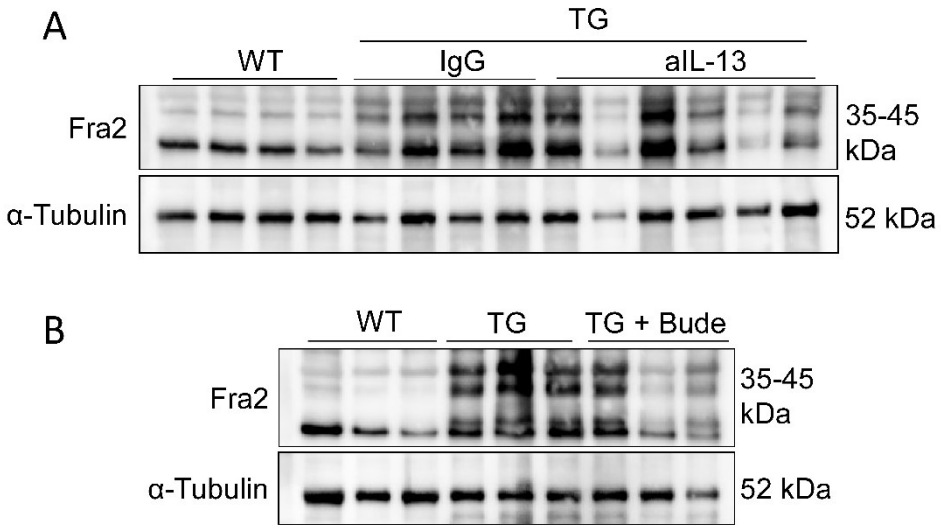

Figure 63: Anti-inflammatory treatment decreases Fra2 protein levels in Fra2 TG mice. Western blot analysis of Fra2 in lung homogenates of A) WT mice and Fra2 TG mice treated with isotype control (IgG) or anti-IL-13 antibodies (aIL-13); or B) WT mice and Fra2 TG mice with or without budesonide (Bude) treatment. For B) one representative of two western blots is shown. α-Tubulin served as a loading control. (Figure adapted from (117))

These results indicate that the increased total amount of Fra2 protein in these mice is not only due to the ectopic overexpression of Fra2 but is also influenced by the increased inflammation in the lungs of these mice.

4. Discussion

4.1. Fra2 overexpressing mice as a model of Systemic sclerosis-associated interstitial lung disease and pulmonary hypertension

Pulmonary complications can manifest as pulmonary fibrosis in the parenchyma and in the vasculature as pulmonary hypertension (PH). These complications are the leading cause of mortality in patients with SSc (137). It was shown that ectopic overexpression of the AP-1 transcription factor family member Fra2 in the mouse leads to fibrotic changes of the skin and to pulmonary structural changes similar to those observed in SSc patients, such as vascular remodelling to the point of pulmonary arterial occlusion, aberrant ECM deposition with fibrosis, and inflammation (16, 42, 138). These structural changes manifest in severe functional impairment, characterized by restrictive lung function and elevated pulmonary pressure, as can be seen in SSc patients, making Fra-2 TG mice a valuable tool to investigate pathophysiological aspects of lung involvement in SSc and to perform pre-clinical proof-of-concept studies.

However, the time-dependency of the Fra2-induced phenotype has been overlooked in most studies published in the last years. The detailed assessment of the time-dependent phenotype conducted in this study showed that restrictive lung function can only be observed in late stages of the disease, in mice <20 weeks of age, whereas in younger mice increased pulmonary compliance was observed. Although no obvious developmental defect in lung morphology was originally described for Fra2 TG mice younger than 12 weeks (42), follow-up studies reported that Fra2 overexpression specifically in α-Sma expressing smooth muscle cells and myofibroblasts impaired myofibroblast function and led to reduced secondary septae formation with alveolar enlargement and emphysema-like phenotype (139). The increase of pulmonary compliance in younger mice (8-16 weeks) observed in this study might therefore be a consequence of this developmental defect of myofibroblast function which are crucial for alveolar septation. We further showed that changes in the vasculature can already be observed at 8 weeks of age, prior to any apparent changes of lung histology. This observation is in line with previous studies showing elevated right ventricular pressure, indicating pulmonary hypertension, at 8 weeks of age (16). In summary, we here described a complex

pulmonary phenotype starting with vascular remodelling at 8 weeks of age, progressive inflammation starting around week 8-12 (16) and culminating in the development of pulmonary fibrosis with restrictive lung function in mice 20-weeks of age and older. However, the severity of the disease can also depend on the genetic background of the mice and the cleanliness of the animal facility as it might influence the progression of the disease. Further, the most severe fibrosis in Fra2 TG mice can be observed in skin and lung (26, 42), two organs which are constantly exposed to the microbiome and exogenous stimuli. This indicates that the development of pulmonary disease in Fra2 TG mice is influenced by environmental factors stimulating the immune system and enhancing inflammation. Regulatory mechanisms which normally take place and limit inflammation to achieve necessary immune tolerance in those organs might be overwritten by the Fra2-induced pro-inflammatory phenotype thereby leading to aberrant inflammation and pro-fibrotic processes. These mice could therefore be a good model to investigate acute exacerbations following subclinical doses of lung pathogens.

To date it is uncertain which factors are responsible for the pulmonary remodelling in SSc patients. Fra2 TG mice have increasingly been used as a model for SSc-associated pulmonary fibrosis and hypertension (140), however a detailed investigation of the time-dependency of its pulmonary phenotype and the involvement of specific inflammatory mediators was missing. We here show that Fra2 TG mice recapitulate several aspects of human disease, including upregulation of inflammatory mediators IL-1, IL-6, the Th2 cytokines IL-4 and IL-13 (117) and chemokines such as Ccl2/MCP-1, and accumulation of immune cells such as B-cells, T-cells and eosinophils in the BAL fluid as well as in the lung tissue (117). The systemic inflammatory state in Fra2 TG mice is not due to the overexpression of Fra2 in bone marrow-derived cells, as shown by Eferl et al, by applying bone marrow reconstitution experiments with TG/WT cells (42). However, it was recently published that Fra2 overexpression in osteoblasts alone is sufficient to induce a systemic pro-inflammatory state, that might drive the disease and manifests predominately in the lung (41). One further similarity to human disease in Fra2 TG mice are elevated levels of matrix metalloproteinase (MMP)-12. MMP-12 is increased in remodelled lung tissue compared to areas of preserved normal lung structure and it correlates with ILD and clinical features of SSc in skin and lung

(123). It was shown to be critically involved in the pathomechanisms of altered vasculature in SSc by inhibiting endothelial urokinase (141, 142). The early upregulation observed in Fra2 TG mice might indicate its involvement in the vasculopathy of the phenotype which is observed much earlier than the fibrotic aspect in Fra2 TG mice.

In some respects, the Fra2-induced phenotype of the mice differs from human disease. For example, the classical pro-fibrotic factor TGFβ which is critically involved in the formation of myofibroblasts and collagen production in SSc is not elevated in Fra2 TG mice. However, it was reported that TGFβ signalling is increased in the lung of these mice and that it plays a critical role in the vasculopathy (143). The TGFβ superfamily pathway includes several cytokines, including bone morphogenetic proteins (BMP), and receptors which are crucially involved in embryonic development, adult tissue homeostasis and in the pathogenesis of various diseases. Signalling is highly complex as receptors and ligands can interact and cross-react thereby antagonising each other to varying degrees and further also cross-react with other signalling pathways (reviewed in (144)). Global TGFβ blockade in Fra2 TG mice ameliorated vascular remodelling and smooth muscle thickening, but did not affect pulmonary fibrosis and even had adverse effects regarding inflammation (143). However, smooth muscle cell specific deletion of the receptor TGFβR2 decreased the smooth muscle cell expansion without affecting inflammation, indicating that TGFβ signalling in smooth muscle cells directly contributes to vascular remodelling in Fra2 TG mice. While TGFβ levels were not altered in Fra2 TG mice, Bmpr2 (BMP receptor 2) levels were decreased (143). BMPR2 is an important antagonist of TGFβ signalling and mutations of it are the most frequent cause of familial or idiopathic PAH (145). In Fra2 TG mice, the amplified TGFβ signalling might therefore be due to the lack of this antagonistic signal rather than due to increase of TGFβ itself (143).

4.2. Development of asthma in Fra2 TG mice

The inflammatory profile of Fra2 TG mice not only closely resembles the changes observed in SSc patients, but also indicates a Th2-predominant, eosinophilic inflammation which can be observed in patients with allergic asthma. Asthma is a

chronic lung disease that affects over 300 million people worldwide (104). Here airway remodelling manifests as mucus cell metaplasia, smooth muscle thickening and sub-epithelial fibrosis, which gives rise to airway obstruction and AHR. The most common form of asthmatic airway disease is atopic (extrinsic) asthma, which is driven by a Th2 allergic response (105). Elevated levels of eosinophils, T-cells and the Th2 cytokines, interleukin (IL)-4, IL-5 and IL-13, cause remodelling and bronchoconstriction (106), and aberrant mucus production (107). Asthma manifests in symptoms such as wheezing, coughing or dyspnoea. We aimed to investigate whether the inflammatory changes observed in Fra2 TG mice lead to airway remodelling and hyperresponsiveness (AHR) as seen in asthmatic patients. To this end, we investigated the asthmatic phenotype of Fra2 TG mice at an early age (16 weeks of age), prior to the development of any apparent lung fibrosis.

4.2.1. Fra2 as a new model of non-allergic asthma

Investigation into the underlying mechanisms of asthma pathogenesis often relies on animal models, which also form the foundation of early pre-clinical testing. As mice do not spontaneously develop asthma, an asthmatic phenotype must first be induced (146). Several different protocols exist that induce acute allergic airway inflammation in mice. These traditionally use intraperitoneal sensitisation of an allergen (typically ovalbumin) and the adjuvant alum to promote the development of a Th2-driven immunological response (146, 147). Several adjuvant free mouse models exist including sub-cutaneous ovalbumin sensitisation (148) or direct exposure of the lung to house dust mite, aspergillus or cockroach aeroallergens (149-151). All these models rely on the application of an exogenous allergen to induce acute allergic airway inflammation. Generally, these models imitate early-onset asthma, which is allergy-induced and associated with elevated IgE levels, Th2 cytokines and responds well to treatment with corticosteroids. In addition to eosinophilic/Th2-driven allergic asthma several other subtypes of asthma have been described, including neutrophil-predominant or mixed eosinophilic/neutrophilic subtypes, which often do not respond to classical glucocorticosteroid treatment (152). These subtypes are however not well-represented regarding animal models. We here have shown that Fra2 TG mice develop an asthmatic phenotype which is severe, possesses key hallmarks of asthma and is independent of any additional allergen challenge (published in (117)). It might therefore be more representative

for non-allergic, late-onset asthma which often poorly benefits from glucocorticoid treatment.

4.2.2. The influence of Fra2 on airway remodelling

Despite their prominent role in cellular differentiation, proliferation and inflammation, little is known about which AP-1 subunits contribute to the pathogenesis of asthma. Bronchial fibroblasts from asthmatic patients have increased AP-1 binding to the DNA compared to non-asthmatic controls (153). Furthermore, inhibition of AP-1 via decoy oligonucleotides has been shown to attenuate OVA-induced experimental asthma (109), however, the contribution of individual AP-1 subunits in the development of asthma is still unclear and studies examining specific subunits are rare. While c-fos was shown to be elevated in OVA-induced asthmatic rats (110), and in bronchial biopsies from asthmatic patients (108), JunB was described as an important factor in Th2 cell differentiation and the production of Th2 cytokines (154). In this study we describe Fra2 as novel factor integrating several features of asthmatic airway disease: It not only influences the immune system leading to a Th2 driven inflammation, but is also directly involved in the regulation of genes important for airway remodelling and mucus production and secretion (25, 117).

Mucus production in the airways is controlled on several levels. It can be increased via upregulation of MUC genes or as a secondary effect of goblet cell hyperplasia/metaplasia and the enhanced secretion of stored mucin (155). We demonstrate that Fra2 upregulates mucus hypersecretion on several different levels (117): First, the production of mucins (MUC5AC) was increased; second, genes necessary for the correct secretion and hydration of newly synthesized mucus such as *Clca1* (156) were increasingly expressed; and third, transcription factors initiating goblet cell differentiation, e.g. *Foxa3* (132), were elevated. Fra2 TG mice also had more collagen around the airways, possible due to the fact that Fra2 increases *Col1a1* and *Col1a2* expression (26, 157) and increased proliferation of smooth muscle cells, leading to thickened airway smooth muscle. In summary, Fra2 overexpression leads to airway remodelling by influencing structure and cellular behaviour on multiple levels.

4.2.3. Fra2 as an inducer of Th2 inflammation

Increased IL-4 expression in Fra2 TG mice was described in the original publication by Eferl and colleagues (42), however the following studies investigated mainly the vascular manifestations and fibrosis development in skin and lung of older Fra2 TG mice (16, 138, 158). In this study we conducted a detailed time-dependent assessment of inflammation in the lungs of Fra2 TG mice. The predominant cell-type involved in Fra2 induced inflammation was eosinophils, together with a Th2 predominant inflammation and highly elevated levels of the effector cytokine IL-13. Neutralising IL-13 diminished the IL-13 levels in the BALF and lung, led to decreased phosphorylation of STAT6, reduced eotaxin expression and eosinophil recruitment, highlighting the crucial role of IL-13 in these processes (159, 160). While IL-13 levels in lung homogenate and BALF decreased after administration of IL-13 blocking antibodies, plasma IL-13 levels significantly increased compared to WT and untreated TG mice. This increase may indicate reduced clearance through internalisation of circulating IL-13 as reported by Kasaian et al. Here the authors state that antibodies directed against IL-13 can have different effects on total IL-13 levels, depending on the targeted epitope and therefore its clearance (134). Furthermore, goblet cell hyperplasia and mucus production were strongly declined by IL-13 inhibition. However, peribronchial collagen thickness was unaltered, further indicating that Fra2 directly influences collagen production. Some structural and morphological changes in the Fra2 TG mouse model may therefore be independent of IL-13, but rather a direct effect of Fra2 overexpression. Nevertheless, we cannot fully exclude that IL-13 neutralisation was incomplete due to duration or dose of treatment.

While blockade of IL-13 signalling decreased the recruitment of eosinophils and T-cells, the numbers of neutrophils and IL-17 levels were elevated. It was previously reported that anti-IL-13 therapy led to increased neutrophilia in the airways of mice sensitized with ovalbumin and ambient particulate matter (161). These effects might be due to the negative regulation of IL-13 on IL-17 production by Th17 cells (133). Neutralising IL-13 might therefore not only have positive effects, but might induce a shift towards Th17 and neutrophil predominant inflammation, as observed in this study. Such observations highlight the importance to choose appropriate treatment strategies for specific disease subtypes, as the described mechanisms might lead

to severe adverse effects in patients with mixed eosinophilic/neutrophilic airway disease.

General anti-inflammatory treatment using the glucocorticoid budesonide partially reversed the Fra2 induced asthmatic phenotype. Recruitment of inflammatory cells to the lungs of Fra2 TG mice was significantly diminished and budesonide further decreased airway smooth muscle thickness. Several mechanisms could explain these positive effects. First, direct interaction of the glucocorticoid receptor (GR) with AP-1/Fra2 could inhibit AP-1 activity (162). Second, accelerated turnover and degradation of Fra2, as seen by diminished Fra2 protein levels following treatment with budesonide. Third, downstream effects of AP-1/Fra2 could be blocked by GR interaction with other pro-inflammatory transcription factors, such as NF-κB, or induction of anti-inflammatory genes by the activated GR (163). However, the Fra2 phenotype could only be partially rescued by treatment with budesonide. Abnormal interaction of GR with AP-1 has been assumed to be a cause for steroid refractory asthma (112). Fra2 overexpression and the consequent change in AP-1 complex composition might therefore decrease the binding affinity to the GR and subsequently explain the incomplete restoration of the Fra2-induced phenotype as well as the steroid-insensitivity in some asthma patients.

4.3. AP-1/Fra2 as therapeutic target

Anti-inflammatory treatment using both IL-13 neutralizing antibodies and glucocorticoids partially decreased protein levels of Fra2 in the lungs of Fra2 TG mice, indicating that some amount of Fra2 protein is not due to the ectopic overexpression, but to the endogenous expression induced by pro-inflammatory stimuli such as IL13 (17). The progressive and irreversible phenotype of Fra2 TG mice might be the result of a vicious cycle caused by the presence of Fra2, triggering pro-inflammatory cytokines which in turn again stimulate Fra2 expression and activation. The constant presence of Fra2 due to the ectopic overexpression could therefore interfere with normal resolution of inflammation.

Fra2/AP-1, due to its global and broad effects on diverse cell and tissue types may have important implications in many inflammatory driven diseases. Therapeutic targeting of AP-1/Fra2 might therefore be a useful possibility to treat unrestrained

inflammatory processes. Inhibition of AP-1 can be achieved through interaction with nuclear receptors such as the glucocorticoid receptor (162) or the oestrogen receptor (164) as part of their anti-inflammatory properties. But due to the broad impact of targeting nuclear receptors and the included adverse effects, it might be of great interest in lung diseases to specifically target AP-1 subunits to achieve better and more targeted therapy. Several studies already reported the feasibility of targeting AP-1. For example, inhibition of the transcriptional activity of redox-regulated AP-1 in an OVA-induced asthma model led to decreased inflammation and ameliorated the asthmatic phenotype (111). Treatment with decoy nucleotides specifically interfering with AP-1 DNA binding attenuated the OVA-induced asthmatic phenotype and improved airway hyperresponsiveness, mucus production and production of Th2 cytokines (109). Furthermore, using a selective small molecular inhibitor of AP-1, dermal fibrosis could be abrogated in two mouse models of SSc (165). Blockade of AP-1 transcriptional activity could therefore be a beneficial therapeutic option in the treatment of systemic sclerosis as well as asthmatic airway disease and might prove effective by targeting several disease pathomechanisms such as inflammation, remodelling and excessive mucus production in the airways.

Furthermore, Fra2 TG mice might provide a valuable new tool to investigate the pathomechanisms of allergen- or viral induced asthma exacerbations. These exacerbations are a common response to viral infections or allergen exposure, leading to abnormal airway inflammation and resulting in increased hospitalisations and health care costs (166). Mechanisms underlying these exacerbations are not yet well studied. Here Fra2 TG mice could serve as a new tool to investigate allergen- or viral-induced exacerbations.

In summary, we have shown that the AP-1 transcription factor family member Fra2 acts strongly pro-inflammatory, leading to a prominent Th2 driven inflammation in the lungs of mice culminating in the development of severe pulmonary fibrosis and restrictive lung function. Additionally, we have shown that without the need for additional allergen challenge, Fra2 TG mice developed severe airway disease including airway remodelling and declined lung function with AHR. This phenotype could only partially be reversed by blocking IL-13 signalling or by anti-inflammatory treatment with glucocorticoids, suggesting that morphological and functional changes were due to a combination of direct Fra2 overexpression and IL-13

pathway activation. However, further investigations are needed to clarify the role of Fra2 in other animal models of experimental asthma and in human airway disease.

5. References

1. Shaulian E, Karin M. AP-1 in cell proliferation and survival. Oncogene. 2001;20(19):2390-400.
2. Angel P, Imagawa M, Chiu R, Stein B, Imbra RJ, Rahmsdorf HJ, et al. Phorbol ester-inducible genes contain a common cis element recognized by a TPA-modulated trans-acting factor. Cell. 1987;49(6):729-39.
3. Glover JN, Harrison SC. Crystal structure of the heterodimeric bZIP transcription factor c-Fos-c-Jun bound to DNA. Nature. 1995;373(6511):257-61.
4. Hai T, Curran T. Cross-family dimerization of transcription factors Fos/Jun and ATF/CREB alters DNA binding specificity. Proceedings of the National Academy of Sciences of the United States of America. 1991;88(9):3720-4.
5. Karin M, Liu Z, Zandi E. AP-1 function and regulation. Curr Opin Cell Biol. 1997;9(2):240-6.
6. Kerppola TK, Curran T. Maf and Nrl can bind to AP-1 sites and form heterodimers with Fos and Jun. Oncogene. 1994;9(3):675-84.
7. Reddy SP, Mossman BT. Role and regulation of activator protein-1 in toxicant-induced responses of the lung. American journal of physiology Lung cellular and molecular physiology. 2002;283(6):L1161-78.
8. Chinenov Y, Kerppola TK. Close encounters of many kinds: Fos-Jun interactions that mediate transcription regulatory specificity. Oncogene. 2001;20(19):2438-52.
9. Matsui M, Tokuhara M, Konuma Y, Nomura N, Ishizaki R. Isolation of human fos-related genes and their expression during monocyte-macrophage differentiation. Oncogene. 1990;5(3):249-55.
10. Nishina H, Sato H, Suzuki T, Sato M, Iba H. Isolation and characterization of fra-2, an additional member of the fos gene family. Proceedings of the National Academy of Sciences of the United States of America. 1990;87(9):3619-23.
11. Lallemand D, Spyrou G, Yaniv M, Pfarr CM. Variations in Jun and Fos protein expression and AP-1 activity in cycling, resting and stimulated fibroblasts. Oncogene. 1997;14(7):819-30.
12. Yoshida T, Suzuki T, Sato H, Nishina H, Iba H. Analysis of fra-2 gene expression. Nucleic acids research. 1993;21(11):2715-21.
13. Sonobe MH, Yoshida T, Murakami M, Kameda T, Iba H. fra-2 promoter can respond to serum-stimulation through AP-1 complexes. Oncogene. 1995;10(4):689-96.
14. Suzuki T, Okuno H, Yoshida T, Endo T, Nishina H, Iba H. Difference in transcriptional regulatory function between c-Fos and Fra-2. Nucleic acids research. 1991;19(20):5537-42.
15. Virolle T, Monthouel MN, Djabari Z, Ortonne JP, Meneguzzi G, Aberdam D. Three activator protein-1-binding sites bound by the Fra-2.JunD complex cooperate for the regulation of murine laminin alpha3A (lama3A) promoter activity by transforming growth factor-beta. The Journal of biological chemistry. 1998;273(28):17318-25.
16. Biasin V, Marsh LM, Egemnazarov B, Wilhelm J, Ghanim B, Klepetko W, et al. Meprin beta, a novel mediator of vascular remodelling underlying pulmonary hypertension. The Journal of pathology. 2014;233(1):7-17.

17. Fichtner-Feigl S, Strober W, Kawakami K, Puri RK, Kitani A. IL-13 signaling through the IL-13alpha2 receptor is involved in induction of TGF-beta1 production and fibrosis. Nature medicine. 2006;12(1):99-106.
18. Yue J, Mulder KM. Requirement of Ras/MAPK pathway activation by transforming growth factor beta for transforming growth factor beta 1 production in a Smad-dependent pathway. The Journal of biological chemistry. 2000;275(40):30765-73.
19. Chuang JY, Huang YL, Yen WL, Chiang IP, Tsai MH, Tang CH. Syk/JNK/AP-1 signaling pathway mediates interleukin-6-promoted cell migration in oral squamous cell carcinoma. International journal of molecular sciences. 2014;15(1):545-59.
20. Barnes PJ, Adcock IM. Transcription factors and asthma. The European respiratory journal. 1998;12(1):221-34.
21. Masuda A, Yoshikai Y, Kume H, Matsuguchi T. The interaction between GATA proteins and activator protein-1 promotes the transcription of IL-13 in mast cells. Journal of immunology. 2004;173(9):5564-73.
22. Mori A, Kaminuma O, Mikami T, Inoue S, Okumura Y, Akiyama K, et al. Transcriptional control of the IL-5 gene by human helper T cells: IL-5 synthesis is regulated independently from IL-2 or IL-4 synthesis. The Journal of allergy and clinical immunology. 1999;103(5 Pt 2):S429-36.
23. Rooney JW, Hoey T, Glimcher LH. Coordinate and cooperative roles for NF-AT and AP-1 in the regulation of the murine IL-4 gene. Immunity. 1995;2(5):473-83.
24. Tang W, Yang L, Yang YC, Leng SX, Elias JA. Transforming growth factor-beta stimulates interleukin-11 transcription via complex activating protein-1-dependent pathways. The Journal of biological chemistry. 1998;273(10):5506-13.
25. Gensch E, Gallup M, Sucher A, Li D, Gebremichael A, Lemjabbar H, et al. Tobacco smoke control of mucin production in lung cells requires oxygen radicals AP-1 and JNK. The Journal of biological chemistry. 2004;279(37):39085-93.
26. Reich N, Maurer B, Akhmetshina A, Venalis P, Dees C, Zerr P, et al. The transcription factor Fra-2 regulates the production of extracellular matrix in systemic sclerosis. Arthritis and rheumatism. 2010;62(1):280-90.
27. Biasin V, Wygrecka M, Marsh LM, Becker-Pauly C, Brcic L, Ghanim B, et al. Meprin beta contributes to collagen deposition in lung fibrosis. Scientific reports. 2017;7:39969.
28. Busnadiego O, Gonzalez-Santamaria J, Lagares D, Guinea-Viniegra J, Pichol-Thievend C, Muller L, et al. LOXL4 is induced by transforming growth factor beta1 through Smad and JunB/Fra2 and contributes to vascular matrix remodeling. Molecular and cellular biology. 2013;33(12):2388-401.
29. Eferl R, Wagner EF. AP-1: a double-edged sword in tumorigenesis. Nat Rev Cancer. 2003;3(11):859-68.
30. Trop-Steinberg S, Azar Y. AP-1 Expression and its Clinical Relevance in Immune Disorders and Cancer. Am J Med Sci. 2017;353(5):474-83.
31. Tulchinsky E. Fos family members: regulation, structure and role in oncogenic transformation. Histol Histopathol. 2000;15(3):921-8.
32. Murakami M, Ui M, Iba H. Fra-2-positive autoregulatory loop triggered by mitogen-activated protein kinase (MAPK) and Fra-2 phosphorylation sites by MAPK. Cell growth & differentiation : the molecular biology journal of the American Association for Cancer Research. 1999;10(5):333-42.

33. Zenz R, Eferl R, Scheinecker C, Redlich K, Smolen J, Schonthaler HB, et al. Activator protein 1 (Fos/Jun) functions in inflammatory bone and skin disease. Arthritis research & therapy. 2008;10(1):201.
34. Riera-Sans L, Behrens A. Regulation of alphabeta/gammadelta T cell development by the activator protein 1 transcription factor c-Jun. Journal of immunology. 2007;178(9):5690-700.
35. Jochum W, David JP, Elliott C, Wutz A, Plenk H, Jr., Matsuo K, et al. Increased bone formation and osteosclerosis in mice overexpressing the transcription factor Fra-1. Nature medicine. 2000;6(9):980-4.
36. Wagner EF. Bone development and inflammatory disease is regulated by AP-1 (Fos/Jun). Annals of the rheumatic diseases. 2010;69 Suppl 1:i86-8.
37. Eferl R, Zenz R, Theussl HC, Wagner EF. Simultaneous generation of fra-2 conditional and fra-2 knock-out mice. Genesis. 2007;45(7):447-51.
38. Karreth F, Hoebertz A, Scheuch H, Eferl R, Wagner EF. The AP1 transcription factor Fra2 is required for efficient cartilage development. Development. 2004;131(22):5717-25.
39. Wagner EF, Eferl R. Fos/AP-1 proteins in bone and the immune system. Immunological reviews. 2005;208:126-40.
40. McCabe LR, Banerjee C, Kundu R, Harrison RJ, Dobner PR, Stein JL, et al. Developmental expression and activities of specific fos and jun proteins are functionally related to osteoblast maturation: role of Fra-2 and Jun D during differentiation. Endocrinology. 1996;137(10):4398-408.
41. Luo Y, Grotsch B, Hannemann N, Jimenez M, Ipseiz N, Uluckan O, et al. Fra-2 Expression in Osteoblasts Regulates Systemic Inflammation and Lung Injury through Osteopontin. Molecular and cellular biology. 2018;38(22).
42. Eferl R, Hasselblatt P, Rath M, Popper H, Zenz R, Komnenovic V, et al. Development of pulmonary fibrosis through a pathway involving the transcription factor Fra-2/AP-1. Proceedings of the National Academy of Sciences of the United States of America. 2008;105(30):10525-30.
43. Maurer B, Busch N, Jungel A, Pileckyte M, Gay RE, Michel BA, et al. Transcription factor fos-related antigen-2 induces progressive peripheral vasculopathy in mice closely resembling human systemic sclerosis. Circulation. 2009;120(23):2367-76.
44. Johnson SR. New ACR EULAR guidelines for systemic sclerosis classification. Current rheumatology reports. 2015;17(5):32.
45. Jordan S, Maurer B, Toniolo M, Michel B, Distler O. Performance of the new ACR/EULAR classification criteria for systemic sclerosis in clinical practice. Rheumatology. 2015;54(8):1454-8.
46. LeRoy EC, Black C, Fleischmajer R, Jablonska S, Krieg T, Medsger TA, Jr., et al. Scleroderma (systemic sclerosis): classification, subsets and pathogenesis. The Journal of rheumatology. 1988;15(2):202-5.
47. van den Hoogen F, Khanna D, Fransen J, Johnson SR, Baron M, Tyndall A, et al. 2013 classification criteria for systemic sclerosis: an American College of Rheumatology/European League against Rheumatism collaborative initiative. Arthritis and rheumatism. 2013;65(11):2737-47.
48. Denton CP, Khanna D. Systemic sclerosis. Lancet. 2017;390(10103):1685-99.
49. Elhai M, Meune C, Boubaya M, Avouac J, Hachulla E, Balbir-Gurman A, et al. Mapping and predicting mortality from systemic sclerosis. Annals of the rheumatic diseases. 2017;76(11):1897-905.

50. Tyndall AJ, Bannert B, Vonk M, Airo P, Cozzi F, Carreira PE, et al. Causes and risk factors for death in systemic sclerosis: a study from the EULAR Scleroderma Trials and Research (EUSTAR) database. Annals of the rheumatic diseases. 2010;69(10):1809-15.
51. Kalluri R, Weinberg RA. The basics of epithelial-mesenchymal transition. The Journal of clinical investigation. 2009;119(6):1420-8.
52. Akter T, Silver RM, Bogatkevich GS. Recent advances in understanding the pathogenesis of scleroderma-interstitial lung disease. Current rheumatology reports. 2014;16(4):411.
53. Rock JR, Barkauskas CE, Cronce MJ, Xue Y, Harris JR, Liang J, et al. Multiple stromal populations contribute to pulmonary fibrosis without evidence for epithelial to mesenchymal transition. Proceedings of the National Academy of Sciences of the United States of America. 2011;108(52):E1475-83.
54. van Caam A, Vonk M, van den Hoogen F, van Lent P, van der Kraan P. Unraveling SSc Pathophysiology; The Myofibroblast. Frontiers in immunology. 2018;9(2452).
55. Klingberg F, Hinz B, White ES. The myofibroblast matrix: implications for tissue repair and fibrosis. The Journal of pathology. 2013;229(2):298-309.
56. Silver RM, Miller KS, Kinsella MB, Smith EA, Schabel SI. Evaluation and management of scleroderma lung disease using bronchoalveolar lavage. Am J Med. 1990;88(5):470-6.
57. White B, Moore WC, Wigley FM, Xiao HQ, Wise RA. Cyclophosphamide is associated with pulmonary function and survival benefit in patients with scleroderma and alveolitis. Ann Intern Med. 2000;132(12):947-54.
58. Song E, Ouyang N, Horbelt M, Antus B, Wang M, Exton MS. Influence of alternatively and classically activated macrophages on fibrogenic activities of human fibroblasts. Cellular immunology. 2000;204(1):19-28.
59. Higashi-Kuwata N, Jinnin M, Makino T, Fukushima S, Inoue Y, Muchemwa FC, et al. Characterization of monocyte/macrophage subsets in the skin and peripheral blood derived from patients with systemic sclerosis. Arthritis research & therapy. 2010;12(4):R128.
60. Huang J, Maier C, Zhang Y, Soare A, Dees C, Beyer C, et al. Nintedanib inhibits macrophage activation and ameliorates vascular and fibrotic manifestations in the Fra2 mouse model of systemic sclerosis. Annals of the rheumatic diseases. 2017;76(11):1941-8.
61. Hancock A, Armstrong L, Gama R, Millar A. Production of interleukin 13 by alveolar macrophages from normal and fibrotic lung. American journal of respiratory cell and molecular biology. 1998;18(1):60-5.
62. Kodelja V, Muller C, Politz O, Hakij N, Orfanos CE, Goerdt S. Alternative macrophage activation-associated CC-chemokine-1, a novel structural homologue of macrophage inflammatory protein-1 alpha with a Th2-associated expression pattern. Journal of immunology. 1998;160(3):1411-8.
63. Luzina IG, Atamas SP, Wise R, Wigley FM, Xiao HQ, White B. Gene expression in bronchoalveolar lavage cells from scleroderma patients. American journal of respiratory cell and molecular biology. 2002;26(5):549-57.
64. Stein M, Keshav S, Harris N, Gordon S. Interleukin 4 potently enhances murine macrophage mannose receptor activity: a marker of alternative immunologic macrophage activation. The Journal of experimental medicine. 1992;176(1):287-92.
65. Atamas SP, Yurovsky VV, Wise R, Wigley FM, Goter Robinson CJ, Henry P, et al. Production of type 2 cytokines by CD8+ lung cells is associated with greater

decline in pulmonary function in patients with systemic sclerosis. Arthritis and rheumatism. 1999;42(6):1168-78.
66. Chanez P, Lacoste JY, Guillot B, Giron J, Barneon G, Enander I, et al. Mast cells' contribution to the fibrosing alveolitis of the scleroderma lung. Am Rev Respir Dis. 1993;147(6 Pt 1):1497-502.
67. Yamamoto T, Hartmann K, Eckes B, Krieg T. Role of stem cell factor and monocyte chemoattractant protein-1 in the interaction between fibroblasts and mast cells in fibrosis. J Dermatol Sci. 2001;26(2):106-11.
68. Jordana M, Befus AD, Newhouse MT, Bienenstock J, Gauldie J. Effect of histamine on proliferation of normal human adult lung fibroblasts. Thorax. 1988;43(7):552-8.
69. Trautmann A, Toksoy A, Engelhardt E, Brocker EB, Gillitzer R. Mast cell involvement in normal human skin wound healing: expression of monocyte chemoattractant protein-1 is correlated with recruitment of mast cells which synthesize interleukin-4 in vivo. The Journal of pathology. 2000;190(1):100-6.
70. Cox D, Earle L, Jimenez SA, Leiferman KM, Gleich GJ, Varga J. Elevated levels of eosinophil major basic protein in the sera of patients with systemic sclerosis. Arthritis and rheumatism. 1995;38(7):939-45.
71. Hesselstrand R, Wildt M, Bozovic G, Andersson-Sjoland A, Andreasson K, Scheja A, et al. Biomarkers from bronchoalveolar lavage fluid in systemic sclerosis patients with interstitial lung disease relate to severity of lung fibrosis. Respiratory medicine. 2013;107(7):1079-86.
72. Shock A, Rabe KF, Dent G, Chambers RC, Gray AJ, Chung KF, et al. Eosinophils adhere to and stimulate replication of lung fibroblasts 'in vitro'. Clinical and experimental immunology. 1991;86(1):185-90.
73. Lafyatis R. Transforming growth factor beta--at the centre of systemic sclerosis. Nat Rev Rheumatol. 2014;10(12):706-19.
74. Kissin EY, Lemaire R, Korn JH, Lafyatis R. Transforming growth factor beta induces fibroblast fibrillin-1 matrix formation. Arthritis and rheumatism. 2002;46(11):3000-9.
75. Varga J, Rosenbloom J, Jimenez SA. Transforming growth factor beta (TGF beta) causes a persistent increase in steady-state amounts of type I and type III collagen and fibronectin mRNAs in normal human dermal fibroblasts. Biochem J. 1987;247(3):597-604.
76. Frazier K, Williams S, Kothapalli D, Klapper H, Grotendorst GR. Stimulation of fibroblast cell growth, matrix production, and granulation tissue formation by connective tissue growth factor. J Invest Dermatol. 1996;107(3):404-11.
77. Sato S, Nagaoka T, Hasegawa M, Tamatani T, Nakanishi T, Takigawa M, et al. Serum levels of connective tissue growth factor are elevated in patients with systemic sclerosis: association with extent of skin sclerosis and severity of pulmonary fibrosis. The Journal of rheumatology. 2000;27(1):149-54.
78. Ludwicka A, Ohba T, Trojanowska M, Yamakage A, Strange C, Smith EA, et al. Elevated levels of platelet derived growth factor and transforming growth factor-beta 1 in bronchoalveolar lavage fluid from patients with scleroderma. The Journal of rheumatology. 1995;22(10):1876-83.
79. Distler O, Pap T, Kowal-Bielecka O, Meyringer R, Guiducci S, Landthaler M, et al. Overexpression of monocyte chemoattractant protein 1 in systemic sclerosis: role of platelet-derived growth factor and effects on monocyte chemotaxis and collagen synthesis. Arthritis and rheumatism. 2001;44(11):2665-78.

80. Hussein MR, Hassan HI, Hofny ER, Elkholy M, Fatehy NA, Abd Elmoniem AE, et al. Alterations of mononuclear inflammatory cells, CD4/CD8+ T cells, interleukin 1beta, and tumour necrosis factor alpha in the bronchoalveolar lavage fluid, peripheral blood, and skin of patients with systemic sclerosis. Journal of clinical pathology. 2005;58(2):178-84.
81. Maekawa T, Jinnin M, Ohtsuki M, Ihn H. Serum levels of interleukin-1alpha in patients with systemic sclerosis. The Journal of dermatology. 2013;40(2):98-101.
82. Kawaguchi Y, Hara M, Wright TM. Endogenous IL-1alpha from systemic sclerosis fibroblasts induces IL-6 and PDGF-A. The Journal of clinical investigation. 1999;103(9):1253-60.
83. Postlethwaite AE, Lachman LB, Kang AH. Induction of fibroblast proliferation by interleukin-1 derived from human monocytic leukemia cells. Arthritis and rheumatism. 1984;27(9):995-1001.
84. Chou DH, Lee W, McCulloch CA. TNF-alpha inactivation of collagen receptors: implications for fibroblast function and fibrosis. Journal of immunology. 1996;156(11):4354-62.
85. Sime PJ, Marr RA, Gauldie D, Xing Z, Hewlett BR, Graham FL, et al. Transfer of tumor necrosis factor-alpha to rat lung induces severe pulmonary inflammation and patchy interstitial fibrogenesis with induction of transforming growth factor-beta1 and myofibroblasts. The American journal of pathology. 1998;153(3):825-32.
86. Hasegawa M, Fujimoto M, Kikuchi K, Takehara K. Elevated serum tumor necrosis factor-alpha levels in patients with systemic sclerosis: association with pulmonary fibrosis. The Journal of rheumatology. 1997;24(4):663-5.
87. Ihn H, LeRoy EC, Trojanowska M. Oncostatin M stimulates transcription of the human alpha2(I) collagen gene via the Sp1/Sp3-binding site. The Journal of biological chemistry. 1997;272(39):24666-72.
88. Ihn H, Tamaki K. Oncostatin M stimulates the growth of dermal fibroblasts via a mitogen-activated protein kinase-dependent pathway. Journal of immunology. 2000;165(4):2149-55.
89. De Lauretis A, Sestini P, Pantelidis P, Hoyles R, Hansell DM, Goh NS, et al. Serum interleukin 6 is predictive of early functional decline and mortality in interstitial lung disease associated with systemic sclerosis. The Journal of rheumatology. 2013;40(4):435-46.
90. O'Donoghue RJ, Knight DA, Richards CD, Prele CM, Lau HL, Jarnicki AG, et al. Genetic partitioning of interleukin-6 signalling in mice dissociates Stat3 from Smad3-mediated lung fibrosis. EMBO molecular medicine. 2012;4(9):939-51.
91. Santarlasci V, Cosmi L, Maggi L, Liotta F, Annunziato F. IL-1 and T Helper Immune Responses. Frontiers in immunology. 2013;4:182.
92. Atamas SP, White B. Cytokine regulation of pulmonary fibrosis in scleroderma. Cytokine Growth Factor Rev. 2003;14(6):537-50.
93. Oriente A, Fedarko NS, Pacocha SE, Huang SK, Lichtenstein LM, Essayan DM. Interleukin-13 modulates collagen homeostasis in human skin and keloid fibroblasts. J Pharmacol Exp Ther. 2000;292(3):988-94.
94. Saito A, Okazaki H, Sugawara I, Yamamoto K, Takizawa H. Potential action of IL-4 and IL-13 as fibrogenic factors on lung fibroblasts in vitro. International archives of allergy and immunology. 2003;132(2):168-76.
95. Huang XL, Wang YJ, Yan JW, Wan YN, Chen B, Li BZ, et al. Role of anti-inflammatory cytokines IL-4 and IL-13 in systemic sclerosis. Inflammation research : official journal of the European Histamine Research Society [et al]. 2015;64(3-4):151-9.

96. Wynn TA. Fibrotic disease and the T(H)1/T(H)2 paradigm. Nature reviews Immunology. 2004;4(8):583-94.
97. Hasegawa M, Fujimoto M, Kikuchi K, Takehara K. Elevated serum levels of interleukin 4 (IL-4), IL-10, and IL-13 in patients with systemic sclerosis. The Journal of rheumatology. 1997;24(2):328-32.
98. Wynn TA, Vannella KM. Macrophages in Tissue Repair, Regeneration, and Fibrosis. Immunity. 2016;44(3):450-62.
99. Kodera T, McGaha TL, Phelps R, Paul WE, Bona CA. Disrupting the IL-4 gene rescues mice homozygous for the tight-skin mutation from embryonic death and diminishes TGF-beta production by fibroblasts. Proceedings of the National Academy of Sciences of the United States of America. 2002;99(6):3800-5.
100. Rishikof DC, Ricupero DA, Kuang PP, Liu H, Goldstein RH. Interleukin-4 regulates connective tissue growth factor expression in human lung fibroblasts. Journal of cellular biochemistry. 2002;85(3):496-504.
101. Bandinelli F, Del Rosso A, Gabrielli A, Giacomelli R, Bartoli F, Guiducci S, et al. CCL2, CCL3 and CCL5 chemokines in systemic sclerosis: the correlation with SSc clinical features and the effect of prostaglandin E1 treatment. Clinical and experimental rheumatology. 2012;30(2 Suppl 71):S44-9.
102. Gharaee-Kermani M, Denholm EM, Phan SH. Costimulation of fibroblast collagen and transforming growth factor beta1 gene expression by monocyte chemoattractant protein-1 via specific receptors. The Journal of biological chemistry. 1996;271(30):17779-84.
103. Hasegawa M, Sato S, Takehara K. Augmented production of chemokines (monocyte chemotactic protein-1 (MCP-1), macrophage inflammatory protein-1alpha (MIP-1alpha) and MIP-1beta) in patients with systemic sclerosis: MCP-1 and MIP-1alpha may be involved in the development of pulmonary fibrosis. Clinical and experimental immunology. 1999;117(1):159-65.
104. Masoli M, Fabian D, Holt S, Beasley R, Global Initiative for Asthma P. The global burden of asthma: executive summary of the GINA Dissemination Committee report. Allergy. 2004;59(5):469-78.
105. Wenzel SE. Asthma phenotypes: the evolution from clinical to molecular approaches. Nature medicine. 2012;18(5):716-25.
106. Brightling CE, Symon FA, Birring SS, Bradding P, Pavord ID, Wardlaw AJ. TH2 cytokine expression in bronchoalveolar lavage fluid T lymphocytes and bronchial submucosa is a feature of asthma and eosinophilic bronchitis. The Journal of allergy and clinical immunology. 2002;110(6):899-905.
107. Report G. Global Strategy for Asthma Management and Prevention Report 2018 [Available from: http://ginasthma.org/download/832/.
108. Demoly P, Basset-Seguin N, Chanez P, Campbell AM, Gauthier-Rouviere C, Godard P, et al. c-fos proto-oncogene expression in bronchial biopsies of asthmatics. American journal of respiratory cell and molecular biology. 1992;7(2):128-33.
109. Desmet C, Gosset P, Henry E, Garze V, Faisca P, Vos N, et al. Treatment of experimental asthma by decoy-mediated local inhibition of activator protein-1. American journal of respiratory and critical care medicine. 2005;172(6):671-8.
110. Liu H, Yang X, Hou W. Correlation of c-fos protein expression with neuropeptide content in the lung of bronchial asthmatic rat. International journal of clinical and experimental pathology. 2014;7(12):8657-65.
111. Nguyen C, Teo JL, Matsuda A, Eguchi M, Chi EY, Henderson WR, Jr., et al. Chemogenomic identification of Ref-1/AP-1 as a therapeutic target for asthma.

Proceedings of the National Academy of Sciences of the United States of America. 2003;100(3):1169-73.
112. Adcock IM, Lane SJ, Brown CR, Lee TH, Barnes PJ. Abnormal glucocorticoid receptor-activator protein 1 interaction in steroid-resistant asthma. The Journal of experimental medicine. 1995;182(6):1951-8.
113. Jenkins RG, Moore BB, Chambers RC, Eickelberg O, Konigshoff M, Kolb M, et al. An Official American Thoracic Society Workshop Report: Use of Animal Models for the Preclinical Assessment of Potential Therapies for Pulmonary Fibrosis. American journal of respiratory cell and molecular biology. 2017;56(5):667-79.
114. McGovern TK, Robichaud A, Fereydoonzad L, Schuessler TF, Martin JG. Evaluation of respiratory system mechanics in mice using the forced oscillation technique. J Vis Exp. 2013(75):e50172.
115. Shalaby KH, Gold LG, Schuessler TF, Martin JG, Robichaud A. Combined forced oscillation and forced expiration measurements in mice for the assessment of airway hyperresponsiveness. Respiratory research. 2010;11:82.
116. Salazar E, Knowles JH. An Analysis of Pressure-Volume Characteristics of the Lungs. J Appl Physiol. 1964;19:97-104.
117. Gungl A, Biasin V, Wilhelm J, Olschewski A, Kwapiszewska G, Marsh LM. Fra2 Overexpression in Mice Leads to Non-allergic Asthma Development in an IL-13 Dependent Manner. Front Immunol. 2018;9:2018.
118. Park SH, Chen WC, Hoffman C, Marsh LM, West J, Grunig G. Modification of hemodynamic and immune responses to exposure with a weak antigen by the expression of a hypomorphic BMPR2 gene. PloS one. 2013;8(1):e55180.
119. Alevy YG, Patel AC, Romero AG, Patel DA, Tucker J, Roswit WT, et al. IL-13-induced airway mucus production is attenuated by MAPK13 inhibition. The Journal of clinical investigation. 2012;122(12):4555-68.
120. Gour N, Wills-Karp M. IL-4 and IL-13 signaling in allergic airway disease. Cytokine. 2015;75(1):68-78.
121. Hoffmann J, Wilhelm J, Marsh LM, Ghanim B, Klepetko W, Kovacs G, et al. Distinct differences in gene expression patterns in pulmonary arteries of patients with chronic obstructive pulmonary disease and idiopathic pulmonary fibrosis with pulmonary hypertension. American journal of respiratory and critical care medicine. 2014;190(1):98-111.
122. Kreft L, Soete A, Hulpiau P, Botzki A, Saeys Y, De Bleser P. ConTra v3: a tool to identify transcription factor binding sites across species, update 2017. Nucleic acids research. 2017.
123. Manetti M, Guiducci S, Romano E, Bellando-Randone S, Conforti ML, Ibba-Manneschi L, et al. Increased serum levels and tissue expression of matrix metalloproteinase-12 in patients with systemic sclerosis: correlation with severity of skin and pulmonary fibrosis and vascular damage. Annals of the rheumatic diseases. 2012;71(6):1064-72.
124. Manetti M, Ibba-Manneschi L, Fatini C, Guiducci S, Cuomo G, Bonino C, et al. Association of a functional polymorphism in the matrix metalloproteinase-12 promoter region with systemic sclerosis in an Italian population. The Journal of rheumatology. 2010;37(9):1852-7.
125. Moore KW, de Waal Malefyt R, Coffman RL, O'Garra A. Interleukin-10 and the interleukin-10 receptor. Annu Rev Immunol. 2001;19:683-765.
126. Ponath PD, Qin S, Ringler DJ, Clark-Lewis I, Wang J, Kassam N, et al. Cloning of the human eosinophil chemoattractant, eotaxin. Expression, receptor

binding, and functional properties suggest a mechanism for the selective recruitment of eosinophils. The Journal of clinical investigation. 1996;97(3):604-12.
127. Rose CE, Jr., Lannigan JA, Kim P, Lee JJ, Fu SM, Sung SS. Murine lung eosinophil activation and chemokine production in allergic airway inflammation. Cell Mol Immunol. 2010;7(5):361-74.
128. LaPorte SL, Juo ZS, Vaclavikova J, Colf LA, Qi X, Heller NM, et al. Molecular and structural basis of cytokine receptor pleiotropy in the interleukin-4/13 system. Cell. 2008;132(2):259-72.
129. Murata T, Puri RK. Comparison of IL-13- and IL-4-induced signaling in EBV-immortalized human B cells. Cellular immunology. 1997;175(1):33-40.
130. Munitz A, Cole ET, Karo-Atar D, Finkelman FD, Rothenberg ME. Resistin-like molecule-alpha regulates IL-13-induced chemokine production but not allergen-induced airway responses. American journal of respiratory cell and molecular biology. 2012;46(5):703-13.
131. Park KS, Korfhagen TR, Bruno MD, Kitzmiller JA, Wan H, Wert SE, et al. SPDEF regulates goblet cell hyperplasia in the airway epithelium. The Journal of clinical investigation. 2007;117(4):978-88.
132. Rajavelu P, Chen G, Xu Y, Kitzmiller JA, Korfhagen TR, Whitsett JA. Airway epithelial SPDEF integrates goblet cell differentiation and pulmonary Th2 inflammation. The Journal of clinical investigation. 2015;125(5):2021-31.
133. Newcomb DC, Zhou W, Moore ML, Goleniewska K, Hershey GK, Kolls JK, et al. A functional IL-13 receptor is expressed on polarized murine CD4+ Th17 cells and IL-13 signaling attenuates Th17 cytokine production. Journal of immunology. 2009;182(9):5317-21.
134. Kasaian MT, Raible D, Marquette K, Cook TA, Zhou S, Tan XY, et al. IL-13 antibodies influence IL-13 clearance in humans by modulating scavenger activity of IL-13Ralpha2. Journal of immunology. 2011;187(1):561-9.
135. Ratman D, Vanden Berghe W, Dejager L, Libert C, Tavernier J, Beck IM, et al. How glucocorticoid receptors modulate the activity of other transcription factors: a scope beyond tethering. Molecular and cellular endocrinology. 2013;380(1-2):41-54.
136. Biola A, Andreau K, David M, Sturm M, Haake M, Bertoglio J, et al. The glucocorticoid receptor and STAT6 physically and functionally interact in T-lymphocytes. FEBS letters. 2000;487(2):229-33.
137. Steen VD, Medsger TA. Changes in causes of death in systemic sclerosis, 1972-2002. Annals of the rheumatic diseases. 2007;66(7):940-4.
138. Maurer B, Reich N, Juengel A, Kriegsmann J, Gay RE, Schett G, et al. Fra-2 transgenic mice as a novel model of pulmonary hypertension associated with systemic sclerosis. Annals of the rheumatic diseases. 2012;71(8):1382-7.
139. Tsujino K, Li JT, Tsukui T, Ren X, Bakiri L, Wagner E, et al. Fra-2 negatively regulates postnatal alveolar septation by modulating myofibroblast function. American journal of physiology Lung cellular and molecular physiology. 2017;313(5):L878-L88.
140. Maurer B, Distler JH, Distler O. The Fra-2 transgenic mouse model of systemic sclerosis. Vascular pharmacology. 2013;58(3):194-201.
141. D'Alessio S, Fibbi G, Cinelli M, Guiducci S, Del Rosso A, Margheri F, et al. Matrix metalloproteinase 12-dependent cleavage of urokinase receptor in systemic sclerosis microvascular endothelial cells results in impaired angiogenesis. Arthritis and rheumatism. 2004;50(10):3275-85.

142. Serrati S, Cinelli M, Margheri F, Guiducci S, Del Rosso A, Pucci M, et al. Systemic sclerosis fibroblasts inhibit in vitro angiogenesis by MMP-12-dependent cleavage of the endothelial cell urokinase receptor. The Journal of pathology. 2006;210(2):240-8.
143. Tsujino K, Reed NI, Atakilit A, Ren X, Sheppard D. Transforming growth factor-beta plays divergent roles in modulating vascular remodeling, inflammation, and pulmonary fibrosis in a murine model of scleroderma. American journal of physiology Lung cellular and molecular physiology. 2017;312(1):L22-L31.
144. Guo X, Wang XF. Signaling cross-talk between TGF-beta/BMP and other pathways. Cell Res. 2009;19(1):71-88.
145. Ma L, Chung WK. The genetic basis of pulmonary arterial hypertension. Hum Genet. 2014;133(5):471-9.
146. Aun MV, Bonamichi-Santos R, Arantes-Costa FM, Kalil J, Giavina-Bianchi P. Animal models of asthma: utility and limitations. Journal of asthma and allergy. 2017;10:293-301.
147. Brewer JM, Conacher M, Hunter CA, Mohrs M, Brombacher F, Alexander J. Aluminium hydroxide adjuvant initiates strong antigen-specific Th2 responses in the absence of IL-4- or IL-13-mediated signaling. Journal of immunology. 1999;163(12):6448-54.
148. Conrad ML, Yildirim AO, Sonar SS, Kilic A, Sudowe S, Lunow M, et al. Comparison of adjuvant and adjuvant-free murine experimental asthma models. Clinical and experimental allergy : journal of the British Society for Allergy and Clinical Immunology. 2009;39(8):1246-54.
149. Campbell EM, Kunkel SL, Strieter RM, Lukacs NW. Temporal role of chemokines in a murine model of cockroach allergen-induced airway hyperreactivity and eosinophilia. Journal of immunology. 1998;161(12):7047-53.
150. Johnson JR, Wiley RE, Fattouh R, Swirski FK, Gajewska BU, Coyle AJ, et al. Continuous exposure to house dust mite elicits chronic airway inflammation and structural remodeling. American journal of respiratory and critical care medicine. 2004;169(3):378-85.
151. Mehlhop PD, van de Rijn M, Goldberg AB, Brewer JP, Kurup VP, Martin TR, et al. Allergen-induced bronchial hyperreactivity and eosinophilic inflammation occur in the absence of IgE in a mouse model of asthma. Proceedings of the National Academy of Sciences of the United States of America. 1997;94(4):1344-9.
152. Trevor JL, Deshane JS. Refractory asthma: mechanisms, targets, and therapy. Allergy. 2014;69(7):817-27.
153. Jacques E, Semlali A, Boulet LP, Chakir J. AP-1 overexpression impairs corticosteroid inhibition of collagen production by fibroblasts isolated from asthmatic subjects. American journal of physiology Lung cellular and molecular physiology. 2010;299(2):L281-7.
154. Hartenstein B, Teurich S, Hess J, Schenkel J, Schorpp-Kistner M, Angel P. Th2 cell-specific cytokine expression and allergen-induced airway inflammation depend on JunB. The EMBO journal. 2002;21(23):6321-9.
155. Rose MC, Voynow JA. Respiratory tract mucin genes and mucin glycoproteins in health and disease. Physiological reviews. 2006;86(1):245-78.
156. Brett TJ. CLCA1 and TMEM16A: the link towards a potential cure for airway diseases. Expert review of respiratory medicine. 2015;9(5):503-6.
157. Bozec A, Bakiri L, Jimenez M, Schinke T, Amling M, Wagner EF. Fra-2/AP-1 controls bone formation by regulating osteoblast differentiation and collagen production. The Journal of cell biology. 2010;190(6):1093-106.

158. Avouac J, Konstantinova I, Guignabert C, Pezet S, Sadoine J, Guilbert T, et al. Pan-PPAR agonist IVA337 is effective in experimental lung fibrosis and pulmonary hypertension. Annals of the rheumatic diseases. 2017;76(11):1931-40.
159. Grunig G, Warnock M, Wakil AE, Venkayya R, Brombacher F, Rennick DM, et al. Requirement for IL-13 independently of IL-4 in experimental asthma. Science. 1998;282(5397):2261-3.
160. Kumar RK, Herbert C, Yang M, Koskinen AM, McKenzie AN, Foster PS. Role of interleukin-13 in eosinophil accumulation and airway remodelling in a mouse model of chronic asthma. Clinical and experimental allergy : journal of the British Society for Allergy and Clinical Immunology. 2002;32(7):1104-11.
161. Park SH, Chen WC, Esmaeil N, Lucas B, Marsh LM, Reibman J, et al. Interleukin 13- and interleukin 17A-induced pulmonary hypertension phenotype due to inhalation of antigen and fine particles from air pollution. Pulmonary circulation. 2014;4(4):654-68.
162. De Bosscher K, Vanden Berghe W, Haegeman G. Glucocorticoid repression of AP-1 is not mediated by competition for nuclear coactivators. Molecular endocrinology. 2001;15(2):219-27.
163. Petta I, Dejager L, Ballegeer M, Lievens S, Tavernier J, De Bosscher K, et al. The Interactome of the Glucocorticoid Receptor and Its Influence on the Actions of Glucocorticoids in Combatting Inflammatory and Infectious Diseases. Microbiology and molecular biology reviews : MMBR. 2016;80(2):495-522.
164. Carthy JM, Sundqvist A, Heldin A, van Dam H, Kletsas D, Heldin CH, et al. Tamoxifen Inhibits TGF-beta-Mediated Activation of Myofibroblasts by Blocking Non-Smad Signaling Through ERK1/2. Journal of cellular physiology. 2015;230(12):3084-92.
165. Avouac J, Palumbo K, Tomcik M, Zerr P, Dees C, Horn A, et al. Inhibition of activator protein 1 signaling abrogates transforming growth factor beta-mediated activation of fibroblasts and prevents experimental fibrosis. Arthritis and rheumatism. 2012;64(5):1642-52.
166. Dougherty RH, Fahy JV. Acute exacerbations of asthma: epidemiology, biology and the exacerbation-prone phenotype. Clinical and experimental allergy : journal of the British Society for Allergy and Clinical Immunology. 2009;39(2):193-202.